Experimental Investigation of Effect of Cement Content and Sulphate Concentration on Loading Rate-Dependent Fracture Behaviour of CPB under Mode I, II, and III Loading Conditions

by

Suman Poudel

A thesis

submitted to the Faculty of Graduate Studies in partial fulfillment of the requirements for the Degree of Master of Science
in Civil Engineering

Civil Engineering Supervisor

Dr. Liang Cui

Associate Professor – Dept. of Civil Engineering

Lakehead University Thunder Bay, Ontario December 2023

Author's Declaration Page

I, Suman Poudel hereby affirm that this thesis, named "Experimental Investigation of the Effect of Cement Content and Sulphate Concentration on Loading Rate-Dependent Fracture Behaviour of CPB under Mode I, II, and III Loading Conditions" presented in partial fulfilment of the requirements for the M.Sc. in Civil Engineering at Lakehead University, is entirely my work.

I declare that:

- Lakehead University citation style guidelines have been followed when citing and referencing all sources used in this thesis.
- This thesis credits any co-authors' or other people's contributions.
- I haven't applied for any other degree or certification with this thesis or substantially similar work at any other university or institution.
- The information and findings contained in this thesis are authentic and have not been altered or faked.

I am aware that any violation of academic honesty or data manipulation may have serious repercussions, including the cancellation of my degree. I reaffirm my dedication to following the ideals of academic integrity and honesty.

Year: 2024

Signature: 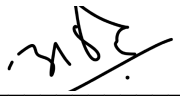

Suman Poudel

.

Abstract

Cement paste backfill (CPB) technology is becoming the standard mine backfilling approach in the mining industry as an environmentally friendly and cost-effective way to manage tailings. Most importantly, CPB plays a critical role in ground support to the surrounding rock mass to ensure the safe and effective operation of the mine. After placement into the mined-out voids, the CPB structure is subjected to complex loading conditions. Due to the dependency of mechanical behaviour on the loading rate, CPB may demonstrate distinctive response and fracture failure characteristics under field loading conditions. However, previous research has primarily concentrated on traditional geomechanical behaviours, ignoring the impact of loading rate on the fracture behaviour of CPB, which significantly influences the assessment of mechanical behaviour and performance of in-stope CPB. Meanwhile, as a cementitious composite, the chemical factors, including cement content and sulphate concentration, dominate the evolution of the mechanical properties of CPB. Therefore, it is of theoretical and practical importance to investigate the effects of cement content and sulphate concentration on CPB's loading rate dependent fracture behaviour. The research aims to evaluate the loading rate dependent fracture behaviour and properties of CPB under different loading conditions. The specific objectives of this study are to experimentally investigate the effect of, cement content (2 wt.%, 4.5 wt.%, and 7 wt.%) and sulphate concentration (5000 ppm, 15000 ppm, and 25000 ppm) on the displacement rate (0.2 mm/min, 1 mm/min, 5 mm/min, and 10 mm/min) dependent fracture behaviour of CPB under different loading conditions (mode I, II, and III) at different curing times (7 days, 28 days, and 90 days). The experimental testing program consists of a series of semi-circular bend (SCB) and edge-notched disc bend (ENDB) tests. In addition to SCB and ENDB tests, a mould-based monitoring program and scanning electron microscope analysis were carried out to characterise the mechanisms responsible for the evolution of loading-rate dependent fracture behaviour and properties of CPB. The results show that the CPB possesses a steeper pre-peak response and a higher peak resistance load as the loading rate increases. The increases in cement content can enhance the sensitivity of pre-peak response, peak load, and fracture properties to the changes in loading rates. However, increasing sulphate concentration adversely influences the early-age CPB matrix integrity due to the generation of expansive ettringite and leads to a reduction in fracture properties, especially at a sulphate concentration of 25000ppm. As the curing time increases to 90 days, CPB consistently improves loading rate dependent fracture properties as the sulphate concentration increases. The

findings from this study can contribute to the reliable assessment of in-situ engineering performance of CPB under complex field loading conditions and thus facilitate the successful implementation of mine backfill technology in practice.

Keywords: Cemented paste backfill, Cement content, Sulphate concentration, Fracture behaviour, Fracture properties.

Acknowledgments

In embarking on this journey of academic pursuit and research, I have been privileged to have received advice, support, and encouragement from numerous individuals and institutions who have played pivotal roles in my MSc study.

First and foremost, I extend my profound gratitude to Dr. Liang Cui, whose wisdom, patience, and unwavering support have been instrumental throughout my academic journey. Dr. Cui's mentorship has enriched my research and instilled in me the values of dedication and perseverance. His role in my life extends beyond academia, as he has welcomed me into his academic family with open arms.

I am deeply indebted to the esteemed members of my thesis committee, Dr. Jian Deng, Dr. Baoqiang Liao and Dr. Eltayeb Mohamedelhassan, for their invaluable time, insights, and contributions to shaping this work.

Special appreciation goes to Dr. Guosheng Wu for his indispensable assistance during SEM observations and to Cory Hubbard and Michael Sorokopud for their technical expertise in the laboratory, which greatly aided my research endeavours.

The support and assistance provided by Brett Holmberg, Javaughn McLean, and Michael Hartford in material testing and data analysis have been invaluable in the pursuit of knowledge. I extend my heartfelt gratitude to the Department of Civil Engineering and the Faculty of Engineering at Lakehead University for their unwavering support. I am particularly thankful to Femi Mirshekari for her guidance throughout the administrative process.

My dear brother, Keshab Sharma, deserves special mention for his unwavering support, motivation, and the opportunities he made possible for me. His enduring patience and care have been my source of strength and inspiration. I am equally grateful to my brother, Bibek Paudel, for his invaluable assistance during the data analysis phase.

My heartfelt gratitude extends to my family, whose unwavering support has been the cornerstone of my educational journey. I fondly remember my late grandfather ‘Narayan Prasad Paudel’ holding my hand as I embarked on my academic path. I dedicate this work to the memory of my late grandmother ‘Keshari Devi Paudel’, whose inspiration gave me the strength to persevere. With

a profound appreciation for my maternal grandmother ‘Ambika Ghimire’ unwavering love and care, I dedicate this work to the exemplar of wisdom and support that she has been on my path to success.

I am immensely grateful to my father and mother ‘Khim Raj & Indira Paudel’, who have selflessly nurtured and supported me in my pursuit of knowledge. To my extended family, including uncles, aunts, brothers, and sisters, I appreciate their unwavering support and encouragement. I also thank my in-laws for their motivating presence and encouragement throughout this journey.

To my wife ‘Nirmala’, your unwavering encouragement and unwavering belief in me have driven my accomplishments. Thank you for standing by me, for your patience, and for never wavering in your support.

In the intricate tapestry of my academic journey, these individuals and institutions have provided unwavering threads of support, guidance, and encouragement. Without their collective efforts, this work would not have been possible.

Table of Contents

List of Tables

List of Figures

List of Equations

List of Abbreviations

CPB	Cemented Paste Backfill
Sc	Sulphate Concentration (ppm)
Cc	Cement Content (%)
w/c	Water to Cement Ratio
SEM	Scanning Electron Microscopy
SCB	Semicircular Bend
ENDB	Edge-notched disc bend
LVDT	Linear Variable Differential Transformer
LEFM	Linear Elastic Failure Mechanics
VWC	Volumetric Water Content
EC	Electrical Conductivity
SIF	Stress Intensity Factor
UCS	Unconfined Compressive Strength
kPa	Kilo Pascal
C-S-H	Calcium Silicate Hydrate
CH	Calcium Hydrate
Aft	Ettringite
CSA	Calcium Sulfoaluminate
C2S	Dicalcium Silicate
C3S	Tricalcium Silicate
C3A	Tricalcium Aluminate

PC	Portland Cement
PPM	Parts Per Million

Nomenclature

P	Maximum Force (N)
R	Radius (m)
T	Thickness
a	Length of Notch (m)
D	Diameter of Sample (m)
t	SCB Thickness of Sample (m)
B	ENDB Thickness of Sample (m)
S	Distance between Load Frame Support Bars (m)
W	Width of Sample (m)
K_{IC}	Mode-I Fracture Toughness ($kPa \cdot m^{1/2}$)
K_{IIC}	Mode-II Fracture Toughness ($kPa \cdot m^{1/2}$)
K_{IIIC}	Mode-III Fracture Toughness ($kPa \cdot m^{1/2}$)
Y_I	Mode-I Normalized Stress Intensity Factor
Y_{II}	Mode-II Normalized Stress Intensity Factor
Y_{III}	Mode-III Normalized Stress Intensity Factor
w	Gravimetric Moisture Content (%)
α	Crack Angle under SCB (°)
β	Crack Angle under ENDB (°)
Ec	Work to crack initiation (Nmm)

Chapter 1 Introduction

1.1 Cemented paste backfill technology

Underground mining is exposed to complex field loading conditions like an earthquake, blasting operations, machinery-induced vibrations, violent rock bursts, pillar bursts, and long walls, causing overburden in strata and disturbance in geological structure over time (Alainachi & Fall, 2021; Cui & Fall, 2015; Wu et al., 2016). Generally, compressive, tensile, and shear stress widely exist in rock mass under these loading conditions (McLean & Cui, 2021; Wang et al., 2014). Cement paste backfill (CPB) is the typical cementitious composite with high fragility, weak fracture resistance, and inadequate durability. These attributes result in unique mechanical behaviours of CPB compared with conventional cement-based materials (Xu et al., 2020). Moreover, as shown in Figure 1.1, the engineering performance of the CPB structure also depends on the complex field loading conditions. For instance, Liu et al. (2017) reported that backfill-rock wall interface interaction not only leads to the development of shear stress near the relatively weak CPB walls but also significantly influences the stress distribution. A more uniform stress distribution was due to stronger rock and thicker backfills (Liu et al., 2017). Moreover, the mined-out voids (called stopes) are commonly featured with rough rock surfaces, which causes the formation of concave and convex wedges on the soft CPB surfaces. The resultant wall notches serve as the local stress concentration regions, resulting in crack initiation and propagation inside the CPB structure when the nominal stress falls below the design strength (Libos and Cui, 2020; Liu et al., 2016). Thus, a reliable assessment of the mechanical stability of the backfill structure requires a full understanding of the fracture behaviour of CPB materials under complex loading conditions (Libos, 2020).

Cemented Paste Backfill (CPB) typically meets compressive loading while supporting the surrounding rock mass, leading the development of a strength-based design technique (SB-DM) for backfill design (Cui & Fall, 2019; Fu et al., 2016; Yilmaz, 2018). The unconfined compressive strength (UCS) is critical in the SB-DM of CPB technology, and determining it is vital to assuring adequate support. Vertical stress analysis is widely used to forecast the stress on the CPB mass, leading the determination of the needed strength in relation to a factor of safety (FS) that is normally in the 1.5-2.5 range. Following this determination, a specific CPB mix design is

developed to meet the identified strength criteria. Significant research efforts have been focused on understanding the UCS of CPB technology, providing useful insights into its mechanical behavior under compression loads. It is worth noting that CPB can be installed at depths exceeding 100 meters below earth, and after curing, it is subjected to complex loading conditions caused by the surrounding ore body and ongoing mining operations such as blasting or equipment usage. However, CPB intrinsic brittleness presents a significant difficulty, increasing the danger of catastrophic failure due to the potential abrupt release of strain energy. This brittle character, along with difficult loading conditions, poses a significant risk to the use of CPB, potentially delaying mining production progress and endangering worker safety. As a result, it is critical to investigate techniques for improving CPB technology deployment and limiting the danger of catastrophic failure. The fiber reinforcing technique appears to be a promising solution in this situation. Figure 1.1 depicts the positioning of CPB as well as the various loading scenarios that it may meet within the underground stope.

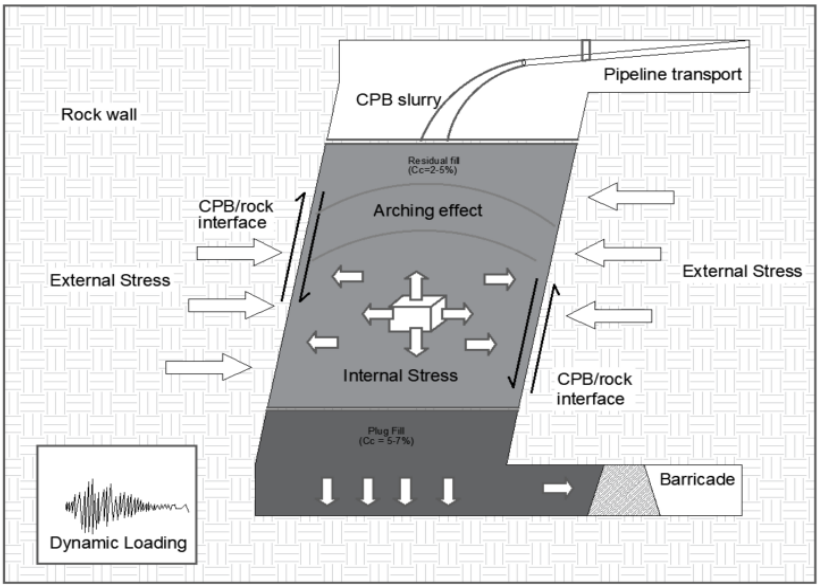

Figure 1.1. CPB mass subjected to complex field loading conditions (modified from (Yin et al., 2023)).

Waste tailings, hydraulic binders, additives, and mixing water are needed to prepare the CPB materials. For hydraulic binders, cement is the primary binding agent used in practice, which reacts with pore water and forms the bond strength between tailings particles (Ercikdi et al., 2009; C. Wang et al., 2014). Therefore, the cement hydration process dominates the development of macro-scale mechanical properties and thus plays a crucial role in the mechanical behaviour of CPB under

field loading conditions (Lura et al., 2009). Besides the hydration process, tailings mainly contain considerable amounts of sulphide minerals such as pyrite, which may react with interstitial water and oxygen. Consequently, sulphate ions may appear in the pore solution and interfere with the cement hydration process. The sulphate ions can react with gypsum and generate expansive ettringite (AFt) in the CPB matrix (Wang, Cao, et al., 2020) . As a result, the crystallization pressure induced by AFt adversely affects the integrity of the CPB matrix and thus causes the degradation of the mechanical properties of CPB. Thus, this chemical process is also called a sulphate attack (Ercikdi et al., 2013; Fall et al., 2010). Based on the sources of sulphate ions in pore solution, a sulphate attack can be further classified into an internal sulphate attack (ISA) and an external sulphate attack (ESA). According to the previous study conducted by Fall and Benzaazoua (2005), sulphate attack on concrete and mortars often occurs in exteriors, whereas CPB is more susceptible to internal sulphate attack. In addition, CPB microstructure and cracks impact fluid movement and durability (Bentz et al., 2002; Lura et al., 2009; Xu et al., 2018).

Likewise, microcrack fusion, which results in considerable deformation in the plastic phase (Cui & Fall, 2016a), dissipates energy in CPB (McLean & Cui, 2021). It has also been confirmed that lower water-cement ratios enhanced fracture toughness while higher cement concentration decreased it (Fang et al., 2021). Fracture toughness increases with curing temperature, while sulphate concentration may lead to a decrease or increase in fracture toughness depending on sulphate concentration and curing time. Meanwhile, saturation conditions did not significantly impact fracture toughness (Libos & Cui, 2020). According to a study performed by Xu & Cao (2018), CPB's fracture toughness increases with extended heat treatment, but it decreases when there is an existing crack. Furthermore, Liu et al. (2013) investigated the deformation and fracture behaviour of CPB samples under various cement-to-tailings ratios and loading circumstances conducted using the acoustic emission (AE) approach to build a damage constitutive model (Liu et al., 2013). These findings emphasize the importance of chemical factors, including cement hydration and sulphate attack, in the mechanical behaviour and properties of CPB. Most importantly, the complex field loading conditions inevitably cause variations in the loading rate acting on CPB mass. It is to be noted that changes in loading rate can considerably impact material behaviour. The effect of varied loading rates on UCS tests in rock and concrete has been widely researched (Rosa et al., 2012; Wisetsaen et al., 2015). For rock materials, loading strain rates are commonly classed as static (about $5x10^{-4}$ s^{-1}) or quasi-dynamic (varying from 5

$x10^{-4}$ s^{-1} to 10^{2} s^{-1}) (Xiu et al., 2021). Additionally, inter-fibre failure (IFF) fracture angle studies indicated improved forecasts at high loading rates (Thomson et al., 2017). Similarly, dynamic Brazilian testing on rocks revealed that higher loading rates increased dynamic indirect tensile strength (Zhu et al., 2015). Furthermore, research into strain-rate-based models for member connections revealed accurate modelling of strain-rate-induced hardening and damage rotation reduction in joints under dynamic settings (Stoddart et al., 2013).

1.2 Problem statement and objectives

As a type of cementitious composite, the failure process in CPB can be characterized by its crack growth. Correspondingly, it is crucial to understand the fracture behaviour and properties of CPB under mode-I, mode-II, and mode-III loading conditions (Aliha et al., 2015). Moreover, the critical stress intensity factor, i.e., fracture toughness, is commonly considered a strength-related fracture property (Libos & Cui, 2020). Therefore, it can serve as the key parameter for the CPB design in practice, which is similar to the role played by material strengths such as UCS. Meanwhile, apart from the fracture toughness, other fracture properties, including stiffness and fracture work, can also provide valuable information for the understanding of the fracture response of CPB under complex loading conditions, especially considering the finite deformation loading conditions.

To explore the characteristics of fracture properties, it is pivotal to consider the effects of chemical factors, including cement hydration and sulphate attack. In CPB technology, optimizing cement usage is crucial as it represents a significant portion of CPB expenses, often accounting for 75% of total expenditures (Wagner et al., 2022). The strength of CPB is highly dependent on the composition of tailings, binder, and water. Tailings composition can vary based on the source, providing opportunities for better control over cement and water content ratio (Carvalho et al., 2018). Careful regulation of cement content is necessary to achieve the desired strength, with Ordinary Portland Cement (OPC) commonly used as the binder due to its influence on CPB workability. Thus, thoroughly understanding the cement hydration process is critical for gradual strength development over time (Benzaazoua et al. 2004). Moreover, sulphate concentration is a crucial component influencing CPB characteristics (Ghirian & Fall, 2014). Since the primary source of sulphate in the CPB material is the tailings from sulphide-bearing minerals in polymetallic mines, which contain low to high levels (2% to 60%) of sulphide that can transform

to sulphate as a result of the chemical reaction (Fall and Benzaazoua 2005, Sheshpari 2015). Sulphate is considered the most common corrosive mineral throughout the environment, including rivers, lakes, soil, and groundwater (Haufe & Vollpracht, 2019; Liu et al., 2020; Zhao et al., 2020). The sulphate affects the rheological characteristics of CPB, which may change how CPB flows, making it less steady and more challenging to control (Xiapeng et al., 2019). When working in the laboratory with dry artificial synthetic tailings, addressing the residual water content in tailings after dewatering from tailings ponds and maintaining the appropriate sulphate concentration is critical. Thus, water content and sulphate concentration integration must be adequately accounted for accurately reproducing real-world situations (Wang et al., 2021). CPB structure has been widely adopted as a crucial ground support measure in underground mining operations to maintain the stability of stopes and safeguard the safety of mining workers and their equipment. Despite extensive research into the conventional geomechanical behaviours (such as compressive, shear, and tensile behaviours) of CPB, there still exists a significant gap in understanding the loading rate-dependent fracture behaviour under various loading conditions, especially considering the effect of chemical factors (i.e., cement content and sulphate concentration).

Most importantly, complex field loading conditions lead to variations in the loading rate and thus influence the fracture response of backfill materials. Therefore, the reliable assessment of the engineering performance of CPB mass requires a comprehensive understanding of the loading rate-dependent fracture behaviour and properties of CPB. Based on previous studies on the geomechanical behaviour of CPB, it has been concluded that changes in loading rate can considerably impact the mechanical behaviour and properties of backfill materials. Previous laboratory studies on the compressive behaviour of CPB were performed using loading rates of 0.2 mm/min, 0.5 mm/min, and 1 mm/min (Fall and Pokharel 2010; Chen et al. 2018; Jiang et al. 2019). When the loading rate was increased from 2 mm/min to 8 mm/min, Li et al. (2016) detected a significant rise in CPB compressive strength. Huang et al. (2011) evaluated CPB strength changes at high loading rates (varying from 10^2 to 10^3 s^{-1}) and found connections between strength and loading rates. Although loading rate-dependent behaviour has been identified as a significant factor influencing material response, its interaction with variable cement content and sulphate concentration in the context of CPB fracture has received less attention. Despite various research characterizing the geomechanical behaviour of CPB, very few studies have been conducted to probe the fracture behaviour of CPB, particularly the dependence of fracture response

on the loading rate. Therefore, it is essential to thoroughly examine CPB's fracture behaviour under different loading rates, which can promote the successful implementation of CPB technology in deep mining operations.

To bridge the present research gap, this research aims to address the following objectives:

(1) Objective I: To experimentally study the loading-rate dependent fracture behaviour of CPB under mode-I (i.e., tensile stress), mode-II (in-plane shear stress), and mode-III (out-of-plane shear stress) loading conditions when considering the effect of chemical factors, including cement content and sulphate concentration.

(2) Objective II: To examine the effect of cement content and sulphate concentration on the evolution of CPB's fracture properties (stiffness, fracture toughness and fracture energy) at various loading rates.

(3) Objective III: To investigate the effect of cement content and sulphate concentration formation of cement hydration products and changes in matrix microstructure and identify the correlation between matrix microstructure and macroscale fracture response and properties.

(4) Objective IV: To explore the influence of cement content and sulphate concentration on the development of matric suction, volumetric water content, and electrical conductivity in CPB from early to advanced ages and thus offer an in-depth insight into the mechanisms responsible for the evolution of fracture properties of CPB.

1.3 Research methodology

This study focuses on understanding the fracture behaviour of CPB materials. A crucial aspect of the present study involves the examination of the impact of cement content and sulphate concentration on the loading rate-dependent fracture behaviour properties of CPB under mode-I, mode-II, and mode-III loading conditions.

To address the objective I, a series of semicircular bend (SCB) tests and edge notched disc bend (ENDB) tests will be conducted on CPB at four different loading rates, including 0.2, 1, 5, and 10 mm/ min from early to advanced ages (7, 28, and 90 days). The SCB tests will be utilized to examine the loading rate-dependent fracture behaviour of CPB under mode-I and mode-II loading conditions, while ENDB tests were specifically designed to explore mode-III fracture behaviour. The testing program will consider two chemical factors influencing the fracture behaviour of CPB: cement content and sulphate concentration. To investigate the influence of chemical factors, three different cement content levels Cc (including 2 wt.%, 4.5 wt.%, and 7 wt.%) and four sulphate concentrations Sc (including 0 ppm, 5000 ppm, 15000 ppm, and 25000 ppm) will be employed. Meanwhile, a constant water-to-tailings ratio (WTR) of 0.36 is adopted to prepare CPB paste, which facilitates the maintenance of the constant mixing proportion of tailings and mixing water. This approach enables the independent evaluation of the effects of Cc and Sc, eliminating their potential confounding influence on the experimental results.

To tackle the objective II, the obtained load-displacement curves from SCB tests and ENDB tests will be used to determine the fracture characteristics, which include material stiffness, fracture toughness, and fracture work. Moreover, the peak load obtained from the load-displacement curves will be used to calculate the critical stress intensity factors, mode-I fracture toughness K_{IC}, mode-II fracture toughness K_{IIC}, mode-III fracture toughness K_{IIIC}. Despite fracture toughness being a measure of material resistance to crack propagation, it does not account for deformation tolerance in its assessment. Importantly, backfill structures often experience substantial deformation loads due to the contraction of the surrounding rock mass. For a thorough grasp of the engineering behaviour of CPB materials, evaluating how energy dissipation changes during a failure is crucial. In line with this, the fracture work was determined by the area under the load-displacement curves.

To deal with the objective III: Scanning electron microscopy (SEM) observation will be conducted on CPB samples prepared with different cement content (2 wt.%, 4.5 wt.%, and 7 wt.%) and sulphate concentrations (0 ppm, 5000 ppm, 15000 ppm, and 25000 ppm) at three different curing times (7, 28, and 90 days). The SEM images will be used to identify the matrix structure changes induced by the precipitation of cement hydration products. Through the identification of hydration products, the influence of cement content and sulphate concentration on the microstructure changes can be obtained and thus used to interpret the evolution of fracture properties of CPB.

To handle the objective IV: a mould-based monitoring program will be developed through the integration of matric suction, water content, and electrical conductivity sensors. The matric suction, water content, and electrical conductivity will be continuously measured over a period of 90 days for CPB samples with different cement content and sulphate concentrations. The obtained results will be used to identify the evolutionary trends of matric suction and water content and thus reveal their contribution to the development of fracture properties of CPB. Meanwhile, the electrical conductivity measurements will be used to explain the changes in cement hydration rates and thus confirm the effect of chemical factors on the internal cement hydration process.

The findings obtained from this experimental testing program will provide in-depth insights into the loading-rate dependent fracture behaviour and properties of CPB and reveal the key mechanisms that influence the fracture response and characteristics under varying loading speeds, with a particular focus on the impact of cement content and sulphate concentration. The results garnered from this study are expected to enhance the understanding of CPB's mechanical performance under real-world field conditions, thereby aiding in the practical application of CPB technology in underground mining operations.

1.4 Organization of the Thesis

This thesis will be presented in five chapters, briefly explained in the following section for a more straightforward presentation and organization. Chapter one provides background information, objectives for the research, methodology, and thesis structure. Chapter two includes an in-depth analysis of backfilling technologies focusing on CPB and thoroughly examining mining operation processes. This chapter also emphasizes the existing studies through the literature review and determining the research gap in this area. The testing materials and apparatus used in this study

are thoroughly described in chapter three, along with the laboratory procedures, test planning, and standards used. Detailed information about the development of a mould-based monitoring program and microstructure analysis will be discussed in this chapter. Chapter four presents and discusses the experimental findings on the loading rate-dependent fracture behaviour of CPB with various cement content and sulphate concentrations. All the derived fracture properties, including stiffness, fracture toughness, and fracture work, will be presented in chapter four. In addition, the findings from the auxiliary analysis (i.e., monitoring program and SEM observations) will be summarized in this chapter. Finally, Chapter five summarizes the most significant findings from the study and offers insightful suggestions for prospective future research to enhance the field of study in this area.

Chapter 2 Literature review

2.1 Introduction

Underground mining operations are inevitably exposed to complex field loadings condition like an earthquake, blasting operations, machinery-induced vibrations, violent rock bursts, pillar bursts, and long walls causing overburden in strata and disturbance in geological structure, etc. over time (Alainachi & Fall, 2021; Cui & Fall, 2015; Wu et al., 2016). Generally, compressive, tensile, shear stress can be developed in mine backfill mass under these loading conditions (McLean & Cui, 2021; Wang et al., 2014). After backfilling in voids and stopes, the hardened CPB must satisfy the specific requirement of mechanical stability (Fall & Benzaazoua, 2005). The research of Fall et al. (2010) listed the major constituents of CPB as (70-80) % by weight of dewater tailing material, and (3-7) % by weight of dry paste used as hydraulic binders usually Ordinary Portland Cement (OPC). Meanwhile, CPB may also be prepared with fly ash sulphate resistance cement and mixing of fresh or mine processed water (Fall et al., 2010). The increase in cement content will reduce ductility and raise stiffness in CPB, whereas the increase in binder content using coarse or medium-grained tailing shows higher strength on CPB than fine-grained tailing (Fall et al., 2007; Wu et al., 2018). Additionally, the strength of the CPB is gained by applying particle size distribution and using admixture and fibres (Fall et al., 2007; Qi & Fourie, 2019). The strength of CPB is an essential factor in its effectiveness as a support structure, and particle size distribution is a crucial factor in determining its strength (Wu et al., 2018). However, composition and chemical constituents determine CPB's short-term and long-term mechanical behaviour (Kesimal et al., 2003). According to Fall & Benzaazoua (2005), 3-7% by weight of cement binder in the CPB gives sufficient strength for the backfilling purpose (Fall & Benzaazoua, 2005). To eliminate the liquefaction, the early-age CPB must have a UCS value greater than 150 kPa (Fall & Pokharel, 2010). Generally, the UCS value of CPB required depends on the function and usage, such as for backfilling purpose on stopes and void UCS range between 150 to 300 kPa, for free-standing wall UCS up to 1 kPa and roof support value higher than 4 MPa. is recommended (Fall & Benzaazoua, 2005; Fall & Pokharel, 2010; Wang et al., 2020). As the typical cementitious material, CPB possesses high fragility, weak fracture resistance, and inadequate durability. These attributes have reduced the popularity of CPB technology (Xu et al., 2020).

The prominent source of sulphate in CPB material is mine tailings containing minerals rich in sulphide, which can have sulphide concentrations ranging from 2% to 60% that can transform to sulphate as a result of the chemical reaction (Fall & Benzaazoua, 2005; Sheshpari, 2015). In various environmental contexts, including rivers, lakes, soil, and groundwater, sulphate is widely consider as a prevalent corrosive element (Haufe & Vollpracht, 2019; Liu et al., 2020; Zhao et al., 2020). The laboratory tests to examine how sulphate affected the rheological characteristics of CPB discovered that adding sulphate to CPB decreased its yield stress while increasing its viscosity. This implies that sulphate may change the way CPB flows, making it less steady and more challenging to control (Xiapeng et al., 2019). The cementitious material tends to deteriorate in sulphate concentration, often characterized as an internal sulphate attack (ISA) and an external sulphate attack (ESA). According to Fall and Benzaazoua (2005), sulphate attack on concrete and mortars often occurs in exteriors, whereas CPB is more susceptible to internal sulphate attack (Fall & Benzaazoua, 2005). Sulphide-rich tailings used in CPB could have issues with strength and stability. ISA on these CPB materials is frequently linked to strength loss and pore characteristic changes (Liu et al., 2020). Generally, the sulphate attack on cement concrete has three modes of deterioration: i.) Gypsum is the acidic type of sulphate attack, leading to losing strength, ii.) Ettringite or Candlot's is the expansive type of sulphate attack developing in expansion and cracking and iii.) Onion-peeling type is scaling or shelling of the surface (Mehta, 1983; Cohen & Bentur, 1988; Al-Amoudi, 1998; Dehwah, 2007). The deteriorations brought on by sulphate include expansion, cracking, loss of stiffness and strength, and disintegration. On the same note, Mehta (1983) found that ettringite formation due to the reaction between water, cement, and sulphate exhibits dual characteristics of the expansion stage (loss of strength) and gaining strength. The sulphate concentration, type of cement, and cation associated with sulphate ions (Na^{+}, Mg^{+2}) will determine the intensity of the sulphate attack on the cement concrete (Dehwah, 2007). In the event of a sodium sulphate attack, the chemical interaction between sulphate, calcium hydroxide ($Ca(OH)_2$), and calcium aluminate (C_3A) result in the formation of gypsum and ettringite. In contrast, a magnesium sulphate attack will form brucite, ettringite, and gypsum (Bonen & Cohen, 1992).

The complex loading condition inside the underground mines also dominate the stress state of CPB. The geomechanical behaviour of CPB can only be determined by studying the compressive, tensile, shear and fracture behaviour of CPB materials (Libos, 2020). Moreover, when the CPB surfaces

are exposed to complex loading conditions when it interacts with the rough rock wall surface having sharp concave and convex wedges. The tensile stress concentration on these notches increased, and the fracture induced in CPB mass at the macroscale since nominal stress became less than design strength (Libos & Cui, 2020; Liu et al., 2016). When backfill and rock mass interact, it becomes clear that many factors are at play, and the interaction is complex. It is noted that the behaviour of the backfill system is greatly influenced by the mechanical characteristics of the surrounding rock mass as well as the backfill material. The performance of the backfill system is affected by the shape of the stope and the stress distribution within the stope under various loading circumstances (Aubertin et al., 2003). As a brittle cement-based material, CPB's deformation behaviour, fracture properties including fracture toughness, development of cracks, and failure pattern of CPB mass under mode I, II, and III loading conditions are critical to understanding the in-situ mechanical performance of CPB. Particularly, the fracture toughness is relevant for CPB because it is often used in mines with irregular and uneven wall geometries, which might result in thin CPB stope sections with pre-existing flaws that are more prone to collapse. As noted, mode I fracture toughness refers to the resistance of a material to crack propagation under tensile stress perpendicular to the plane of crack, whereas mode II fracture toughness refers to the resistance to crack growth under shear stress parallel to the plane of crack (Libos & Cui, 2020). The tearing shear mode under torsion applied perpendicular to the plane of crack refer as mode III fracture toughness which provide resistance to out of plane crack growth (Aliha et al., 2015). Fracture toughness testing involves subjecting a material to controlled loading under different conditions, such as tension or bending, and measuring the critical stress intensity factor at which a crack begins to propagate. This critical stress intensity factor, or fracture toughness, is a measure of the material's ability to resist crack growth and is used in the design and analysis of structures and components to ensure their safety and reliability (Landes, 1996). The testing procedures for fracture toughness, specifically the linear-elastic and nonlinear testing procedures. Testing for linear-elastic fracture toughness involves both slow and fast loading, crack initiation, and crack arrest techniques. The crack tip opening displacement (CTOD) method, J-R curve evaluation, and J_{IC} testing are all examples of nonlinear testing. Other techniques include the weldment fracture testing technique, the common fracture toughness test, the combined J standard method, and the transition fracture toughness test (Landes, 1996; Xiu et al., 2021).

Liu et al. (2017) analysis of the stress distribution in backfilled stopes reveals the significance of considering the interfaces between the backfill and rock walls. In numerical simulations with different backfill thicknesses, rock mass characteristics, and interface circumstances, the scientists discovered that frictional resistance between the backfill and rock walls significantly influenced the distribution of stresses. They also observed that more tough, stiffer rock masses and thicker backfills resulted in a more uniform stress distribution (Liu et al., 2017). McLean & Cui (2021) conducted a comprehensive review of the energy dissipation mechanisms in cementitious materials and identified the fusing of microcracks into macrocracks as the main mechanism for energy dissipation in plain cementitious materials. The evolutive elasto-plastic model developed by Cui & Fall, (2016a) considering the time-dependent behaviour of CPB and its response to changes in loading conditions shows that the non-linear response of the CPB with a significant portion of the deformation occurs during the plastic phase.

Additionally, plastic deformation is associated with the rearrangement of the granular particles and the development of microcracks in the cement matrix (Cui & Fall, 2016). The study by Fang et al. (2021) showed that an increase in cement content reduced fracture toughness, while a decrease in the water-cement ratio contributed to its acquisition. The temperature positively affected fracture toughness, while varied with sulphate concentration and curing age. Libos & Cui (2020) conducted experiments using a compact tension test which showed that the K_{IC} of CPB increased with increasing cement content and curing time. However, the saturation state did not significantly affect the fracture toughness (Libos & Cui, 2020). The experiment by Xu & Cao (2018) under three-point bending loading found that the fracture toughness of CPB increases with thermal treatment duration. However, the presence of a pre-existing crack decreases fracture toughness. The researchers also found that increasing the loading rate decreases fracture toughness due to the dynamic effect of loading, causing more energy to dissipate in the form of friction and deformation. Finally, Aliha et al. (2015) investigated the brittle and quasi-brittle material to assess the integrity of crack components subjected to Mode-III deformation, which shows that K_{IIIC} value is smaller than those with K_{IC} for all material types.

CPB is an essential material used in underground mining operations to provide ground support and assure the safety and effectiveness of the mine. Despite several research characterizing the mechanical behaviour of CPB, much remains to be discovered regarding the various elements that

influence its fracture behaviour. Notably, the effect of strain rate, sulphate concentration, and cement content with the curing period on CPB's fracture behaviour is poorly understood. While earlier studies concentrated on the conventional geomechanical behaviours of CPB, they generally neglected the impact of loading rate on various cement contents and sulphate concentrations on evolving fracture behaviour. The composition of the paste and the surrounding rock mass are two variables that affect how CPB behaves under different loading circumstances. When sulphate ions are present in CPB, they undergo a complicated set of chemical and physical reactions that may impact their behaviour under various loading situations. The amount of sulphate in the CPB paste affects the mechanical behaviour and characteristics of CPB as cement hydration develops over time. Therefore, it is essential to thoroughly examine CPB's fracture behaviour to ensure it is used appropriately in deep mining operations.

2.2 Mechanical behaviour of CPB

The mechanical properties of CPB, like cohesion and internal friction angle, will be highly influenced by the percentage of the solid content of tailing, binder proportion, water content, thermal loads from hydration, curing time, rate of loading and hydraulic conductivity. Based on the material strength design approach, the UCS term is used to determine the mechanical strength of the hardener CPB (Libos, 2020). Generally, the strength of CPB material with the factor of safety (FS) greater than one (1.5-2.0) is frequently employed in order to achieve the stability of the material (Li, 2014). The strength performance of CPB is most often evaluated using triaxial compressive strength and UCS. However, UCS being more feasible and economical, could easily be incorporated into standard-quality control for regulatory conformity (Fall et al., 2007; Fall & Pokharel, 2010; Xu et al., 2020).

Cui & Fall (2016b) investigated the early-age mechanical and thermal properties of cemented tailings materials and the influence of initial temperature, curing stress, and drainage conditions. Their findings suggest that initial temperature can significantly impact the setting time and early-age strength of the materials. They also found that higher curing stresses resulted in higher compressive strengths. Furthermore, drainage conditions were shown to affect the thermal conductivity of the materials, with reduced drainage leading to higher thermal conductivity (Cui & Fall, 2016). According to Yilmaz et al. (2009), the compressive strength of the CPB increased

significantly when cured under pressure. The study also found that the curing time and pressure level significantly impacted the compressive strength development of the samples. The authors attributed this improvement in strength to the increased compaction and reduced porosity of the samples under pressure (Yilmaz et al., 2009). Chen et al. (2022) looked at the impact of curing stress on different cementitious tailings backfill qualities in their study. The outcomes demonstrated that increasing curing stress had a favourable effect on the backfill stability and microstructural compactness. Moreover, higher curing stress increased the backfills electrical conductivity and matric suction (Chen et al., 2022). Jafari (2020) found that increasing the cement content and curing time led to higher strength and lower permeability. However, increasing the water content negatively affected the material's strength and permeability (Jafari, 2020). Yang et al. (2022) illustrated that the variation in volumetric water content of materials like soil, tailings, and cement-based materials has been successfully monitored using the volumetric water content sensor (5TE) as a result, 5TE can dynamically track the CPB hardening process by continuously monitoring VWC. In support, Cui (2023) concludes that the stronger binder forces developed due to increase in C-S-H while change in matric suction and decrease in VWC lead to and increase in frictional resistance (Cui, 2023). Additionally, the SEM analysis showed that the backfill specimens exhibited a dense and uniform microstructure, which contributed to their high strength and ductility. However, with the increase in stress, the microstructure gradually became loose and porous, leading to the initiation and propagation of cracks (Zhou et al., 2021).

As shown in Figure 2.1, through the process of "arching," the strain on the backfill is distributed among the nearby rock mass, redistributing stresses, and reducing the load on the backfill. A stope with a flat roof, as opposed to one with a curved or uneven roof, will typically have a more noticeable arching effect. When the backfill in a narrow stope is unable to sustain the weight of the rock above it, a significant stress concentration forms at the stope's roof. The backfill is consequently put under a lot of compressive stress, which can lead to deformation and eventual failure. The rock mass's strength and the backfill stiffness are key factors in determining the arching effect. Stronger rock masses will tend to deform more under stress, while weaker rock masses will tend to transfer more load to the surrounding backfill (Aubertin et al., 2003). Fall et al. (2007) reported that the stress-strain behaviour of CPB is nonlinear and exhibits strain-hardening behaviour, indicating that the elastic modulus of CPB varies with strain. The authors found that the elastic modulus of CPB increases with increasing strain, which is consistent with

the strain-hardening behaviour observed in the stress-strain curve (Fall et al., 2007). Zhou et al. (2015) found that micro-cracks form in plain cementitious materials under axial strain, causing an increase in Poisson's ratio due to greater transverse strain relative to axial strain. This increase is known as the "Poisson effect" and becomes more significant as the number and size of micro-cracks increase, resulting in an exponential increase in Poisson's ratio with axial strain.

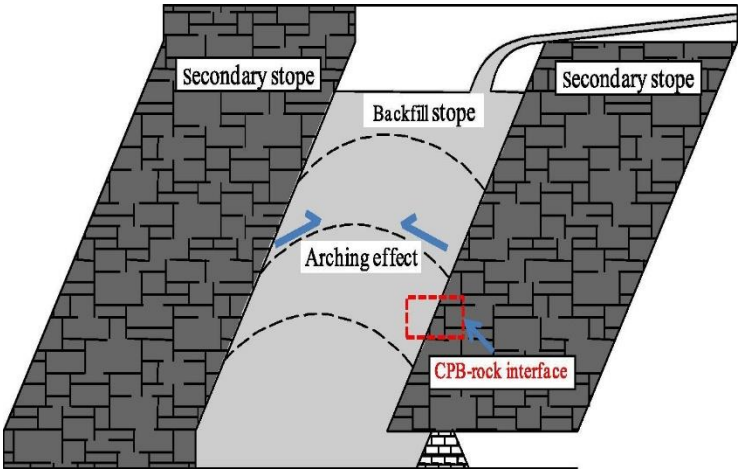

Figure 2.1. Arching Effect CPB-rock interface representation diagram (Weilv et al., 2021).

Additionally, it is well known that different salty corrosive conditions exist for CPB and concrete. A high concentration of sulphate ions and other corrosive substances are exposed to CPB when it is employed as a backfill material in underground mining. While in above-ground constructions, the amount of sulphate ions that concrete is exposed to is often lower. The rate of sulphate attack and sulphate attack mechanism in CPB and concrete are impacted by the various exposure situations (Wang et al., 2020). Sulphate attack on concrete and mortar often takes place in two major sulphate reactions, i) ettringite formation is an expansion phase where cracking of concrete due to the reaction of C_3A and its hydration products takes place ii) gypsum formation due to a reaction between sulphate ion and calcium hydroxide (CH) (Tian & Cohen, 2000).

The stress-strain behaviour and UCS of CPB samples were examined during laboratory testing using sulphate solutions at various concentrations (0 g/L, 0.1 g/L, 1 g/L, and 10 g/L) as shown in Figure 2.2. The study indicates that both a short-term (30 days) and long-term (240 days) sulphate attack had a substantial impact on the compression behaviour of CPB samples. The peak stress and slope of the linear part of the stress-strain curves both steadily grew at 30 days as the sulphate concentration increased. Furthermore, CPB samples immersed in solutions with increasing

sulphate concentrations showed an improved softening tendency during the post-failure stage. However, after being submerged for 240 days, the peak stress decreased as sulphate concentration rose. This was due to the fact that at later ages, increased sulphate concentrations led to additional degradation of the CPB microstructure and a corresponding decrease in CPB's strength and the slope of the elastic stage of the stress-strain curves gradually decreased (Wang et al., 2020). Consequently, it was discovered that a rise in sulphate concentration was advantageous for enhancing short-term strength but detrimental for decreasing CPB strength in advance ages. Thus, this paper presents the comprehensive review on the fracture behaviour of CPB under static loading. The aim is to provide detailed insights into how CPB responds to compressive, tensile, and shear stresses. It primarily concentrates on the geomechanical behaviour of CPB under static loading, the failure patterns that occur, and the mechanical properties of CPB in such scenarios.

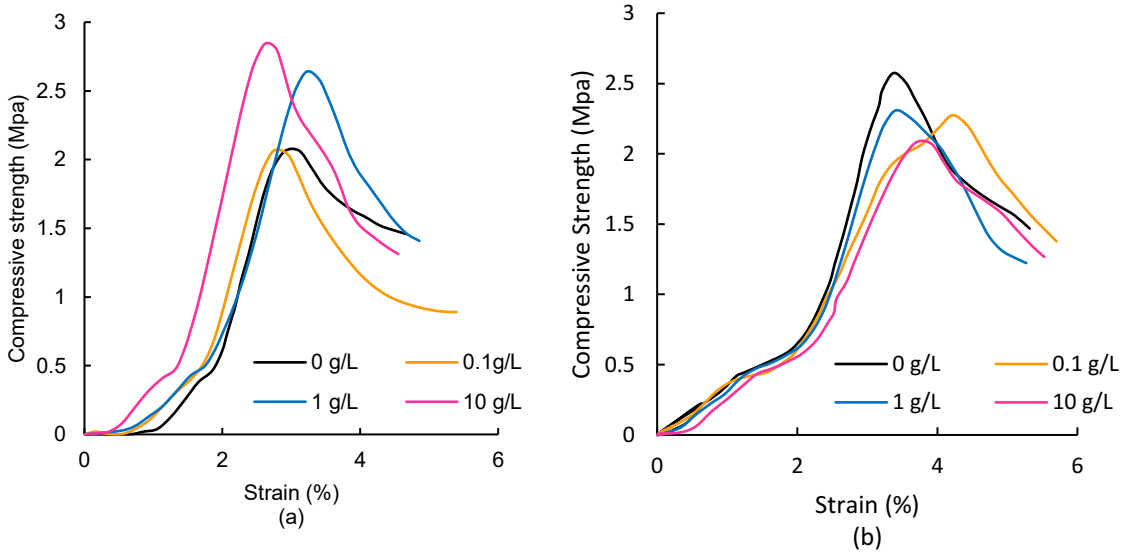

Figure 2.2. Effect of sulphate concentration on the compressive behaviour of CPB (a) 30 days and b(b) 90 days (Wang et al., 2020).

2.3 Compressive behaviour of CPB

The tailing particles surrounded by the hydration product eventually dispersed within the CPB matrix, which accounts for the significant increase in UCS as the curing time increases. Furthermore, with increasing porosity, CPB's UCS and elastic modulus under seepage decline exponentially and exhibit a linearly inverse proportional relationship to the pore area fractal dimension (Ke et al., 2022). The research of Yilmaz et al. (2009) suggests that the increase in UCS

is attributed to the consolidated than those unconsolidated undrained situations of CPB, which is mainly due to the elimination of pore water by applied pressure during the curing process. Shahsavari & Grabinsky (2016) found that pore water pressure in cemented paste backfilled stopes increased during early cement hydration and decreased as it set. This is due to the fact that cement hydration generates heat and releases water, leading to an increase in pore water pressure. As the cement sets, the voids in the backfill become filled with the solidified cement, reducing the pore water pressure (Shahsavari & Grabinsky, 2016).The study on coupled effects of sulphate and temperature showed that the hydraulic conductivity in CPB is inversely related to performance and durability. Hydraulic conductivity rises at a low temperature, and corrosion will occur within CPB because of constraints in cement hydration and sulphate concentration (Pokharel & Fall, 2013). When CPB gets heated to 120 °C, Xu & Cao (2018) discovered that the pore structure dramatically coarsened, and the fracture toughness reduced by 63.5% as the heated temperature rose from 20 °C to 120 °C. However, the significant impact of curing temperature with aging remains. According to Jiang et al. (2023), the mechanical parameter of CPB cured at -6, -1, and 14 °C temperatures significantly impacted mechanical behaviour such as UCS and stress-strain curve. The study suggests that interparticle cohesion and friction are strongly influenced at sub-zero temperatures while it remains in contrast at higher temperatures. The research by Helinski et al (2007); Tian & Fall (2021) provide valuable insight into the behaviour of CPB under non-isothermal conditions; at higher temperature strength of CPB reduces and the pore structure becomes more heterogeneous, which could lead to the formation of cracks and durability. The study also examined CPB's self-desiccation (water consumption during hydration) behaviour, which occurs when water gets removed from a mixture due to evaporation or chemical reactions attributed to the temperature rise (Tian & Fall, 2021). Xu et al. (2018) concluded that the electrical resistivity of the CPB increased gradually during the hydration process, and the rate of increase was related to the water-cement ratio and curing time. The electrical resistivity correlates with CPB mechanical properties, such as compressive strength. Another study by Wenbin et al. (2018) showed that the electrical resistivity of CPB first decreased and gradually increased with increasing curing time and confining pressure and strongly correlated with CPB's compressive strength and elastic modulus. In the same study, the author attests that with the curing time, the formation of more hydration products will contribute to an increase in compressive strength.

The compressive strength of CPB increases with increasing cement content and decreasing water content where as confinement pressure will lead to the different mode of failure (Fall et al., 2007). The effect of aggregate size (particle density, water absorption, flakiness index, degree of agglomeration, surface charging and roughness) on the bearing capacity was less substantial, while curing time significantly impacts its strength, with longer curing times resulting in higher strength values (Zhou et al., 2019). The strain-hardening behaviour of CPB is characterized by an increase in strength and stiffness with increasing strain due to the progressive development of interparticle bonds and cement hydration. Increasing the cement content leads to a denser and more homogeneous cement matrix, resulting in higher strength and stiffness there by reducing ductility (Fall et al., 2007). Conversely, decreasing the water content reduces the porosity of the CPB mixture, resulting in higher strength and stiffness. The longer curing times allow for complete cement hydration and bond development, resulting in higher strength. (Fall et al., 2007). The study by Zhou et al. (2021) investigated the acoustic emission (AE) characteristics, initiation crack intensity, and damage evolution of cement-paste backfill under uniaxial compression.

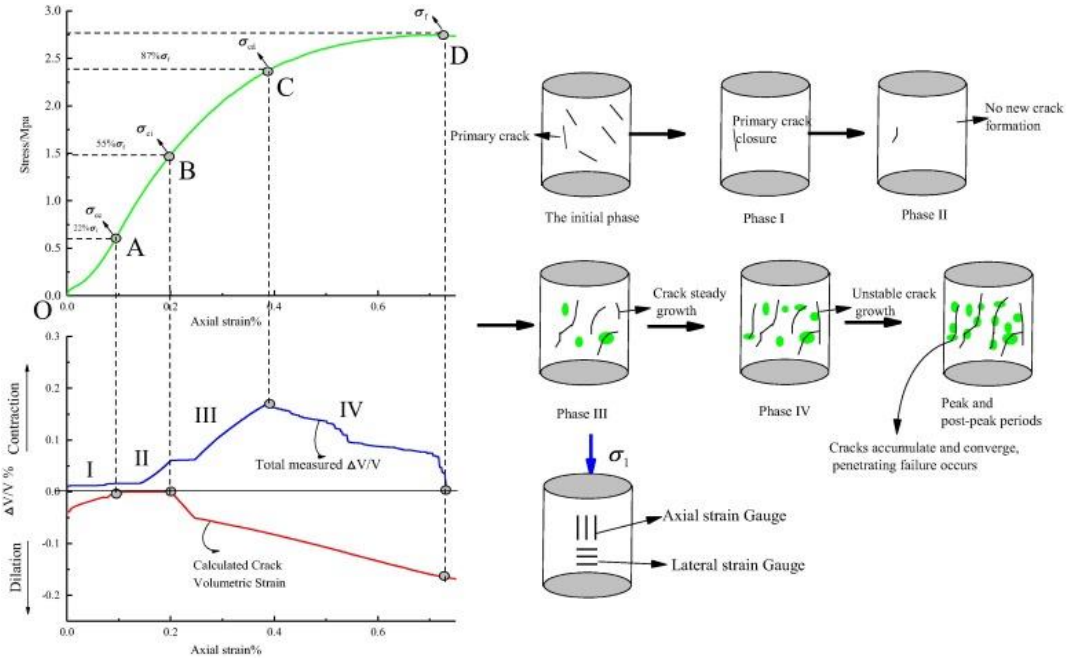

Figure 2.3. Typical stress-strain diagram of CPB sample (Zhou et al., 2021).

The acoustic emission AE characteristic gives valuable insights into the damage progression of CPB under uniaxial compression. The examination of the axial stress-strain, volume strain-axial strain, and crack volume strain-axial strain curves from Figure 2.3 reveal the sample underwent

several stages during the uniaxial compression test, which includes original crack compaction (OA), elastic stage (AB), four stages of crack steady growth (BC) and unstable crack propagation (Zhou et al., 2021). The CPB sample under axial compression (OA) indicates crack closure and pore compaction of samples. The linear axial stress and axial strain curve (AB) indicate the elastic stage of CPB material where no initiation and development of new crack occurs. The volumetric strain gradually increases, and stress corresponding to endpoint B is the crack initiation strength point. The elastoplastic deformation at stage (BC) represents stable crack growth where volumetric strain gradually decreases, and the new crack expands progressively. The unstable crack growth is represented by stage CD, where an increase in axial compression led to damage to the test sample. The crack initiation intensity increases with increasing stress, and the microstructure of the backfill becomes loose and porous, leading to crack initiation and propagation (Zhou et al., 2021). Jafari & Grabinsky (2021) studied the impact of hydration on the failure surface evolution of low sulphide-content cemented paste backfill. They found that the failure surface transformed from smooth and planar to rough and irregular as hydration progressed. The rate of evolution increased with hydration time and decreased with cement content (Jafari & Grabinsky, 2021; Wang et al., 2020).

2.4 Tensile behaviour of CPB

The CPB tensile strength is crucial for building sturdy stopes, but its tensile behaviour is little understood. Many studies were conducted on tensile behaviour on cement concrete; however, tensile behaviour on CPB is minimal. In the study by Schuler et al. (2006) determine the concrete tensile and fracture energy studies entailed applying tensile loads to concrete specimens at high strain rates and watching for spallation through high-speed cameras to monitor the spalled material's velocity. The studies findings demonstrated that concrete's tensile strength and fracture energy rise as the strain rate increases. Also, the researchers noted that the spallation process in concrete is a complicated phenomenon that includes several fracture events, such as cracking, micro-cracking, and the breaking of aggregates (Schuler et al., 2006). The study by Klepaczko & Brara (2001) enables reliable evaluation of critical dynamic tensile parameters like tensile strength, fracture toughness, and strain rate sensitivity, providing insights into concrete behaviour under dynamic loading circumstances. The author insists that the structure's integrity depends on spalling and compression loading due to tensile cracks and the tensile strength of concrete (Klepaczko &

Brara, 2001). Additionally on the research by Pan & Grabinsky (2021) the tensile qualities of the material can be improved by adding more cement and curing time since cement particles serve as a binder to hold the other CPB components together.

The absence of an acceptable test procedure has hampered the advancement of the study in terms of tensile strength. In several instances, for example in cut-and-fill mining or the significant exposure of primary CPB through the ore mining of a secondary stope, the tensile strength is the crucial factor leading to the failure of a cementitious body, even though it can only account for 20%–30% of compressive strength (Fall et al., 2010a; Guo et al., 2022; Komurlu et al., 2016a). Thus, it is crucial to accurately gauge and examine CPB's tensile strength. To improve the current design strategy for undercut CPB using Mitchell's sill mat method, Pan & Grabinsky (2023) proposed combining direct tensile testing with UCS and direct shear tests. The adoption of CPB may increase, resulting in significant operational savings. The research discovered that Mohr-Coulomb parameters provide a more accurate prediction of the tensile strength than the frequently employed UCS ratios of 1:10 or 1:12. However, the Mohr-Coulomb technique is still an empirical correlation, thus whenever possible, direct tensile strength testing is advised (Pan & Grabinsky, 2023). According to Komurlu et al. (2016), the size and form of the specimens as well as the loading apparatus used impact the splitting tensile strength of cement paste backfill materials. Another study by Pan and Grabinsky (2021) stated that the low tensile strength of CPB compared to its high compressive strength is a challenge in producing traditional axisymmetric dogbone-shaped specimens for direct tensile testing of CPB. They pointed out that the Brazilian Split test, an indirect tensile test, is frequently employed for CPB and is simpler to carry out using the same tools as compressive testing. Although it is simple and inexpensive to set up, this indirect test does not yield precise elastic characteristics in tension (Pan & Grabinsky, 2021). The direct shear test and triaxial test are two standard methods used to study the behaviour of the CPB-rock interface. Among them, the former is easier to use, and the latter allows for more varied tests. The direct shear test has also been used to evaluate the shear behaviour of the interface between CPB-rock and CPB-CPB (Pan & Grabinsky, 2021).

According to Li et al. (2016), the specimen's failure modes changed from a mixed mode of tensile-shear failure to a single shear form. Additionally, it has been found that as the loading rate increases, the time needed to reach failure reduces. In other words, the specimen fails more quickly with

larger loading rates. In Figure 2.4 specimen with 60 days curing time depicts that when the loading rate is 2 mm/min, a combination of tensile failure and shear failure parallel to the loading direction are the primary modes of failure. However, the failure mechanism changes to a new pattern involving a longitudinal splitting surface and an oblique shear plane as the loading rate rises to 4 and 6 mm/min (Li et al., 2016).

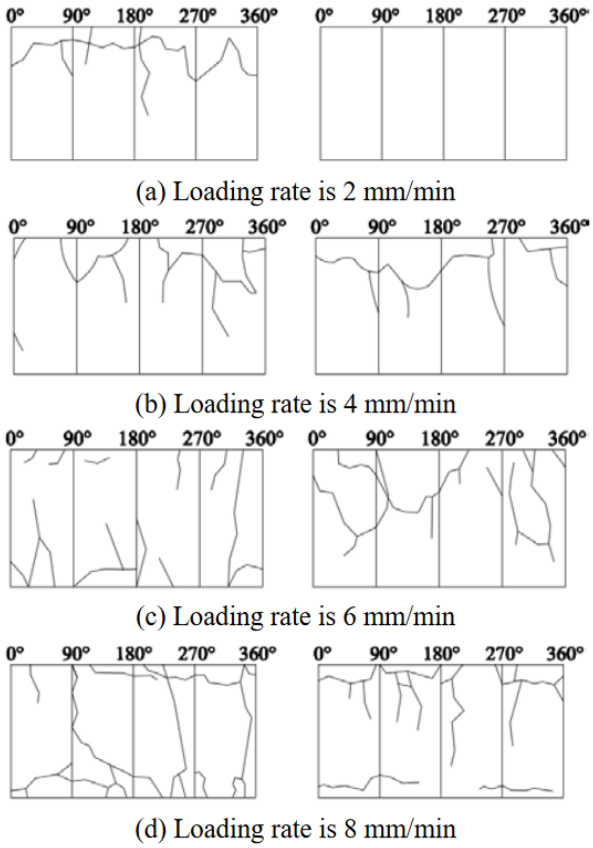

Figure 2.4. Failure pattern of CPB at different loading rate (Li et al., 2016).

2.5 Shear behaviour of CPB

Libos (2020) mentioned that interfacial shear failure predominantly occurs on the soft CPB side because CPB's stiffness and strength are significantly lower than those of the surrounding rock mass. Research studies have shown that the shear strength of CPB increases with curing time and increases with the concentration of cement and tailings in the CPB mix (Fang & Fall, 2018; Jafari, 2020). The shear behaviour of CPB was investigated using a direct shear test by Nasir & Fall (2008); Xiu et al. (2021) found that the shear strength of CPB increased notably as the curing time increased, and the increase was more significant for CPB with a higher cement content (Nasir &

Fall, 2008). According to Koupouli et al (2016), the CPB-rock wall interface's shear strength increased with increasing CPB curing time, indicating that chemical bonding occurred between the CPB and the rock wall. The study also found that the failure mode of the CPB-rock wall interface changed from a cohesive failure mode to a mixed mode failure as the curing time increased (Koupouli et al., 2016). In addition, the shear strength of the CPB-CPB interface was dependent on the ratio of binder to tailings in the CPB mixture. A higher binder content resulted in a higher shear strength of the CPB-CPB interface (Koupouli et al., 2016). Fang & Fall, (2021) investigated the shear behaviour of the CPB-rock interface using a direct shear test. The study found that the CPB-rock interface's shear strength increased with the CPB's curing time and increased with the roughness of the rock surface. When the rock surface is wet, the shear strength of the interface is reduced, and the deformation behaviour becomes more ductile compared to the dry rock surface. The study also showed that the presence of CPB increased the overall shear strength of the interface (Xiu et al., 2021). According to Xiu et al. (2021), the surface characteristics of the rock have an impact on the shear behaviour of the rock-CPB interface. The study demonstrated that water on the rock surface reduces the interlocking effect, so the interface's shear strength is larger under wet conditions than in dry conditions. Additionally, it has been discovered that the interface's failure mode shifts from shear to mixed-mode failure in moist conditions, increasing the risk of tensile failure (Xiu et al., 2021). The study by Fang & Fall, (2018) discovered that the shear strength of the CPB-rock interface strengthens with increasing curing time at 20 °C as shown in Figure 2.5. This is attributed to the increase in the rate of cement hydration at longer curing time, which results in a more rigid CPB matrix. The authors also observed that the failure mode of the interface changed from a cohesive failure at lower curing temperatures to an adhesive failure at higher temperatures.

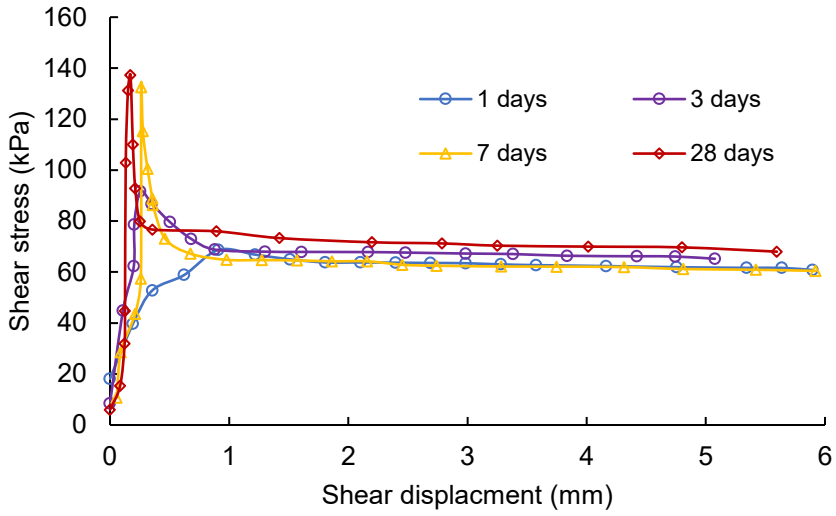

Figure 2.5. Shear stress-displacement curves (Fang & Fall, 2018).

Another study by Fang & Fall (2020) found that curing stress substantially impacts the shear behaviour of the interface between rock and cemented backfill. The higher the curing stress, the higher the peak shear strength and the stiffer the interface response. The researchers also found that drainage conditions played a role in the shear behaviour, with the dry interface exhibiting higher peak shear strength than the wet interface. Furthermore, the backfilling rate was found to have a limited effect on the shear behaviour of the interface (Fang & Fall, 2020). According to a study by Weilv et al. (2021) using a series of triaxial tests on CPB specimens with different interface angles and cement contents, the failure mode shifts from bulging deformation to shear slipping as the angle increases. This is because the interface angle affects the shear strength of the CPB-rock interface. The study also discovered that increasing the cement content of the CPB can improve its stiffness and shear strength, but too much cement content can result in brittle failure (Weilv et al., 2021). The shear strength of CPB increased with increasing confining pressure, as demonstrated by a series of triaxial compression experiments on CPB samples at various confining pressures up to 2.0 MPa (Araújo et al., 2017). When the confining pressure increased from 0.2 MPa to 2.0 MPa, the cohesiveness and angle of internal friction increased by almost 40% and 30%, respectively. According to the authors, the CPB showed strain-hardening behaviour at high confining pressure, indicating that it may withstand large deformation before failing (Araújo et al., 2017). Moreover, there is no linear correlation between the cement concentration and the mechanical shear characteristics of CPB-rock specimens. In other words, increasing the cement content may not result in a proportionate increase in strength after a certain point (Weilv et al.,

2021). This is because there is an ideal cement content that strikes a balance between the advantages of higher strength and the expense of using more cement. The strength of the CPB-rock specimens can also be impacted by the angle at which the CPB meets the rock surface. A rougher surface may result in more mechanical interlocking and higher shear strength (Weilv et al., 2021). An issue frequently arises in mining operations when groundwater has high sulphate concentrations, affecting CPB, a form of backfill material used in underground mining. Fang & Fall (2022) investigated that the shear properties of the interface between rock and cemented tailings were significantly impacted by sulphate attack. The interface's shear strength declined as the level of sulphate attack progressed, and the failure mode switched from cohesive to adhesive (Fang & Fall, 2022). It is noted that sulphate attack caused changes in the microstructure of the cemented tailings, weakening the link between the tailings and rock by forming crystals of ettringite and gypsum. In a study on the coupled effects of temperature and sulphate on the strength of CPB, Fall & Pokharel (2010) discovered that independent of the sulphate level, a greater curing temperature would result in higher CPB strength in the early stage. Fang & Fall (2018) illustrate that various studies have demonstrated that increased matric suction increases the shear strength and elastic modulus of porous media and the soil structure. It is found that higher matric suction is produced at the CPB-rock interface because of temperature-induced self-desiccation that raises the shear strength of the CPB material (Fang & Fall, 2018). It is shown that the shear strength, friction angle, cohesiveness, and interface failure morphology are significantly affected by the dryness or moisture of the rock surface. Under dry conditions, the shear strength of the CPB-Rock interface is more sensitive to the curing time, and the cohesiveness and friction angle both rise as the curing time increases. The study also demonstrated that a longer curing time is more beneficial to the durability of filled underground cavities under dry conditions (Fang & Fall, 2018).

2.6 Summary

A comprehensive understanding of a CPB's mechanical behaviour and properties in underground operation under different loading conditions and chemical composition is crucial for designing structures and predicting their performance. The study emphasises the interconnected relationship between cement hydration, pore water pressure, and mechanical properties of CPB, including its electrical resistivity as an indicator of compressive strength. The tensile behaviour of CPB in underground mining is a critical aspect that is often overlooked in research. Existing studies

primarily focus on concrete tensile behaviour, with limited attention given to CPB. Furthermore, research indicates that sulphate attack, curing time, cement content, tensile and shear characteristics have complex interactions that require a thorough understanding of these variables to guarantee CPB's stability and efficacy in mining applications. The assessment draws attention to the complexity of field loadings in underground mines, such as seismic activity, blasting activities, and vibrations caused by machinery that subject CPB to shear, tensile, and compressive stress. CPB's mechanical stability and strength are primarily determined by its composition, which is mainly made up of dewatered tailings, cement binders, and additives. The strength and stability of CPB may be impacted by internal sulphate attacks, which are a major concern when sulphate is present in mine tailings. Furthermore, research on the behaviour of CPB fractures under various loading scenarios is conducted in the literature, highlighting the significance of comprehending fracture behaviours in order to guarantee the dependability and safety of underground mines.

Despite extensive research on CPB's mechanical, compressive, tensile and shear behaviour, several gaps in understanding are identified. First of all, the effects of cement content, sulphate concentration, and loading rates on the fracture behaviour of CPB have not been thoroughly investigated. According to the review, previous research concentrated more on traditional geomechanical behaviours while ignoring the dynamic effects of varying cement and sulphate content as well as loading rates. Second, nothing is known about how loading rate affects fracture behaviour, particularly at different cement contents and sulphate concentrations. Finally, the review emphasises how crucial it is to look into how sulphate ions affect CPB in terms of fracture behaviour because sulphate concentration significantly impacts CPB's long-term performance in deep mining operations. The highlighted research gap and future research possibilities are related to the systematic investigation of CPB fracture behaviour under dynamic loading circumstances, taking into account the effects of cement content, sulphate concentration, and loading rates. Examining these variables may help optimise CPB formulations in specific mining situations and provide insightful information for real-world implementations in underground mining settings. A thorough examination of these features would broaden our comprehension of CPB's fracture behaviour and improve its application for ground support and safety assurance in deep mining activities.

Chapter 3 Experimental testing program

3.1 Introduction

CPB mixture comprised of tailings (70-85%), cement (3-7% wt.), and water (15-20%), which gives sufficient strength for backfilling purposes (Benzaazoua et al., 2004; Fall & Pokharel, 2010; Pokharel & Fall, 2013). CPB structure effectively maintains mine workers' safety, ensures the stability of underground structures serving as a secondary ground support pillar, reduces adverse environmental effects by decreasing the concentration of sulphide-bearing tailing on the earth's subsurface and adds economic value to the mining operation (Alainachi & Fall, 2021; Fang & Fall, 2019; W. Li & Fall, 2016; Kesimal et al., 2004). CPB has been widely adopted worldwide, particularly in Canada, to minimize the surface footprint of sulphide-rich tailing, which account for approximately 50-60% of surface tailing waste deposits. It serves as the best alternative for controlling the problem associated with acid mine drainage and provides secondary support to extract available ore reserves from the mine (Cui & Fall, 2020; Ghirian & Fall, 2015; Hustrulid et al., 2001). Several research has been conducted to characterize the factor affecting the compressive strength behaviour of CPB (Fang et al., 2021; Komurlu et al., 2016; Fall et al., 2010; Yilmaz et al., 2003). Research on the tensile properties, cement and sulphide concentration, and CPB fracture behaviour is quite limited (Fall et al., 2010; Fang et al., 2021). As a cementitious composite, the tensile fracture resistance plays a crucial role in the stability of CPB structures in many cases (Chhorn et al., 2018; Jaber et al., 2018). Prior research, however, mainly concentrated on conventional geomechanical behaviours and disregarded the impact of loading rate on CPB's fracture behaviour and properties. This oversight significantly impacts the assessment of CPB's mechanical performance and behaviour inside mining stopes. No studies have been found to systematically investigate the loading rate-dependent fracture behaviour and properties of CPB under mode-I (tensile stress), mode-II (in-plane shear stress), and mode-III (out-of-plane shear stress) loading conditions, considering various cement and sulphate concentrations. Therefore, it is vital to experimentally investigate how the cement and sulphate concentration affects the loading-rate-dependent fracture behaviour of CPB. The purpose of this study is to conduct experimental investigations to determine how changes in cement content (2 wt.%, 4.5 wt.%, and 7 wt.%) and sulphate concentration (5000 ppm, 15000 ppm, and 25000 ppm) that affect the fracture behaviour of CPB under various loading rates (0.2 mm/min, 1 mm/min, 5 mm/min, and 10 mm/min)

and to determine the fracture response and fracture properties, including stiffness, fracture toughness, and work of crack initiation. Meanwhile, the volumetric water content (VWC), electrical conductivity (EC) and matric suction through mould base monitoring are utilized to understand the mechanisms behind CPB's fracture behaviour and properties. Additionally, scanning electron microscope (SEM) observation to understand the mechanisms of microstructural development in the CPB matrix. This research work and obtained findings will have the potentials to promote our understanding of CPB's fracture behaviour by offering new insights into how CPB reacts to changing loading events.

3.2 Materials

3.2.1 Tailings

Ground tailings (silica) were mainly made up of silicon dioxide SiO_2 (99.7%), with only trace levels of aluminium oxide (0.17%) and iron oxide (0.035%), as shown in Table 3.1. The physical properties of the tailings, particularly their particle size distribution as shown in Figure 3.1, were interrelated to the averaged qualities of hard rock Canadian mines, allowing for better uniformity and comparability in investigating the effects and characteristics of tailings (Fall & Pokharel, 2010). Particle size distribution parameters for quartz tailings such as D_{10} (1.87 μm), D_{30} (8.47 μm), D_{60} (25.67 μm), C_u (13.72), and C_c (1.50) offer essential details regarding the range and properties of the particle sizes. According to these criteria, 10% of the particles have a diameter of less than 1.87 μm, 30% less than 8.47 μm, and 60% less than 25.67 μm. The coefficient of uniformity (C_u) value suggests a wide range of particle sizes. However, the curvature coefficient (Cc) value indicates a somewhat skewed distribution. These variables make it easier to characterize and consider potential uses for the quartz tailings by helping to comprehend their size distribution and homogeneity. These synthetic tailings were convenient, cost-effective, and easy to use, and they reduced the uncertainties associated with natural tailing due to oxidation of other components.

Table 3.1 Chemical composition of quartz tailing.

Compound – (%) content	Compound – (%) content
SiO_2 – 99.70	CaO – 0.02
Al_2O_3 – 0.17	Na_2O – 0.01
Fe_2O_3 – 0.035	K_2O – 0.02
FeO – 0.024	TiO_2 – 0.02
MgO – 0.01	P_2O_5 – 0.01

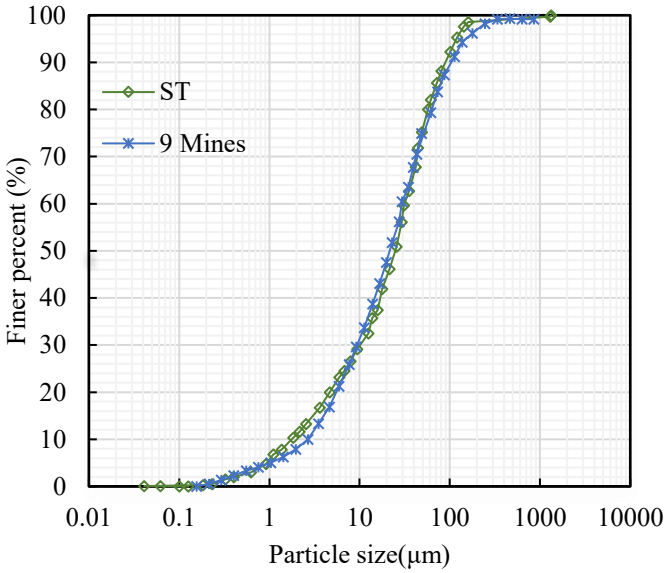

Figure 3.1. Particle size distribution of silica tailing (ST: silica tailings).

3.2.2 Cement

Portland cement (CSA Type GU) is being used as the binder in this study to examine the impact of cement content on the fracture toughness of CPB-related structures (Sheshpari, 2015; Tariq & Yanful, 2013). The water-to-cement ratios (w/c) of samples with cement contents of 2 wt.%, 4.5 wt.%, and 7 wt.% (wt.%: weight percentage measured with reference to the total weight of solid materials, including tailings and cement). The primary cement components, as listed in Table 3.2, are crucial in defining the overall composition and characteristics of the cementitious matrix.

Table 3.2. Chemical composition and relative density of cement.

Elements	CaO	SiO_2	Al_2O_3	MgO	Fe_2O_3	SO_3	K_2O
Content (wt.%)	62.86	18.03	4.53	2.65	2.70	3.82	0.819

3.2.3 Water and sulphate solution

This research combined tap water with a precise amount of ferrous sulphate heptahydrate ($FeSO_4.7H_2O$). The water-to-cement ratio (w/c) used in the study was 0.36, meaning that 0.36 water units were added for every cement unit. The study investigated sulphate concentrations of 5000 ppm, 15000 ppm, and 25000 ppm. As we know, underground stopes frequently include sulphate-rich mine water, up to 2000 mg/L concentrations (Kinnunen, 2018; Walker et al., 2015). Fall & Benzaazoua (2005) illustrated that the oxidation of sulphides present in tailings from polymetallic mines like (FeS_2, ZnS, $CuFeS_2$ and PbS) is the primary source of sulphate in CPB. Sulphide concentration on these tailings ranges from 2% to 60%, with Pyrite (FeS_2) being the primary mineral content. Other sources of sulphate include the cyanide oxidation process in the presence of sulphur dioxide and air from gold mine tailing; the addition of gypsum or anhydrite accelerates early strength development and sulphate accumulation in mill tailing and mine water (Xu et al., 2020; Sheshpari, 2015; Fall & Benzaazoua, 2005b; Akcil, 2003)

3.3 Mix proportions and specimen preparation

This study aims to evaluate the influence of loading rate (0.2 mm/min, 1 mm/min, 5 mm/min, and 10mm/min) on the characteristics and performance of the CPB specimens after various curing times by altering the cement content (2 wt.%, 4.5 wt.%, and 7 wt.%) and sulphate concentration (5000 ppm, 15000 ppm, and 25000 ppm) while keeping a constant water-to-cement ratio of 0.36. A curing period of 7 days, 28 days, and 90 days is employed to evaluate the early-age and long-term effects on the specimens' properties, such as stiffness, fracture toughness, and fracture energy needed for crack propagation.

Table 3.3. Summary of mix recipe, curing times, and loading rates.

Chemical Factor	Group	Water to tailings ratio	Cc (wt.%)	Sc (ppm)	Loading rate (mm/min)	Curing time (days)
Cement content	A1-0	0.36	2	0	0.2, 1, 5, and 10	7, 28, and 90
	B1-0	0.36	4.5	0	0.2, 1, 5, and 10	7, 28, and 90
	C1-0	0.36	7	0	0.2, 1, 5, and 10	7, 28, and 90
sulphate concentration	D1-0	0.36	4.5	5,000	0.2, 1, 5, and 10	7, 28, and 90
	E1-0	0.36	4.5	15,000	0.2, 1, 5, and 10	7, 28, and 90
	F1-0	0.36	4.5	25,000	0.2, 1, 5, and 10	7, 28, and 90

Note: Cc: cement content; Sc: sulphate concentration

3.4 Mechanical testing program

3.4.1 Semicircular bend (SCB) test

A hydraulic air hose was used to withdraw the sample from cylindrical mould once the curing process has reached predetermined times. The specimens were then cut to sizes and shaped using a BOSCH Mitre Saw with a diamond masonry blade. At least 1 cm is removed from either side of the CPB (20 cm × 10 cm) cylinder to ensure consistency between samples. The cylinders were subsequently split into three discs, each with a thickness of 5 cm. Each circular dish was split in half by placing in a specially designed wooden frame where the vertical notch was introduced on the spliced semi-circular dish. In the mode I Semi-Circular Bend (SCB) test, the loading point was exactly beneath a 25 mm deep vertical notch as shown in Figure 3.2 (a-b). This arrangement sought to evaluate the material's response to mode I fracture, which entails opening the notch in tension. A custom-made base with rolling supports was utilized to hold the specimens during the tests that are set at 8.13 cm difference to meet rock mechanics standards as shown in Figure 3.2 (a-b). Similarly for Mode-II Semi-Circular Bend (SCB) test, samples with cylindrical mould were separated and split into three circular discs of 5 cm thickness. Each circular dish was divided in half using a specially crafted wooden frame, thereby introducing a 54-degree pre-notch of 25 mm length from the center of the resulting semicircular dish as shown in Figure 3.2 (c-d).The

choice of the precise pre-notch angle is based on earlier research, which shows that mode II loading can be accomplished by altering the notch length ratio (a/R) and the half span-to-radius ratio (S/R) within a range of notch inclinations between 26.5 and 63 degrees (Ayatollahi & Aliha, 2006; Kuruppu & Chong, 2012; Mahanta et al., 2017). Similarly, the International Society for Rock Mechanics (ISRM) suggests semicircular bend (SCB) as the testing strategy for examining the fracture behaviour in geomaterials due to its simple setup, effective utilization of testing materials, and a high degree of repeatability (Kuruppu et al., 2014; Obara et al., 2009).

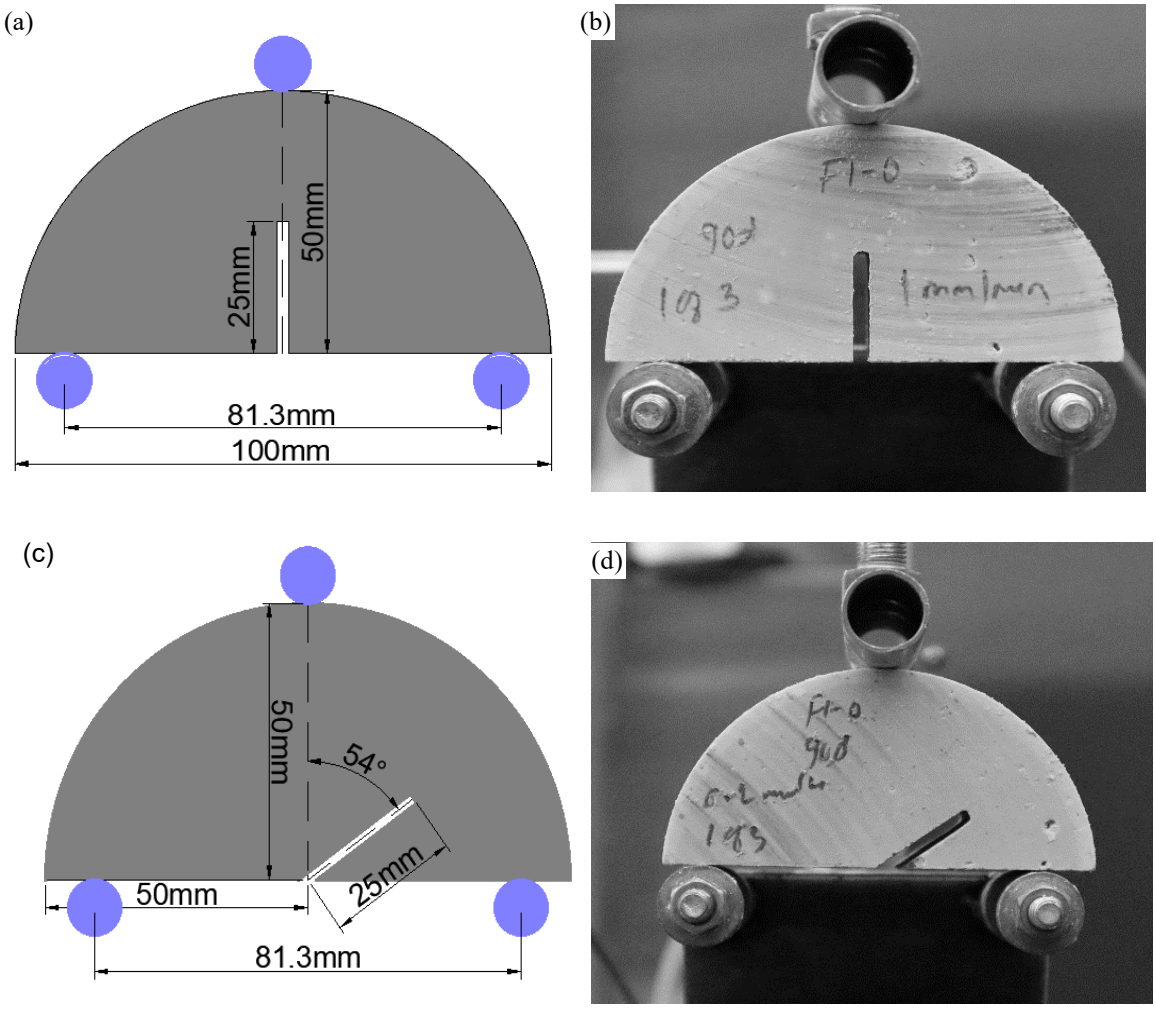

Figure 3.2. Experimental setup for CPB samples under Mode-I (a-b) and Mode-II (d-c) SCB test.

The experimental design featured a Digital Tritest-50 machine with a 5-ton capacity, a Load Cell with a 1000-pound capacity, and a 25 mm Linear Variable Differential Transformer (LVDT)

displacement sensor. The Smart Strain Data Acquisition program was used to integrate these components. The loading rate was changed by toggling the Tritest-50 digital keypad. Three repeated experiments were performed for each loading rate to assure accurate results, for a total of 216 tests for each mode is carried throughout the experimental work. The loading rate used in SCB testing has varied across standards and past studies. The International Society of Rock Mechanics (ISRM) suggests a loading rate of 0.2 mm/min to mitigate dynamic effects, while ASTM D8044-16 recommends a 0.5 mm/min rate. Conversely, the EN 126697-44:2010 standard suggests a loading rate of 5 mm/min, and AASHTO TP124-18 specifies a higher rate of 50 mm/min for SCB testing on asphalt material (Lu et al., 2021). To determine the effect of loading rate on the development of fracture toughness in our study, the loading rate of 0.2 mm/min, 1 mm/min, 5 mm/min, and 10 mm/min is employed.

3.4.2 Edge-notched disc bend (ENDB) test

In order to analyze mode-III fracture behaviour in CPB sample, the ENDB test is employed. The cylindrical sample is divided into three circular samples at a thickness of 5 cm by cutting via the diamond masonry blade of 1.5 mm width as shown in Figure 3.3. Then, at a 60-degree angle to the loading bar, a 2 cm deep notch (width = 2 mm) is made along the circumferential edge of each disc sample as shown in Figure 3.3. In order to study mode-III (out of plane) fracture behaviour, several test configurations have been proposed, including the inclined edge cracked three-point bend beam, circumferentially notched shaft samples under torsion, compact tension shear rotation specimen, edge-cracked plate loading fixture, and edge-notched disc bend (ENDB) test (Aliha et al., 2015; Ayatollahi & Saboori, 2015; Richard et al., 2014). In earlier research, ENDB tests on building materials have been performed at loading rates ranging from 0.05 mm/min to 5 mm/min (Aliha et al., 2015; Hua et al., 2022). In this study, ENDB tests at 0.2 mm/min, 1 mm/min, 5 mm/min, and 10 mm/min loading rates are performed which are alike to the loading rate of the semicircular bend (SCB) test. The selected loading rates are analogous to the various experiments conducted on construction materials. Furthermore, 216 ENDB test samples were prepared, and three replicate tests were run on each loading rate.

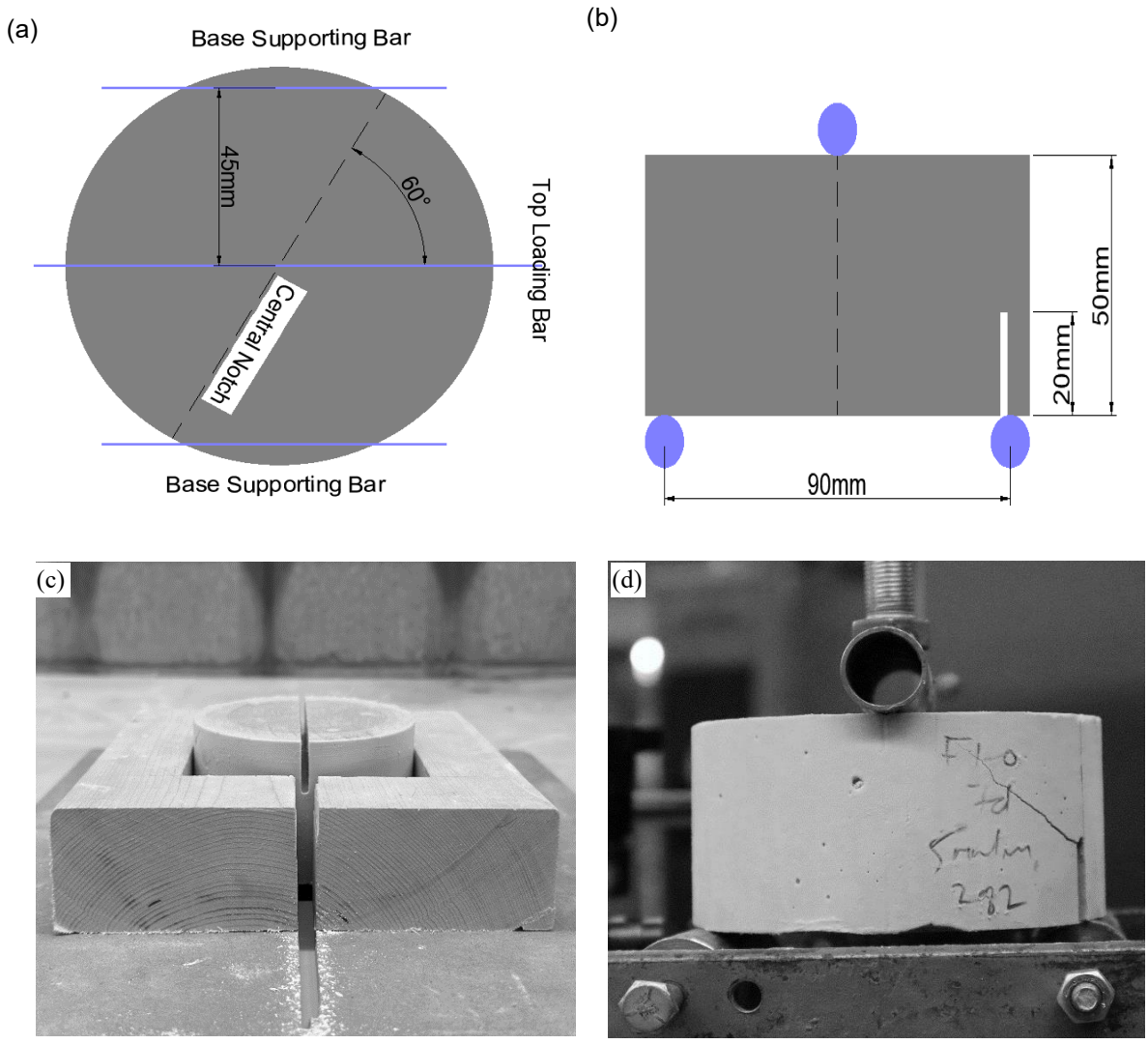

Figure 3.3. CPB samples under mode-II SCB tests.

3.4.3 Determination of fracture properties of CPB

Fracture toughness is a broad material attribute, the values vary according to the specimen sizes used and applied stress to size and shape of crack. The stress intensity factor measures the level of tension at the crack's tip, a crucial aspect in determining how susceptible the material is to crack. A normalized stress intensity factor for each type of fracture (for example, mode I, mode II, and mode III) relates the fracture toughness to the variation in tests for each type of fracture mode. It is critical in underground mines to examine the fracture properties of CPB to provide effective ground support for the surrounding rock. The fracture properties like fracture toughness, material stiffness, and energy of crack initiation of backfill are essential to be analyzed. Fracture toughness is a critical component in determining fracture initiation in CPB. It denotes the critical stress

intensity factor required for crack initiation. The fracture toughness values (K_{IC}, K_{IIC} and K_{IIIC}) of CPB under mode-I, mode-II and mode-III loading conditions are calculated using the peak load obtained in the load-displacement curve. Mathematical calculations incorporate elements such as force, sample size, and the normalized stress intensity factor, along with the initial crack angles. The peak load (P) is employed in the following formulae to determine the fracture toughness values of CPB for mode I, mode II and mode III loading conditions:

$$K_{IC} = \frac{P}{DT}\sqrt{\pi a}Y_I \tag{3.1}$$

$$K_{IIC} = \frac{P\sqrt{\pi a}\,Y_{II}}{2RT}\left(\frac{a}{R}, \frac{S}{R}, \alpha\right) \tag{3.2}$$

$$K_{IIIC} = \frac{6PS\sqrt{\pi a}\,Y_{III}}{RB\text{^}2}\left(\frac{a}{B}, \frac{S}{R}, \beta\right) \tag{3.3}$$

Where,

- P: Maximum force applied (in N)
- R: Radius of the disc-shaped sample (in meters)
- T: Thickness of the SCB (Semicircular Bend) sample (in meters)
- B: Thickness of the ENDB (End-Notched Flexure Beam) sample (in meters)
- a: Length of the notch (in meters)
- α: Initial crack angle under SCB test (in degrees)
- β: Initial crack angle under ENDB test (in degrees)
- S: Half-span length (in meters)
- Y_I: Normalized stress intensity factor under mode-I fracture toughness, Y_I =6.52 at a= 0.025 m, D = 0.10 m T = 0.05 m Y_I = 6.52
- Y_{II}: Normalized stress intensity factor for mode-II fracture toughness, Y_{II} = 1.072 at α = 54°, for SCB tests with a/R = 0.5 and S/R = 0.8
- Y_{III}: Normalized stress intensity factor for mode-III fracture toughness, Y_{III} = 0.0713 at β = 60°, for ENDB tests with a/B = 0.4, S/R = 0.9

Understanding a material's stiffness is critical for engineering applications since it directly affects its capacity to withstand deformation and maintain its shape under diverse conditions. This

calculation is critical for anticipating material behaviour during design procedures and guaranteeing structural integrity. The measurement of material stiffness via load-displacement curve is a standard technique. The behaviour of a material can be determined well by employing a load and measuring the displacement that takes place. The relationship between applied load and displacement is represented by the load-displacement curve, which offers crucial insight into the behaviour of the material. The linear elastic area of the load-displacement curve is examined in this study to determine the stiffness of the material. The linear area is the range in which the material behaves elastically, deforming in proportion to the applied stress but not permanently. Usually, the curve's first component is detected in this region. In this study, the linear region between the peak load displacement's 45% and 55% marks is specifically chosen for analysis. This selection is shown in Figure 3.4. To calculate the material stiffness (k_m), the load-displacement data is utilized. Displacement values, D_{45} and D_{55}, corresponding to the 45% and 55% marks, respectively, are determined. These displacement measurements, along with the peak load (Fp), are used in the formula to estimate the material stiffness as

$$k_m = \frac{55\%F_p - 45\%F_p}{D_{55} - D_{45}} \tag{3.4}$$

Even though fracture toughness aids in crack initiation assessment, it does not explicitly look at the energy dissipation brought on by deformation due to tremendous geo-stress; rock walls in deep underground mines converge. Thus, the area under the load-displacement curves up to the peak load, as shown in Figure 3.4 (b), is calculated to derive the energy of crack initiation (Fracture Work) (E_c), which is used to assess fracture growth in CPB under finite deformation.

The Fracture work (E_c) is determined by the formula as shown.

$$E_c = \frac{(F_1 + F_2)}{2}(D_1 - D_2) \tag{3.5}$$

Where,

F1 and F2 are loads,

D1 and D2 are displacements.

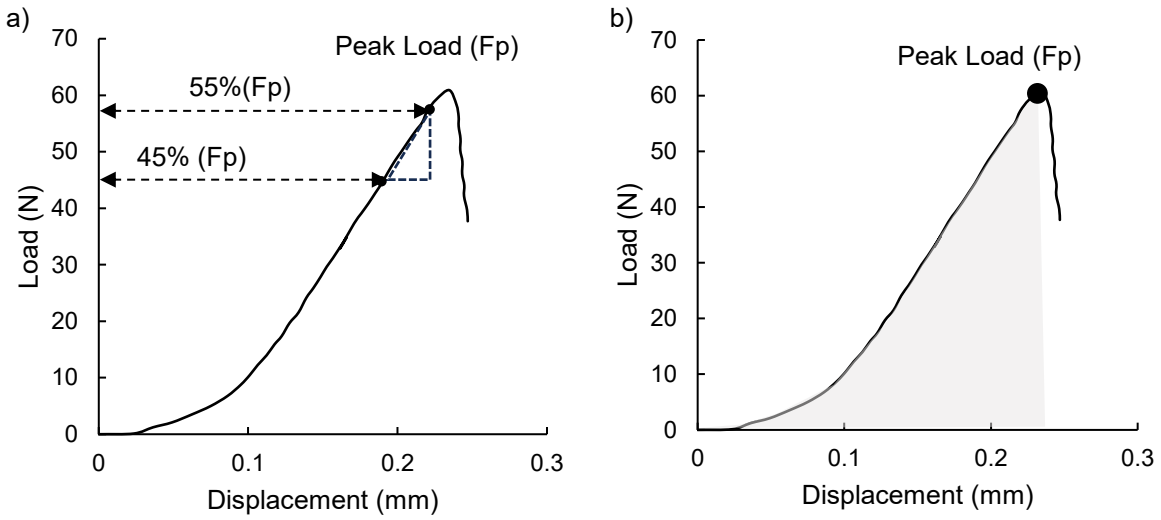

Figure 3.4. Definition of fracture properties of CPB: (a) stiffness and (b) energy of crack initiation.

3.5 Auxiliary analysis

3.5.1 Scanning electron microscope (SEM) analysis

The Hitachi SU-70 scanning electron microscope (SEM) with a high resolution of up to 1nm is used to analyze the microstructure evolution of CPB material. The samples go through careful preparation prior to scanning. In order to ensure that all moisture associated with the CPB matrix is removed, they are first oven-dried for 48 hours at 45°C. The samples are subsequently sealed within a plastic bag to prevent potential moisture absorption. A thin CPB sample is chipped off into a 5 mm-diameter to the thickness of 2 mm segment for observation purposes, which is then firmly fixed on a stand or holder to provide stability throughout the scanning procedure. The sample then gets coated in a thin layer of gold to improve image quality and electron reflectivity. After sample preparation, the coated specimens are put into the vacuum chamber of the Hitachi SU-70 SEM. The SEM investigates the sample's surface using a highly focused electron beam to provide fine photographs of its microstructure. Identifying hydration products and monitoring microstructural changes over time are made possible by this SEM visual imagery, which offers essential insights into the material under study.

3.5.2 Measurement of matric suction, volumetric water content, and electrical conductivity

The mould-based monitoring program aims to measure electrical conductivity (EC), volumetric water content (VWC) and matric suction to evaluate the behaviour of CPB specimens with

different cement contents and sulphate concentrations over 7, 28 and 90 days. A cylindrical specimen (10 cm × 20 cm) with the 5TE sensor (to measure VWC, and EC), and T5X tensiometer (to matric suction) are measured as part of the monitoring procedure where these sensors are connected to a data logger (ZL6) and computer as shown in Figure 3.5. Understanding the specimen's load-displacement behaviour and fracture characteristics under uniform curing conditions depends on these measurements. The VWC measurements reveal the water content of the material. Changes in water content can considerably impact the interparticle friction inside the material.

Due to water's lubricating properties, the interparticle friction decreases as the water content rises. Consequently, there is also a reduction in the resistance to crack propagation. In contrast, interparticle friction rises as the water content drops, improving crack resistance. Therefore, monitoring VWC aids in evaluating changes in water content, which affect a material's ability to resist crack propagation (Fang et al., 2021). Matrix suction, on the other hand, refers to the negative pressure or tension present inside the CPB matrix. It indicates the level of internal drying resulting from cement hydration, known as self-desiccation. The amount of water and solids in the mixture is reduced due to the cement's consumption of some water throughout the reaction process. As a result of this reduction, the substance develops suction. The apparent cohesion of the cemented material could be improved by increased matric suction. The term "cohesion" describes particles' internal cohesiveness or connection where the dried and more compact material results from decreased water content as the matric suction rises. As a result of stronger links between particles being formed in this drier state, the material is more cohesive.

Consequently, the substance exhibits better structural integrity and crack resistance (Fang & Fall, 2018). Monitoring the EC is essential for tracking structural changes in hydrating cementitious materials and evaluating the development of cement hydration. EC measurements give information about the rate of ion movement, which is closely linked to chemical processes and the amount of water in the material. The ion movement is a sign of these changes, and tracking the EC values provides helpful information on how cement hydration and microstructural evolution are developing. The critical point at which the EC value reaches its maximum value tells us how quickly cement hydrates. This peak reflects the most active stage of cement hydration and corresponds to the point where the creation rate of ions reaches its maximum. As hydration

proceeds, ions are consumed faster than they are produced, which causes the EC values to drop (Courard et al., 2014).

Figure 3.5. Mould Base Monitoring Program (A) a 5TE sensor measuring moisture, temperature, and electrical conductivity, (B) a TEROS 21 sensor measuring water potential and temperature, (C) a data logger identified as ZL6, (D) the process of data collection, and (E) the test samples.

Chapter 4 Experimental testing results

4.1 Loading rate dependent fracture behaviour of CPB

4.1.1 Effect of cement content on the loading-rate dependent fracture behaviour of CPB under mode-I loading

Figure 4.1 shows the effect of cement content on mode-I fracture behaviour of CPB at different loading rates. The load-displacement curves for CPB specimens with varying loading rates (0.2, 1, 5, 10 mm/min), cement contents (2, 4.5, and 7 wt.%) represented as group A1-0, B1-0 and C1-0 respectively, at curing durations (7, 28, and 90 days). The load-displacement curves indisputably demonstrate that the rise in loading rate increases linearly with displacement until reaching a fracture, irrespective of the curing period and cement content. The pre-peak response of CPB materials is denoted by the linear relationship between load displacement before the peak load. It suggests that the principles of linear elastic fracture mechanics (LEFM) can be used to describe the fracture behaviour of CPB (Cui, 2023)**.** Thus, it is crucial to thoroughly examine the performance of materials from early to advanced age to comprehend the fracture behaviour of CPB materials. The load-displacement curves for 7 days sample are shown in 4.1 It is noticeable that the maximum force changes as the loading rate increases. Furthermore, samples that can withstand larger loads exhibit significantly shorter displacements before failure. For instance, in group A1-0 7d, the peak at 10mm/min loading rate reached 0.37 mm while it took 0.61 mm displacement to attain peak value at 0.2 mm/min. The improvement of displacement to achieve the peak load can be observed by comparing the early-day CPB of groups A1-0, B1-0 and C1-0. In earlier days, CPB at a higher loading rate, irrespective of Cc and curing time, shows higher stiffness. As a result, the stress intensity factor takes less time to attain mode I fracture toughness. The peak load rises from 24.83 kPa on the 7^{th} day to 32.83 kPa on the 28th day and 56.40 kPa at 90 days under the 10 mm/min loading rate for group A1-0. The percentage increment of peak load for group A1-0 from 28 days to 90 days at 0.2, 1, 5 and 10 mm/min is 71%, 71%, 80% and 71%, respectively. In Figure 4.1b, group B1-0 CPB specimen with the change in loading rate and curing time we can see the intermediate development in peak load, which follows the same trend as group A1-0. The percentage increment with change in loading rate for a group C1-0 at 7-day is 9%, 2%, and 12%

for 0.2 to 10 mm/min. Likewise, the increase in peak load for C1-0 at 90 days is41%, 31% and 7% wrt 0.2mm/min loading rate. Thus, the increment in peak load is time-dependent and sensitive to the loading rate, however the advanced age CPB shows a reducing trend.

The evolution of mode-I fracture behaviour induced by the variation of cement content can be interpreted by the progression of cement hydration in CPB matrix. The CPB matrix produces additional hydration products such as calcium hydroxide (CH) and calcium silicate hydrate (C-S-H) when there is a higher curing time and Cc. As cement hydration products build up over time, the pore structure gets refined, reducing porosity and counteracting the wall effect (Fang & Fall, 2020). These hydration products help the CPB matrix to become more cohesive, improving its bonding strength to withstand crack propagation and raising its peak load. At the lower loading rate viscous effect dominates fracture behaviour, while at a higher loading rate inertia effect is prominent. The interaction between water in voids and porous matrix at a lower loading rate slightly decreases its peak load due to its viscous effect. While at a higher loading rate, the inertia effect becomes more pronounced, increasing the CPB effective stiffness and reducing the time available for crack propagation. The stress wave propagates rapidly through material particles developing higher stress at the crack tip, increasing the peak load. As a result, more energy is required to initiate the crack, increasing the fracture resistance with an increased loading rate (Zhang et al., 2009). The post-peak response of CPB steepens, indicating a decreased capacity for tolerating persistent deformation and development of material brittleness. This material's brittleness reflects its reduced capacity for plastic deformation and suggests that the CPB material becomes more brittle with a higher loading rate, as shown in Figure 4.1.

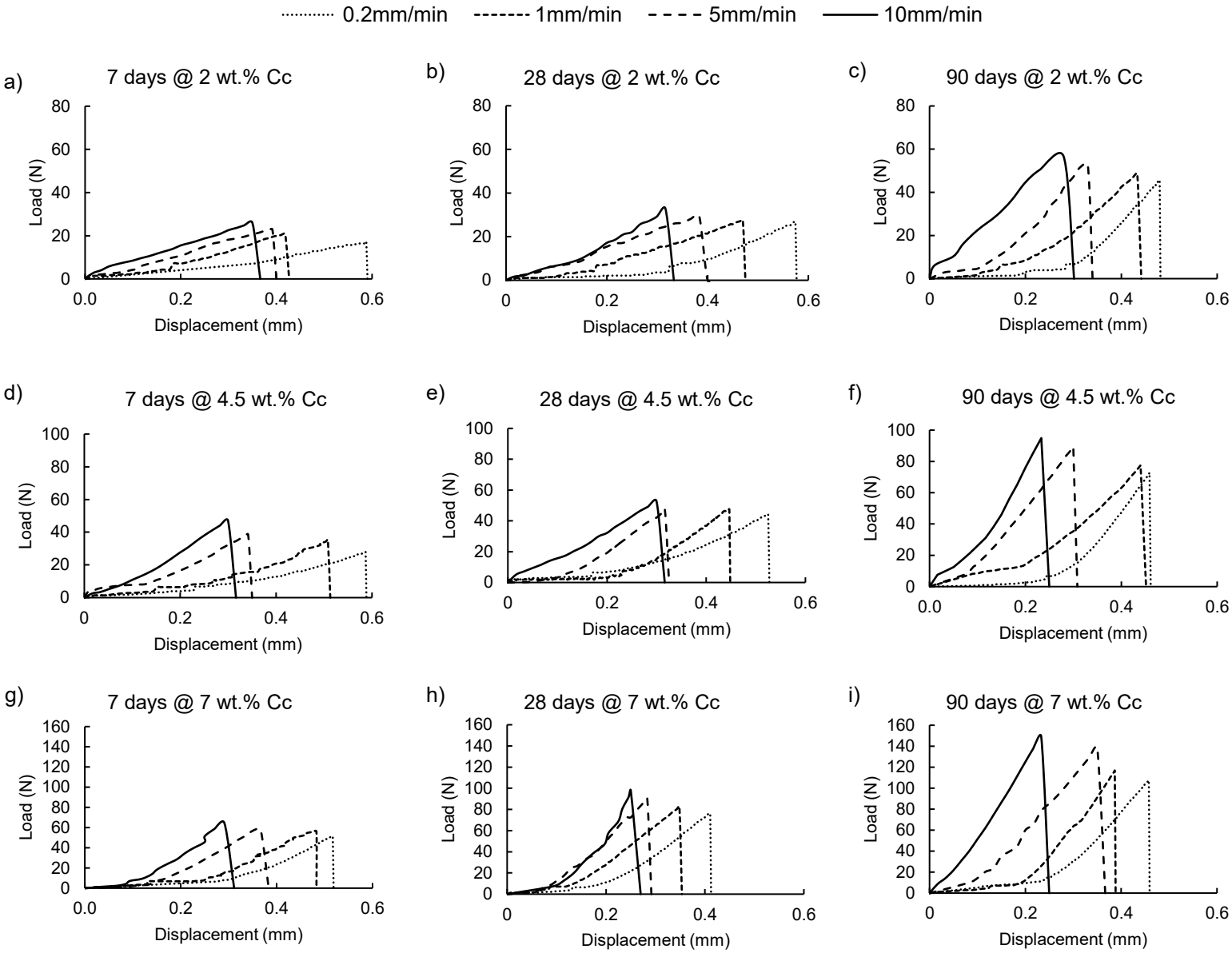

Figure 4.1. Effect of cement content on the loading-rate dependent fracture behaviour of CPB under mode -I loading.

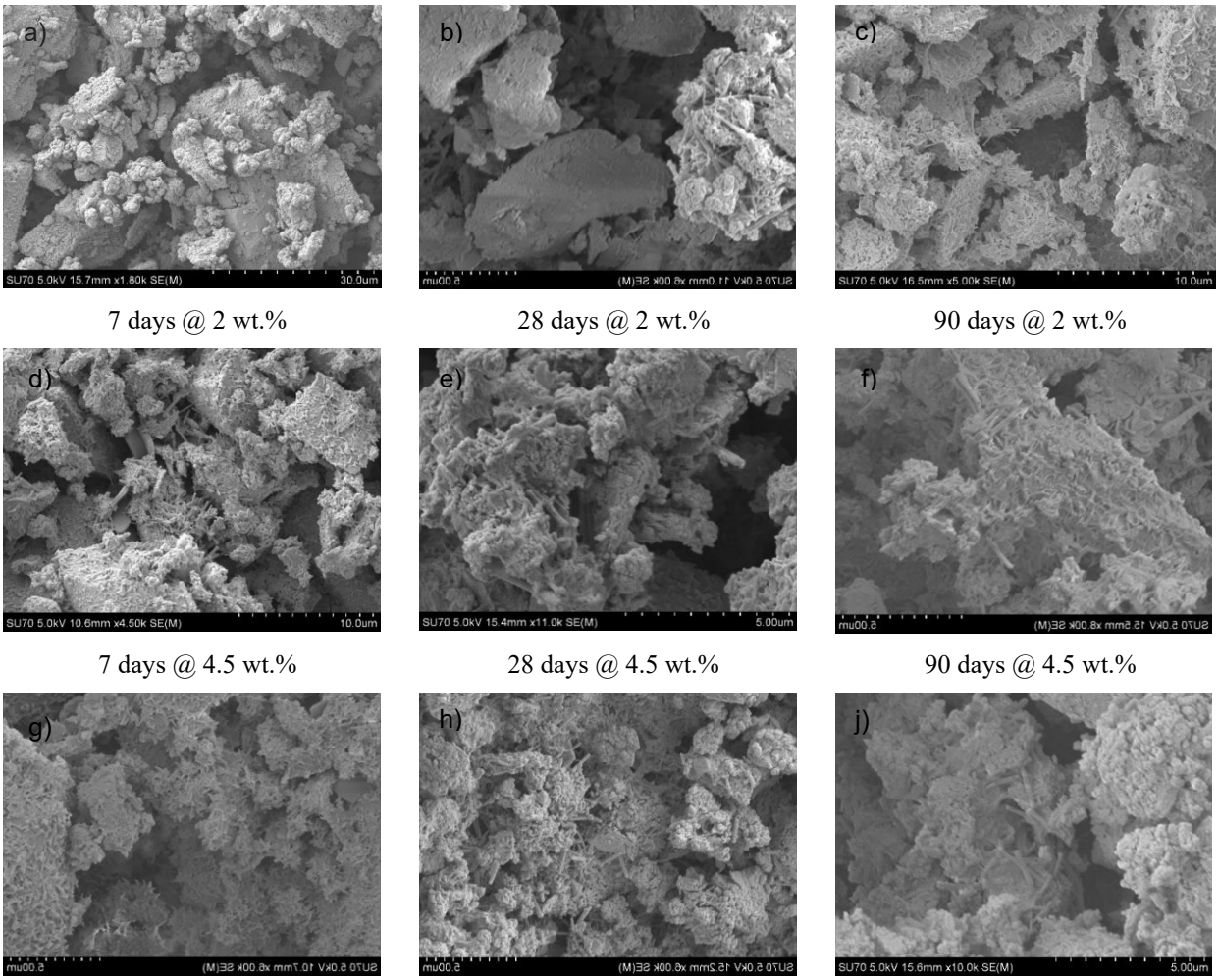

7 days @ 2 wt.% 28 days @ 2 wt.% 90 days @ 2 wt.%

7 days @ 4.5 wt.% 28 days @ 4.5 wt.% 90 days @ 4.5 wt.%

7 days @ 7 wt.% 28 days @ 7 wt.% 90 days @ 7 wt.%

Figure 4.2. SEM images for effect of cementt content on microstructural evolution of CPB: (a-c) 2 wt.%, (d-f) 4.5 wt.%, and (g-i) 7 wt.%.

The SEM images in 4.2a demonstrate that at a 7-day curing period, a sizeable amount of C-S-H and C-H is produced around the surface of tailing particles, varied with the increase in cement content. The SEM images of the samples after 7 days show that a rise in Cc leads to smaller pores and better self-desiccation effects. C-S-H is noticeable, whereas ettringite (AFt) crystals are dispersed randomly. From 4.2b, we can observed that the 28-day samples exhibit larger C-S-H amounts, more evenly spaced, smaller pores, and lower levels of free AFt. The C-S-H forms linkages between C-S-H clusters and encircles the AFt. With little AFt and CH in the 90-day samples, C-S-H dominated the microstructure as shown in Figure 4.2c. The pores in the C-S-H clusters are smaller and more evenly spaced. The 90-day samples show the greatest range of C-S-H cluster volumes between the CPB particles whille comparing between Cc at 2-7% wt.

Furthermore, the wall effect in the CPB can be formed by the size difference between the tailing particle and the cement hydration products (Fang & Fall, 2020a). A microstructure with significant porosity is produced due to this wall effect, which prevents cement grains from gathering and reduces strength at an early age. The early-age matric suction results 4.3 indicated the availability of more capillary water within the pore structure of the CPB matrix. This reduced matrix suction at an early age means less hydration product, which makes the specimen prone to fracture at a small load applied. Matric suction develops in CPB when transitioning from a fully saturated condition to a partially saturated state (Libos & Cui, 2020). The matric suction (i.e., a pressure gradient brought on by the presence of capillary water in a porous material) grew more intense with the increase in cement content and curing period. The rise in cement hydration consequently decreases the water content and increases self-desiccation, eventually leading to higher matric suction within the pores structure of CPB.

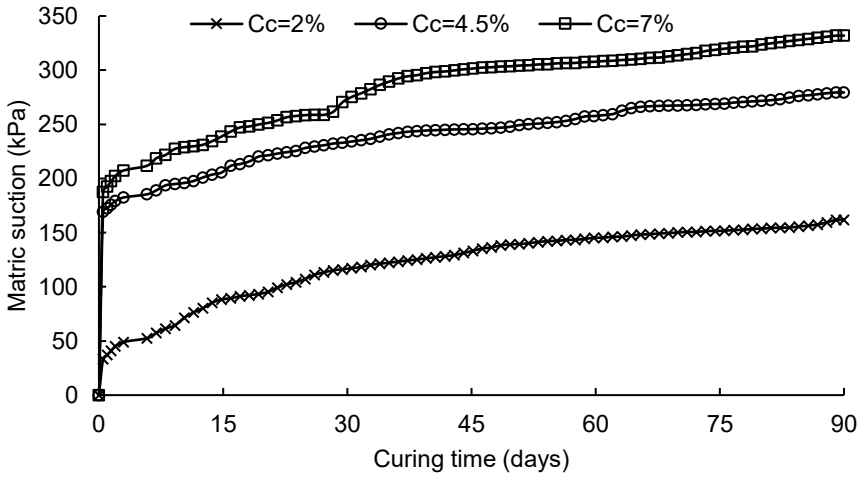

Figure 4.3. Effect of cement content on evolution of matric suction with curing time.

More hydration products, including C-S-H, CH, and ettringite, are formed as the CPB goes through the hydration process. These hydration products enable C-S-H to bind together by filling the pore structure between the particles. This eventually results in a larger peak load, as seen in Figure 4.2, and has two primary causes. First off, more C-S-H increases the binding force, increasing the adherence of the CPB material. As a result, the peak load and K_{IC} are increased. Furthermore, the precipitation of cement hydration products refines the pore structure, resulting in a finer capillary structure with CPB. A large amount of C-S-H is present at the interface, which is further confirmed by SEM images in Figure 4.2, and this amount only grows with increased curing time. The pore

structure is improved, porosity is decreased, and the wall effect is countered over time by the rising amount of cement hydration products.

4.1.2 Effect of sulphate concentration content on the loading-rate dependent fracture behaviour of CPB under mode-I loading

Figure 4.4 illustrates the effect of sulphate concentration on the load-displacement curve of CPB at various loading rates, curing time, and a constant cement content of 4.5 wt.%. After comparing the group B1-0 (0 ppm) with Sc sample of group D1-0 (5000 ppm), E1-0 (15000 ppm) and F1-0 (25000 ppm), it is observed that the sulphate-free sample exhibits the lowest peak load than that with Sc sample for all loading rate and curing time. The sulphate ion's presence promotes cement hydration to gain a higher peak load. However, the presence of sulphate has a significant effect during the hydration process, showing varied reactions and outcomes on the development of fracture behaviour of the CPB. The loading rate effect on the same curing period also increases with the rise in the loading rate. For example, in 4.4, the 7-day sample at 5000 ppm with 5 mm/min loading rate is 48.53N, which increased by 7% (52.07N) at 28-day and 143% (118.13N) at 90-day for the same loading conditions. The sample with 5000 ppm Sc at 7 days shows the highest peak load, followed by 15000 ppm and 25000 ppm for all loading rates. For instance, peak load at 10 mm/min loading rate is 50.25 N at 5000 ppm in 7 days, followed by 48.67 N and 43.93 N for 15000 ppm and 25000 ppm, respectively. The reduction in early age peak load can be explained by the tricalcium aluminate (C_3A) reaction, which gets hydrated when cement and water are combined. This is one of the main processes when sulphate ions are present, and they quickly react with C_3A to generate a substance known as ettringite (AFt). This reaction consumes the Ca^{2+} and decreases its availability to form the hydration products (Li & Fall, 2018). The un-hydrated cement particles then develop a thin layer of ettringite crystals around its surface as shown in Figure 4.5. These ettringite layers prevent water from reaching dicalcium silicate (C_2S) and tricalcium silicate (C_3S), slowing hydration by inhibition effect. Sulphates can interact with the calcium silicate hydrate (C-S-H) gel to produce calcium sulfoaluminate (CSA) compounds and other by-products (Fang & Fall, 2019). These by-products help coarsen the pore structure, resulting in more extensive and linked pores. A material's strength and overall durability are compromised by a coarser pore structure which affects the setting time and strength development at early age CPB (Yilmaz & Fall, 2017).

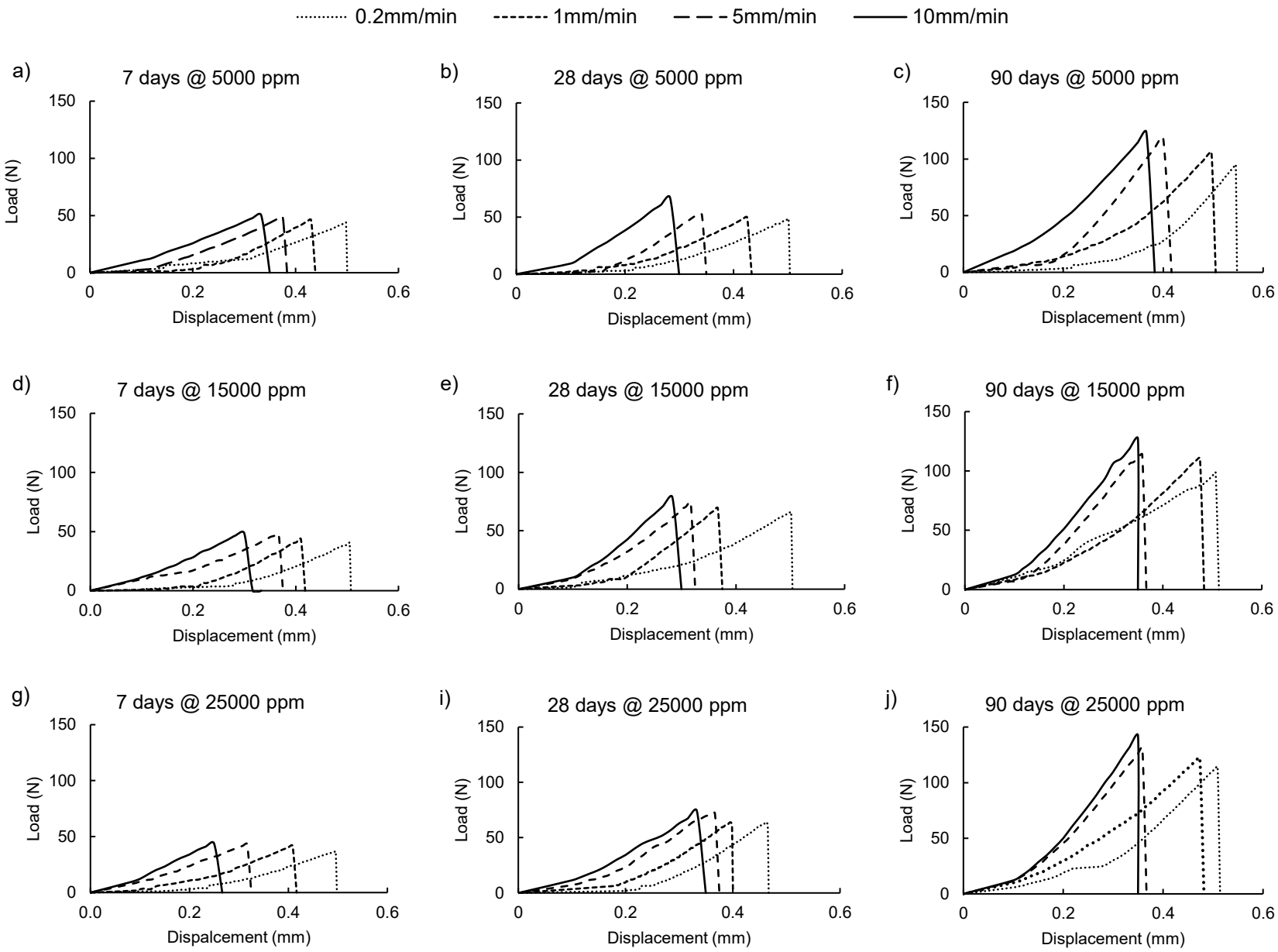

Figure 4.4. Effect of sulphate concentration on the loading-rate dependent fracture behaviour of CPB under mode -I loading condition.

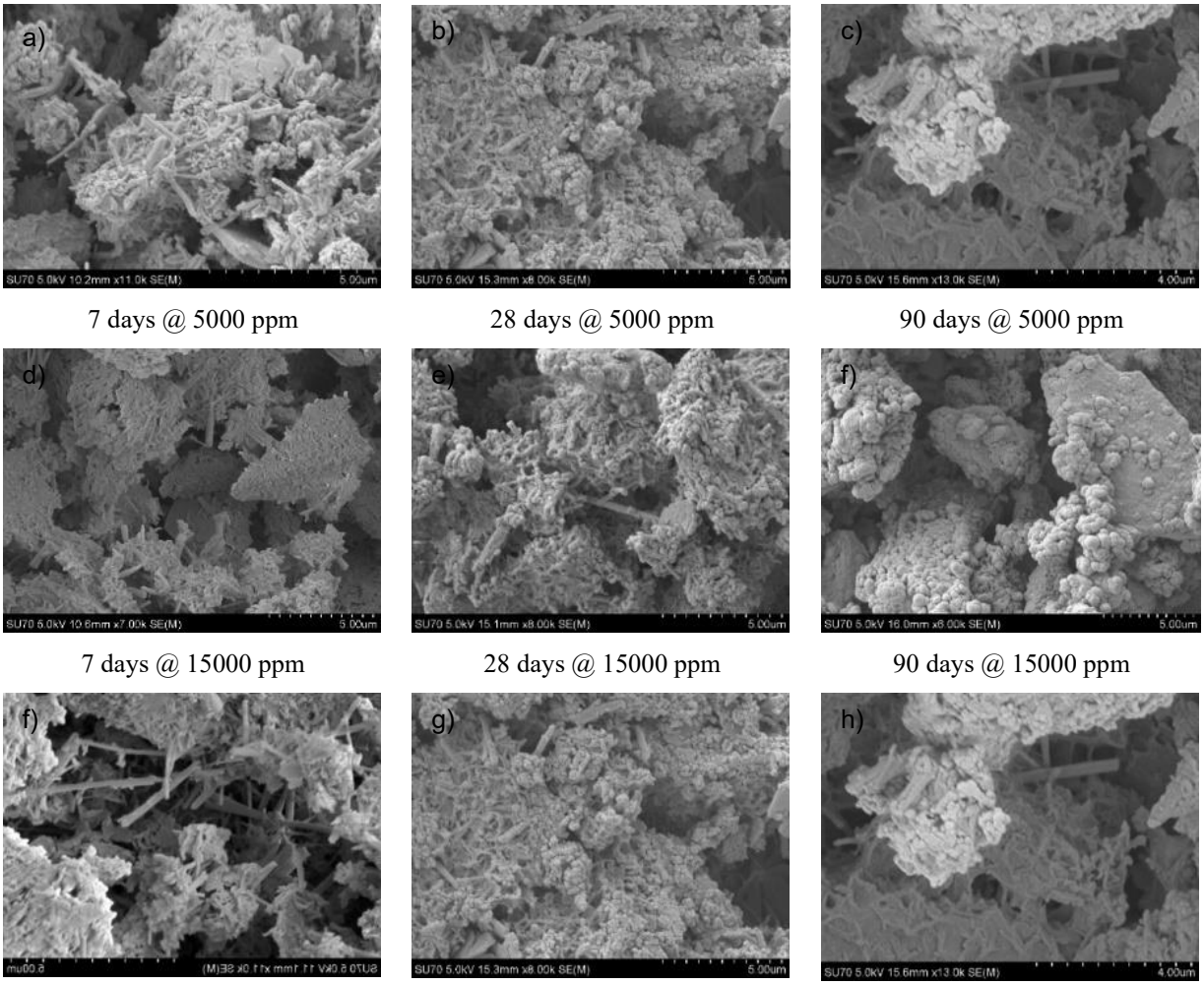

7 days @ 5000 ppm | 28 days @ 5000 ppm | 90 days @ 5000 ppm

7 days @ 15000 ppm | 28 days @ 15000 ppm | 90 days @ 15000 ppm

7 days @ 25000 ppm | 28 days @ 25000 ppm | 90 days @ 25000 ppm

Figure 4.5. SEM images for effect of sulphate concentration on microstructural evolution of CPB (a-c) 5000 ppm (d-f) 15000 ppm and (f-h) 25000 ppm.

During the early age, the sulphate concentration of 5000 ppm negatively impacts the suction development for up to 2.5 days of curing time. This shows that the 5000 ppm of sulphate first hampers the self-desiccation mechanism in the CPB. The sulphate concentration, however, begins to positively affect the CPB's suction development or self-desiccation after 2.5 days. From Figure 4.5, the outcomes further demonstrate that early ages sulphate concentrations of 15,000 ppm and 25,000 ppm took up to 4.5 days and 7.5 days to develop suction, significantly inhibiting the suction development in CPB. This unfavourable result is due to the sulphate ion that delays cement hydration (explained later in EC). Higher sulphate concentrations decrease the amount of pore water that CPB uses, lowering capillary pressure and preventing self-desiccation (Bentz, 2008). For instance, the sample reaches a suction value of 10.2,11.4 and 12.7 kPa after 28 days of curing and gradually increased with advanced age to reach 11.2, 12.4 and 14.1 kPa for 5000, 15000 and

15000 ppm Sc at 90 days. Thus, the development of suction in advanced age CPB helps to promote self-desiccation and thus pull the matrix to a greater extent, which definitely contributes to the improvement of matrix integrity and resistance to deformation and stress.

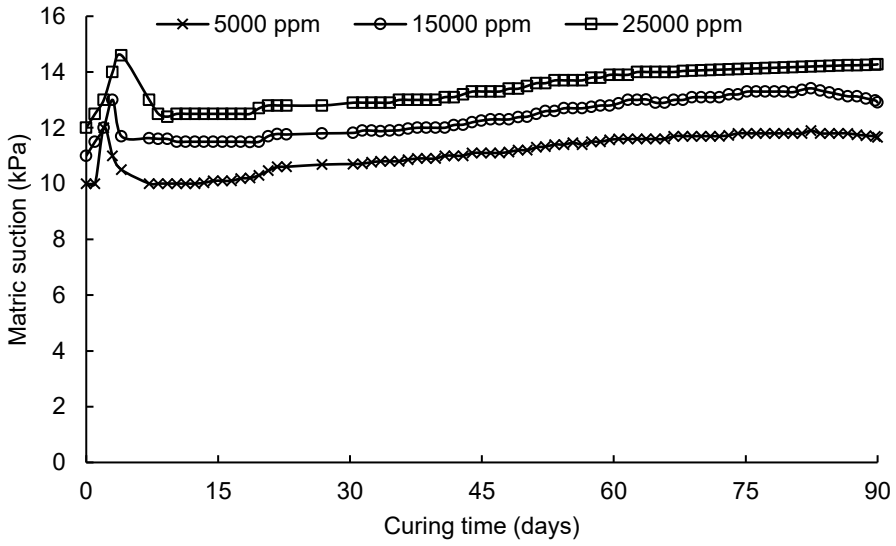

Figure 4.6. Effect of sulphate concentration on evolution of matric suction with curing time.

4.1.3 Effect of cement content on the loading-rate dependent fracture behaviour of CPB under mode-II loading

The mode-II fracture behaviour of CPB is influenced by various factors, including loading rate, cement content, and curing time. Figure 4.7 demonstrates that higher loading rates result in higher peak loads and stiffer material response under mode-II loading condition, leading to smaller displacements before failure. This effect is attributed to the stress intensity factor (SIF), which accelerates modes II fracture toughness and encourages rapid crack propagation. This experimental work brought attention to how loading rates affect CPB's viscoelastic behaviour (Ouattara et al., 2017). Higher peak loads, stiffer material response, and quicker crack propagation were all caused by increasing loading rates. The results highlight the importance of taking loading rates and the related parameters into account when figuring out and differentiating CPB's cracking behaviour. A total of four different loading rates 0.2 mm/m, 1 mm/min, 5 mm/min, and 10 mm/min were used for three groups of sample A1-0 (2 wt. % Cc), B1-0 (4.5 wt.% Cc) and C1-0 (7 wt.% Cc). It was found that higher loading rates resulted in stronger material responses, which accelerated pre-peak slope growth and sharply reduced post-peak slope. Increased stiffness, which

encourages rapid crack propagation, can be the cause of this behaviour (Lu et al., 2021). The A1-0, B1-0 and C1-0 sample group changing trends in peak load were consistent with the loading rates used. These results highlight the CPB's susceptibility to varying loading rates, which is essential for understanding CPB fracture behaviour under various loading rates.

Another significant factor affecting peak load in CPB is the degree of binder hydration. Over time, increased peak loads are attributed to greater binder hydration, resulting in increased density of calcium-silicate-hydrate (C-S-H) and enhanced capillary structure at the CPB-CPB interface. Higher cement content leads to the production of more hydration products such as C-S-H, calcium hydroxide (CH), and ettringite (Fall et al., 2010b). The concentration of C-S-H plays a crucial role in increasing peak load and fracture toughness in mode II by enhancing the bond between the CPB matrix. The main constituents of Portland cement such as tricalcium aluminate (C_3A), dicalcium silicate (C_2S), tricalcium silicate (C_3S), and tetracalcium aluminoferrite (C_4AF) react to form the hydration product. The first interaction of C3A with water increases the effective stress within the CPB due to the consumption of water. Secondly, the hydration of C_3S and C_4AF leads to the formation of calcium silicate hydrate (C-S-H) which mostly determines the CPB initial strength (Fang et al., 2021). Along with this, the hydration of C_2S, which is the slowest reaction, also contributes to the generation of C-S-H (Liu, Zhu, et al., 2019). Moreover, the hydration process involving C3A, C3S, and C4AF generates approximately 60-70% of the hydration products (L. Liu, Song, et al., 2019). In conclusion, the behaviour of CPB is significantly influenced by loading rates, cement content, and curing time. Higher loading rates result in stronger material responses and accelerated crack propagation. Increased cement content leads to greater binder hydration, which increases peak load and fracture toughness due to enhanced C-S-H concentration. The SEM images Figure 4.2 provide visual evidence of the increasing amount of C-S-H with higher cement content and longer curing time, indicating improved capillary structure within the CPB.

Over time, this migration process intensifies the binding attraction between the particles. The higher degree of cement hydration increases the water consumption from pores which lead to the rise in matric suction demonstrates how these events have an impact on the CPB microstructural development process. As shown in Figure 4.8, volumetric water content (VWC) decreases from 0.7 to 0.4 m^3/cm^3 while the matric suction increases from 169.3 kPa to 279.4 kPa for B1-0 (4.5 wt.% Cc) during the period of 90 days, showing that cement hydration is consuming water. In

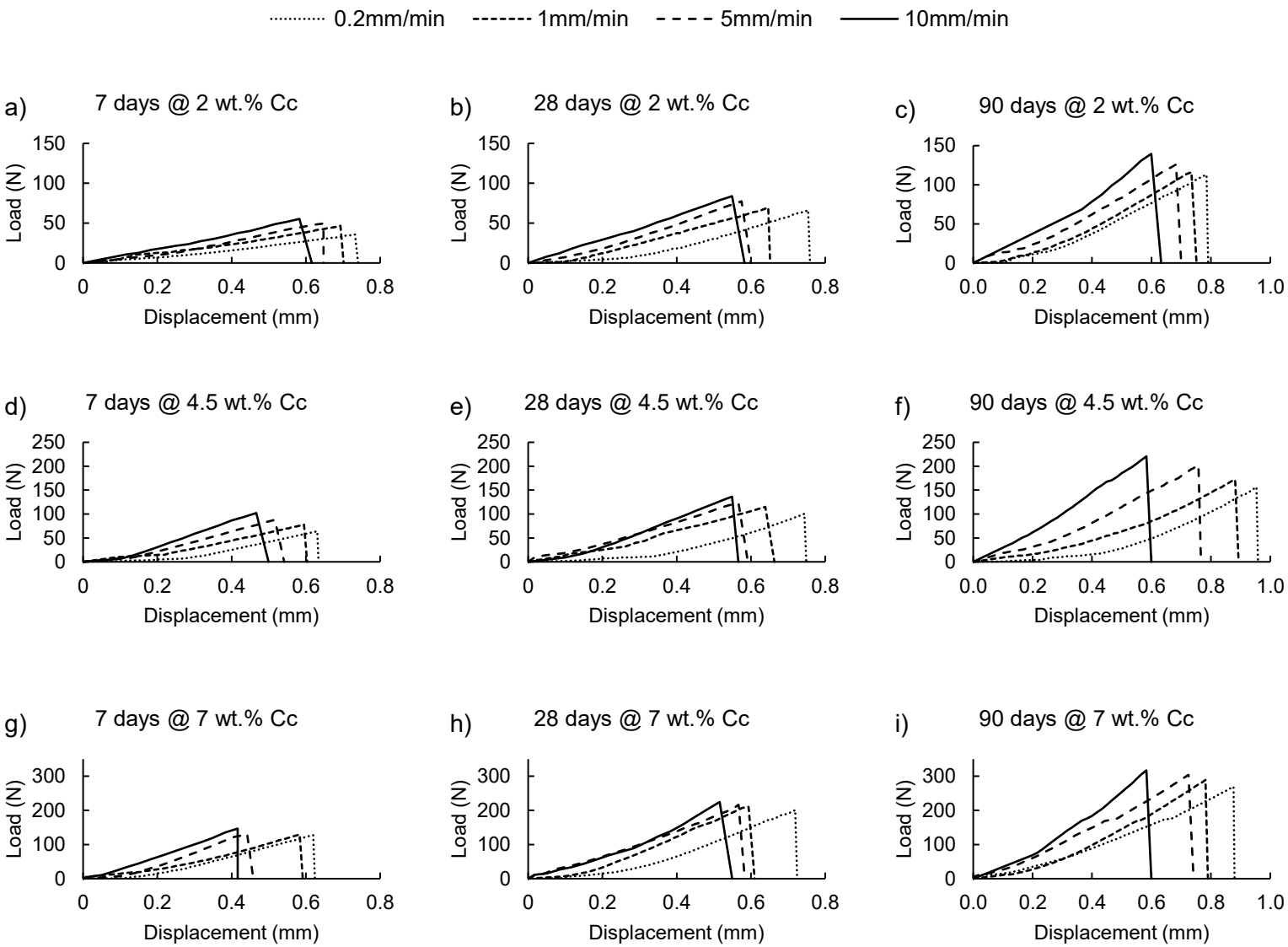

Figure 4.7. Effect of cement content on the loading-rate dependent fracture behaviour of CPB under mode-II loading condition.

parallel, the CPB matrix shows finer structure on the 90 days SEM observation (Figure 4.2), indicating the formation of a more refined pore structure and an increase in effective stress in the substance.

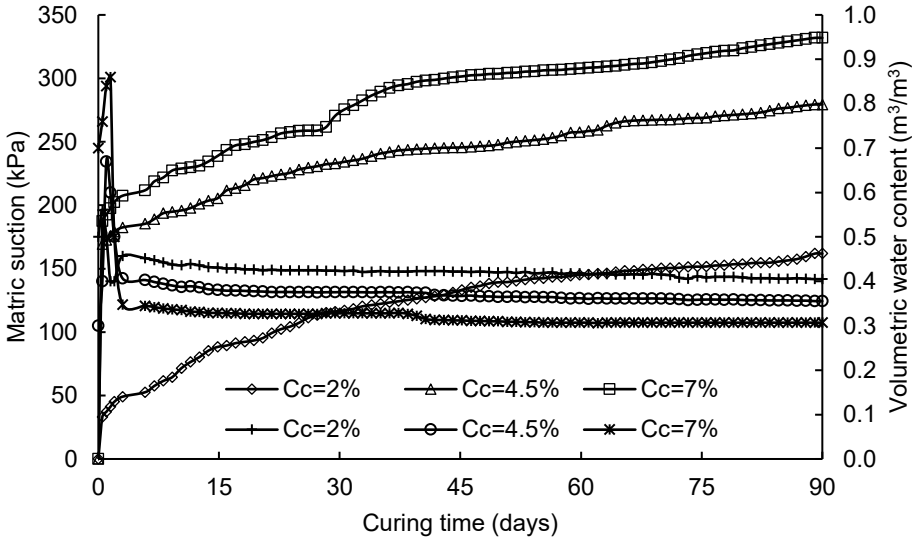

Figure 4.8. Evolution of matric suction and VWC with the change in cement content and curing time.

The higher the cement content on CPB, the more capillary water is consumed during the hydration process there by increasing the effective stress in the CPB structure. The utilization of more water leads to filling the pores within the matrix. Thus from the study of (Fang et al., 2021) can be confirm that CPB gain more bonding strength with the consumption of pore water thereby decreasing the porosity and reducing the lubricating effect within the CPB matrix. However, the effect of matric suction on fracture toughness is complicated. The water content limits matric suction, which works on solid surfaces in contact with water. As cement hydration continues, the pore water content decreases, reducing the contact area between water and solid particles. As a result, the water content limits the contribution of matric suction to fracture toughness (Fang & Cui, 2023). The initial increase in EC values can be related to the rising concentration of ions such Ca^{2+}, OH, and $SO4^{2-}$. However, these ions are eventually consumed as the cement hydration process proceeds. The EC values begin to decrease after the consumption rate overtakes the generation rate (Courard et al., 2014). The peak EC value shows (Figure 4.9) the critical moment when the rate of cement hydration is highest. The evolution of EC can be confirmed from the Figure 8 shows that after 12 hours of curing, the sample containing 7 wt.% Cc by weight reaches

a peak EC value of 5 mS/cm, while the sample containing 4.5 wt.% Cc by weight reaches a peak EC value of 4.2 mS/cm after 48 hours of curing. Likewise, the sample containing Cc 2 wt. % took nearly 3 days to reach its peak value of 1.6 mS/cm.

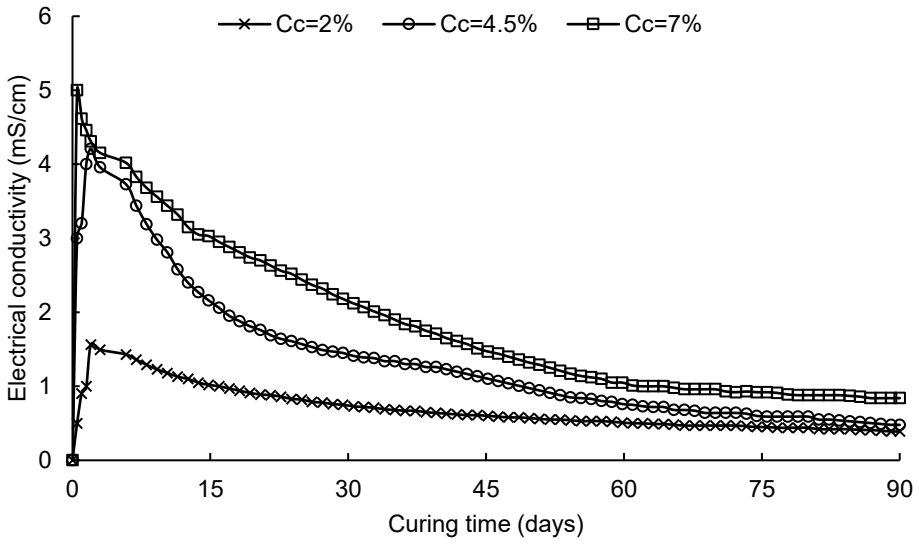

Figure 4.9. Evolution of electrical conductivity (EC) with the change in cement content and curing time.

4.1.4 Effect of sulphate concentration content on the loading-rate dependent fracture behaviour of CPB under mode-II loading

Figure 4.10 shows the effect of sulphate concentration on the loading-rate dependent fracture behaviour of CPB under mode-II loading condition. which indicates that the negative effects of sulphate ions the early-age development of the CPB matrix become more obvious at 7 days as the sulphate concentration rises. The softening behaviour of CPB, which is characterized by lower peak force, inclined pre-peak branch is observed at 7 days which gradually rises with the increase in loading rate. The strength of interparticle bonding significantly impacts the CPB pre-peak behaviour. As a result, the progressive pre-peak slope shows that sulphate solution affects the initial strength development on CPB matrix.

As shown in Figure 4.5, SEM observation of the CPB matrix demonstrates significant microstructural alterations. The presence of acicular crystals of ettringite increases with rising sulphate concentration. Additionally, within the 7-day CPB matrix, these needle-like ettringite crystals gradually change into longer rod-like structures. It is crucial to remember that the strength

of particle connections is unaffected by the ettringite's precipitation. Rather, the substantial growth of expanding ettringite crystals obstructs the hydration process within the relatively soft 7-day CPB matrix. A higher sulphate concentration also results in less calcium hydroxide (CH) tabular crystals in the CPB matrix. The continual consumption of CH by the synthesis of ettringite impairs the early-age hydration of cement there by decreasing the strength of the particle bonding. The observed improvement in resistance against crack propagation results from the interaction between friction resistance and interparticle bonding within the CPB matrix with the increase in curing time. The interlocking particles improve structural integrity and prevent the crack from expanding further, while the frictional forces restrict the displacement of crack surfaces.

The decrease in VWC from 0.9 to 0.3 m^3/cmS and raise in matric suction from 12 to 14.3 kPa for 25000 ppm sample with the span of 90 days can be observed as shown in Figure 4.11. But it is noted that it took 8 days to develop the matric suction for the sample with 25000 ppm Sc. Early age cement hydration is restrained by the higher level of sulphate concentration on the CPB. After that the suction drops down to 12.4 kPa and steadily rises with the span of curing time. Afterward, sulphate solution in the CPB matrix further strengthens these mechanism beneficial effects. Thus, the overall improvement of the sulphate rich CPB sample is due to this synergistic interaction between the ettringite and tailing particles as the curing time advanced. The reduced moisture content from forming solid expanding ettringite requires transforming capillary water into chemically bound water. As a result, there is less pore water to lubricate the tailing particles' contact surfaces by increasing particle friction resistance. From Figure 4.11 we can see the rise in VWC 0.6 to 0.9 m3/m3 in the first 2.1 days that after water contain sharply reduce to 0.7 m3/m3 in 4. 2days.So for the early 7 days of curing the decrease in strength of CPB is observed with higher Sc due to the lubricating effect between the CPB particles due to excess amount of water. While with the consumption of pore water by hydration process VWC steadily reduces to 0.3 m3/m3 in 90 days. The enhanced strength in the CPB material is observed for the higher concentrated sample as the reduce water content and increase matric suction favor the interparticle friction and bonding strength within the CPB matrix. Furthermore, the development of expansive ettringite leads to passive confinement inside the toughened CPB matrix, intensifying the interaction between the matrix and ettringite and enhancing the bonding which eventually leads to the higher peak force.

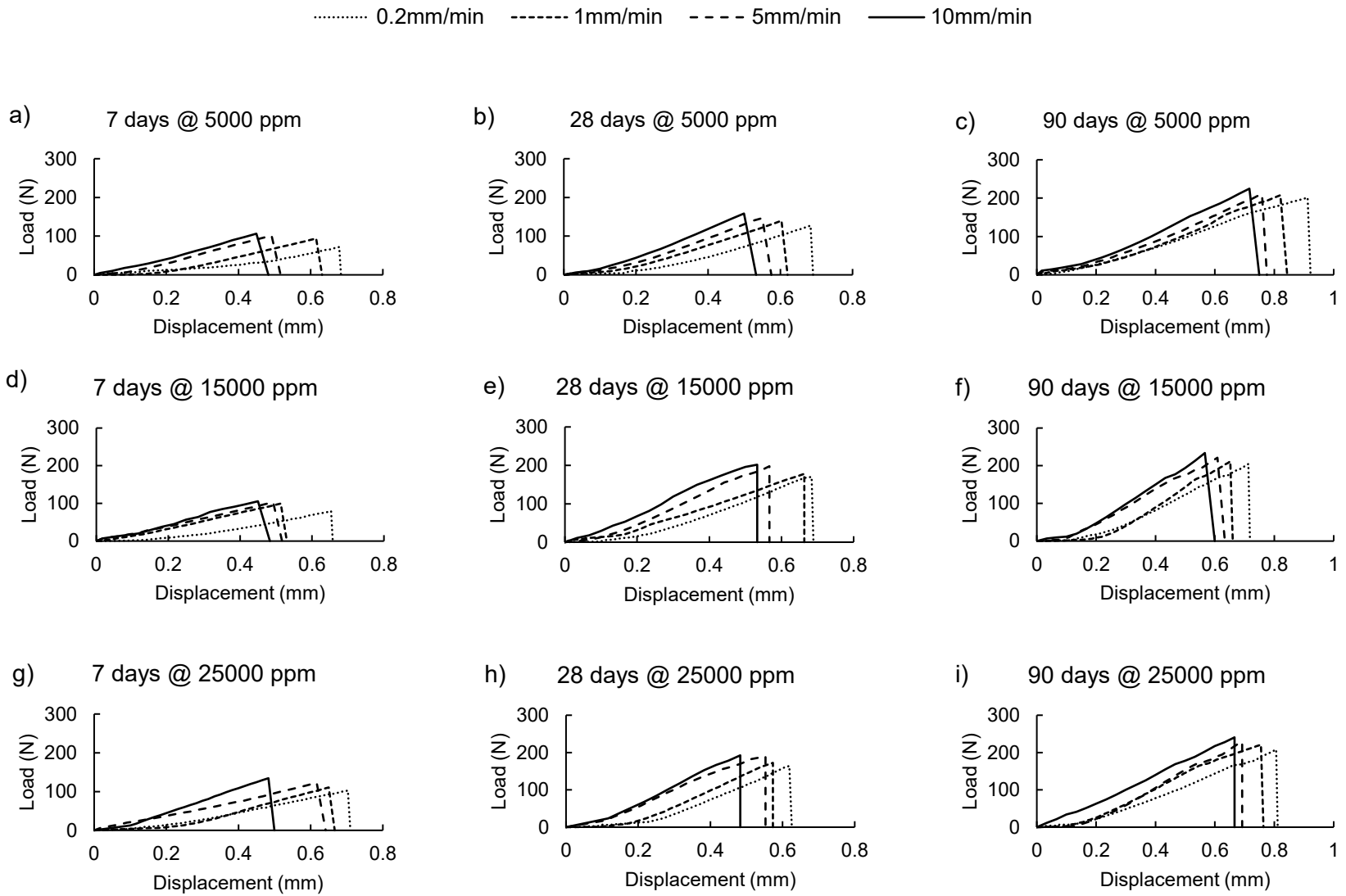

Figure 4.10. Effect of sulphate concentration on the loading-rate dependent fracture behaviour of CPB under mode-II loading condition.

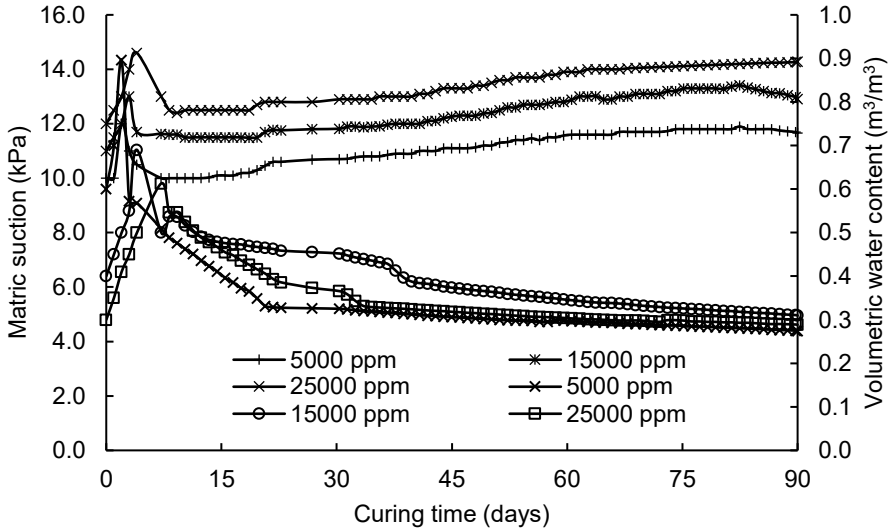

Figure 4.11. Evolution of matric suction and VWC with the increase in sulphate concentration and curing time.

4.1.5 Effect of cement content on the loading-rate dependent fracture behaviour of CPB under mode-III loading

The effect of cement content on the loading-rate dependent fracture behaviour of CPB under mode-III loading condition is presented in Figure 4.12. It can be observed that loading rate is able to impose a strong influence on the mode-III fracture response. More precisely, increasing loading rates result in faster crack propagation, altering fracture behaviour and load-displacement response. Regardless of curing period or cement content (Cc), the Mode-III samples displayed the highest peak forces when subjected to increased loading rates. The load-displacement curve became steeper as the loading rate increased, indicating an elevated gradient in force. Once the peak stress was attained, the samples experienced rapid crack propagation, which continued until the specimen completely collapsed. It is clear that rise in loading rate have incremental effect on acquiring the highest peak load for individual curing conditions. We can observe that peak force smaller difference between the 28 and 90-days curing period C1-0 (7 wt.% Cc) sample, however increment is twice as high we compare with the 7-day sample. Similarly, the A1-0 (2 wt.% Cc) and B1-0 (4.5 wt.% Cc) samples demonstrated a comparable increase in peak force with changes in loading rates, similar to the trend seen in mode II (explanation is provided earlier). The A1-0 7 days sample revealed a prolonged build-up to peak force regardless of loading

rate, but no significant post-peak behaviour is observed. In contrast, the peak forces of the 28-day and 90-day A1-0 samples were attained earlier. This data shows that higher loading rates result in larger peak forces and the longer curing durations contribute to overall strength improvement. However, variations in the material's behaviour and features might arise due to factors such as curing time and cement content, as seen by the variances observed between the A1-0, B1-0 and C1-0 samples at different curing periods. Increases in cement content promote the development of peak load. Changes in cement content and curing time in cementitious materials can greatly affect their mechanical characteristics and fracture behaviour. While curing time impacts the degree of hydration and development of the microstructure, cement content affects the material's overall strength and stiffness. As the mode III loading would see faster crack growth due to the increased loading rate. A steeper load displacement curve due to the increased crack growth would suggest more crack propagation resistance. The SEM images in Figure 4.8 provide compelling evidence to support the idea that the quantity of C-S-H in CPB samples increases as the cement content and curing time increase. These images clearly show the distinct flocculent appearance of C-S-H on the surfaces of the tailing particles. Moreover, it is evident that after a 90-day curing period, there is a significant growth in the amount of C-S-H compared to samples that were cured for only 7 or 28 days. The precipitation of cement hydration products aids in the movement of C-S-H, facilitating its migration and leading to the refinement of the capillary structure within the CPB. This reinforces the understanding that the interaction between cement content, curing time, and C-S-H formation plays a vital role in the behaviour of CPB.

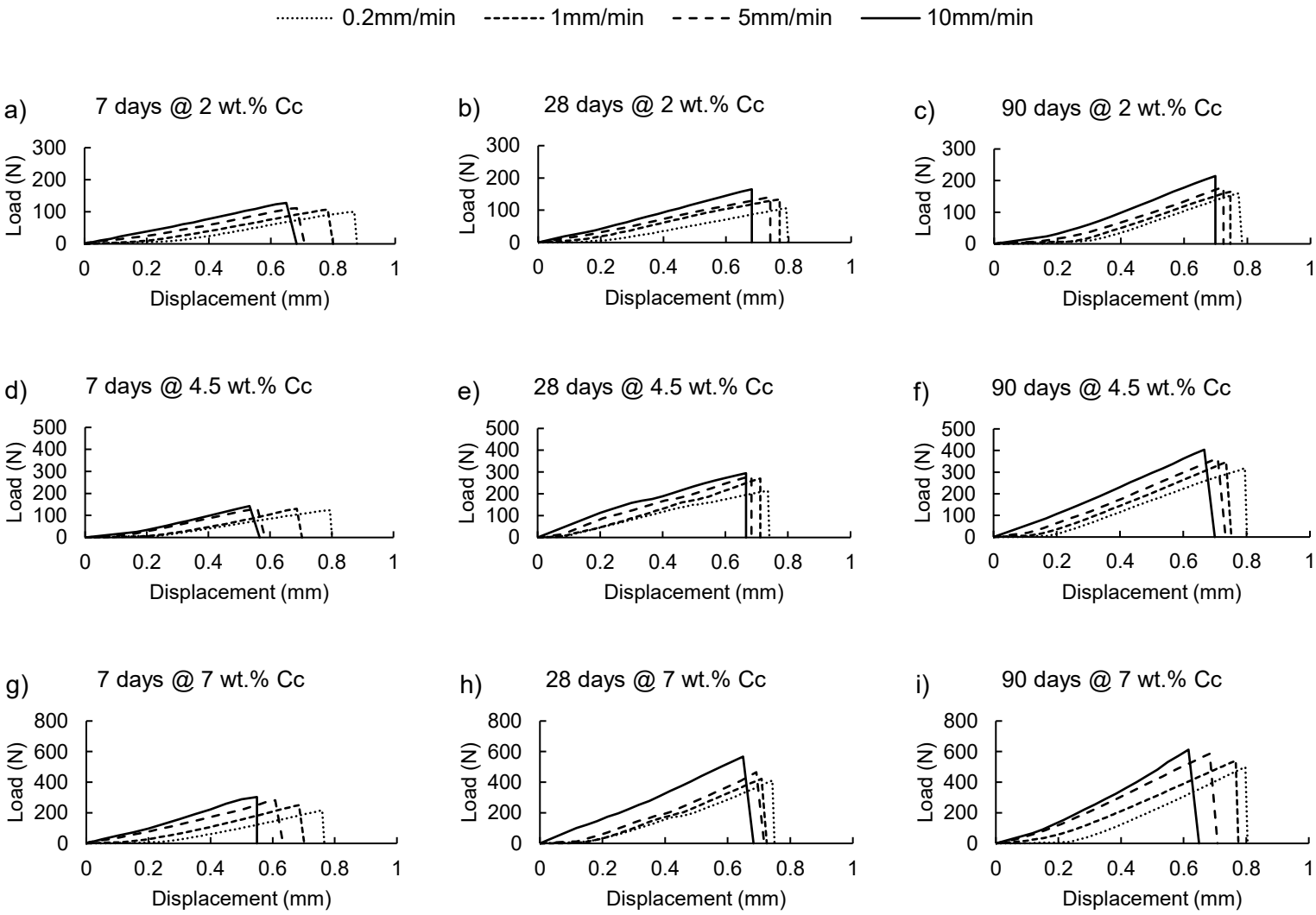

Figure 4.12. Effect of cement content on the loading-rate dependent fracture behaviour of CPB under mode-III loading condition.

4.1.6 Effect of sulphate concentration on the loading-rate dependent fracture behaviour of CPB under mode-III loading

Figure 4.13 illustrates the effect of sulphate concentration on the load-displacement curves under ENDB tests with various loading rates. These curves exhibit the linear and brittle response of the tested CPB material, demonstrating the viability of the linear elastic fracture mechanics (LEFM) framework for studying its fracture behaviour. The peak load from the load-displacement curves is used to calculate the fracture toughness, material stiffness and fracture energy for mode III loading condition. It is possible to determine and assess the fracture toughness of each loading rate by changing the peak load. Peak load from the load-displacement curves is used as a measure of fracture properties and enables analysis and comparison of the fracture behaviour at various loading rates and chemical concentration. The results of mode III loading with various Sc samples across curing periods of 7 days, 28 days, and 90 days at varied loading rates of 0.2, 1, 5, and 10 mm/min are shown in Figure 4.13 where higher loading rates and irrespective of cement content result in an increase in the peak force. Across all curing times and Cc values, mode-III loading consistently shows the highest peak forces, and the load-displacement curve steepens with increase in loading rate. We can observe that peak force is higher in the 90-day C1-0 sample than in the 28-day sample, but both twice as high as in the 7-day sample. However, we can observe the detrimental effect on the early 7 days with the raise in Sc. The sulphate effect on the cement hydration is became constraint with the increase amount of Sc on CPB material (explanation is provided earlier). The evolution of cement hydration products can be seen by through a SEM investigation on a sample that was prepared after 7, 28 and 90 days as shown in Figure 4.5. The C-S-H gel, which makes up the surface products, is the main element seen in the CPB microstructure. CH, another important product with a polycrystalline structure, was discovered in pore spaces. Due to improved cement hydration and self-desiccation, higher Cc has a favorable effect on the behaviour of CPB. The longer curing period encourages more effective binder hydration, which boosts the amount of C-S-H produced. Additionally, the interaction of other byproducts, like ettringite and gypsum, helps to improve the pore structure and create a denser arrangement. The easier movement of C-S-H is made possible by the denser pore structure, which eventually increases the binding force within the CPB. As visible proof for the benefits derived by

higher sulphate concentration CPB, the SEM pictures in Figure 4.5 clearly show the presence of a finer pore structure in advanced aged CPB.

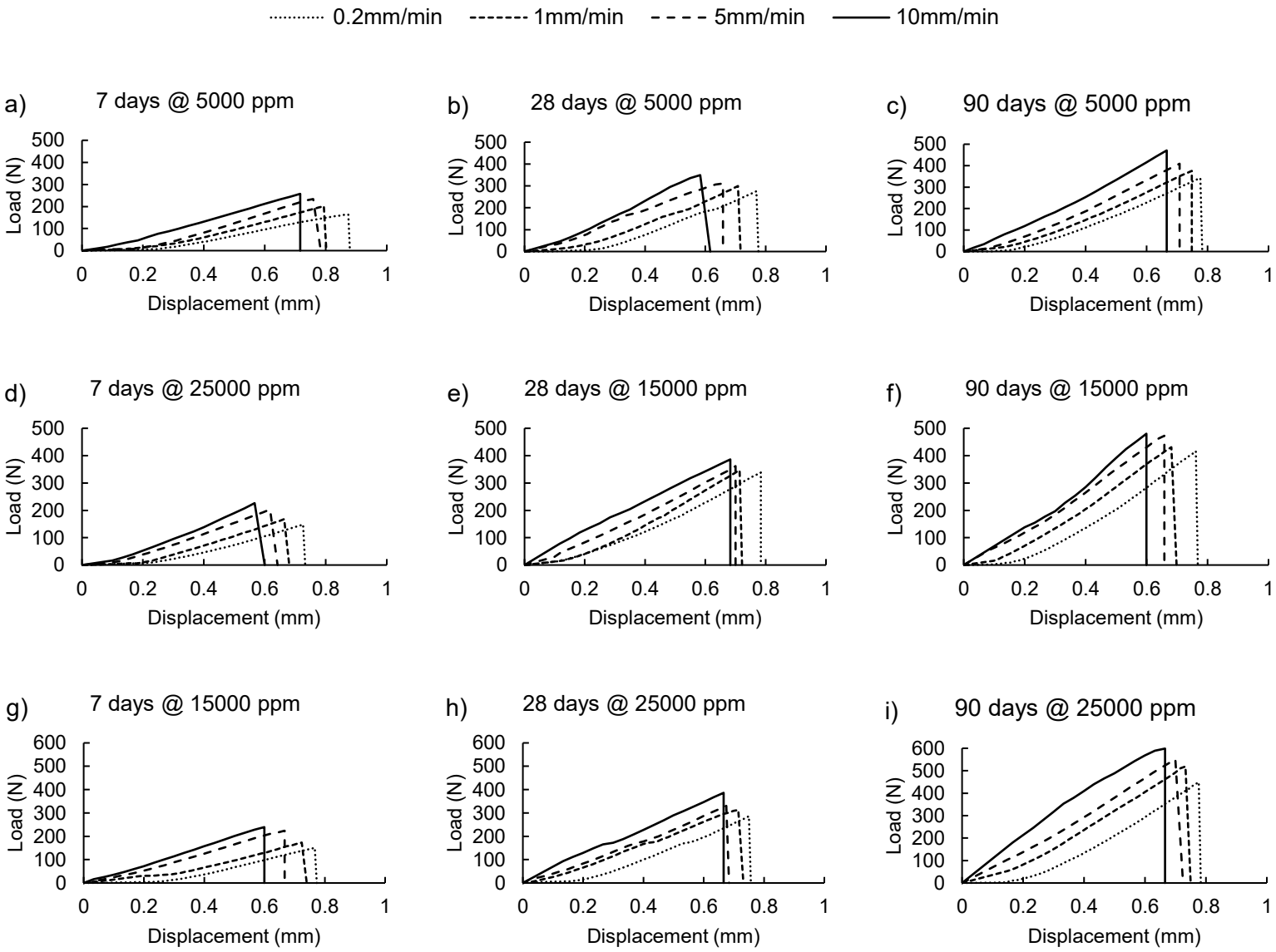

Figure 4.13. Effect of sulphate concentration on the loading-rate dependent fracture behaviour of CPB under mode-III loading conditions.

4.2 Loading rate-dependent material stiffness of CPB

4.2.1 Effect of cement content on the loading-rate dependent material stiffness of CPB under mode-I loading

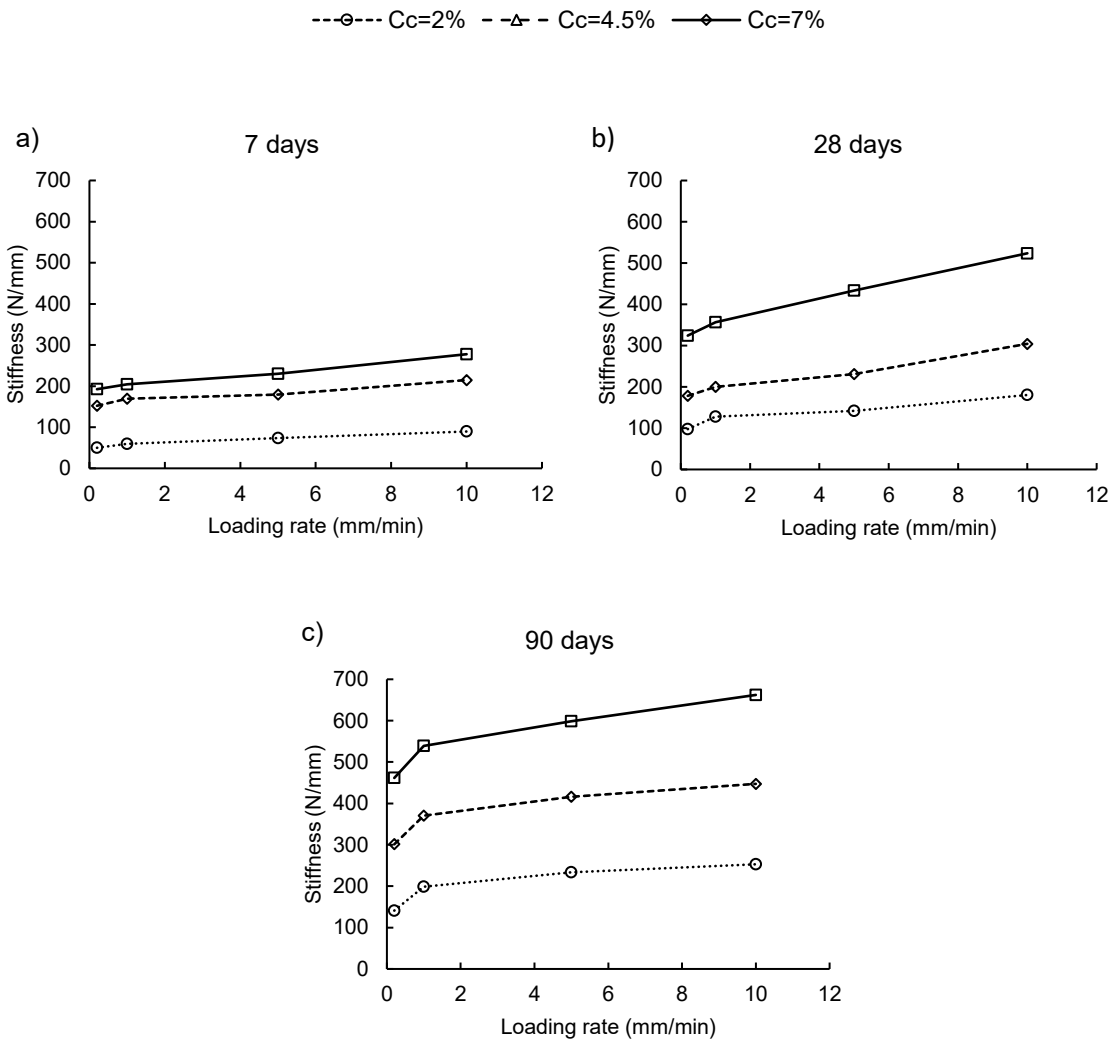

Figure 4.14. Effect of cement content on development of mode-I material stiffness at (a) 7 days, (b) 28 days, and (c) 90 days.

The pre-peak slope of load-displacement curve can describe the material stiffness of CPB. Likewise, the computed stiffness of CPB at different loading rates, cement content and curing times are shown in 4.14. As the loading rate increases, CPB gradually becomes stiffer. For example, the stiffness for a 10 mm/min loading rate in 7 wt.% Cc at 90 days is 138% higher (662.26 N/mm) than for the same conditions in (277.54 N/mm) at 7 days. This improvement in stiffness

suggests a stronger resistance to deformation under stress. As the loading rate progresses, the load-displacement curve exhibits a steeper post-peak response, representing the development of material brittleness, showing a decreased tolerance for permanent deformation.

4.2.2 Effect of sulphate concentration content on the loading-rate dependent material stiffness of CPB under mode-I loading

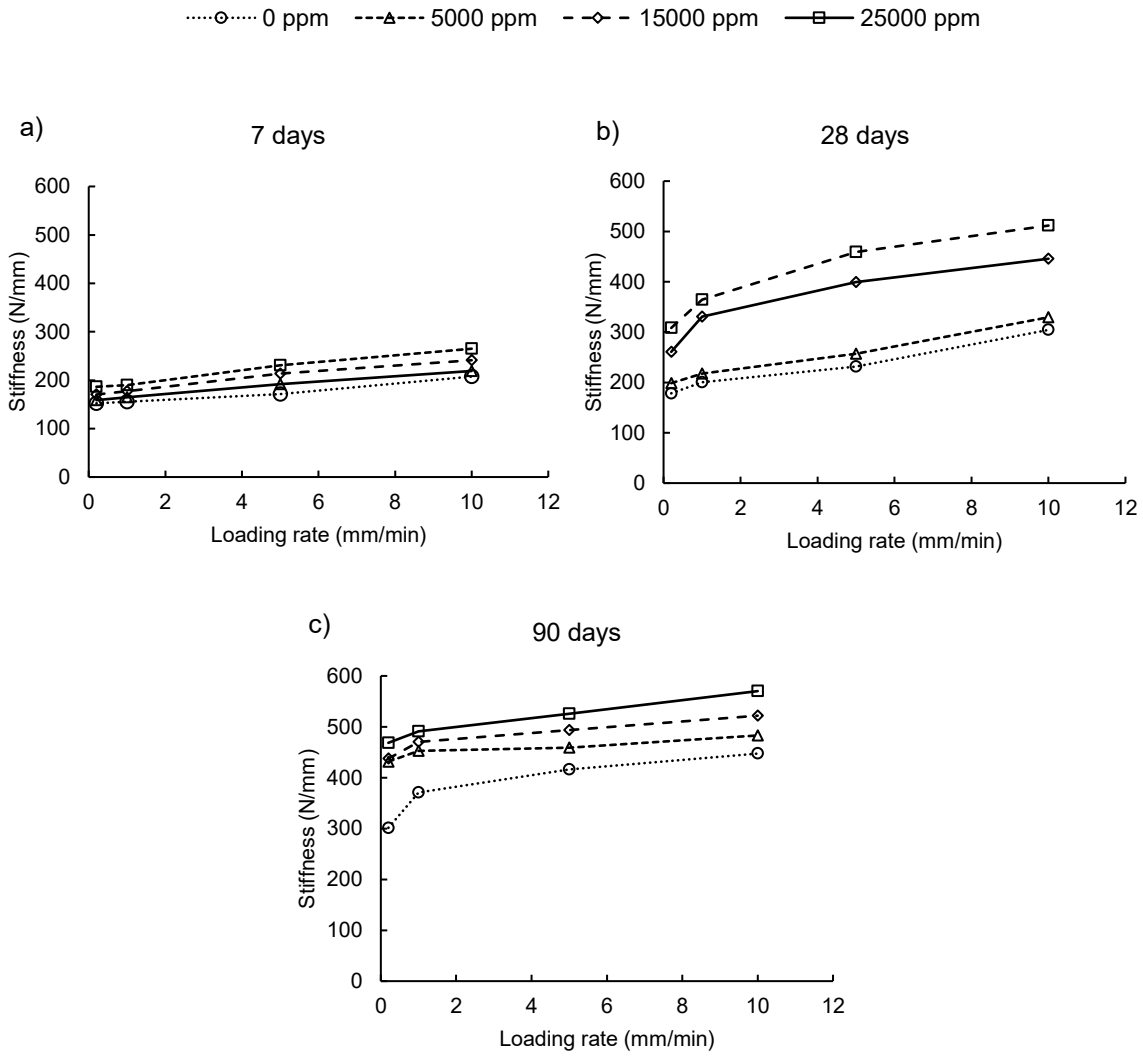

Figure 4.15. Effect of sulphate concentration on development of mode-I material stiffness at (a) 7 days, (b) 28 days, and (c) 90 days.

The evolution of mode-I material stiffness observed decrease in material stiffness at initial stage particularly at higher sulphate content. Hower the material stiffness for all the curing age is higher than that of the control CPB sample. From Figure 4.15 advance age CPB shows significant improvement at 28days. Additionally, the moderation rate of stiffness increment changes occurs

in 90 days cured sample regardless of sulphate content. The enhancement of passive confining pressure is critical in boosting CPB density while trapping expansive phases inside the bulk matrix. This process helps to increase material stiffness, especially in CPB with a high sulphate concentration. The stiffest CPB is observed at the 90-day mark at 25000 ppm, followed by 15000 ppm, 5000 ppm, and 0 ppm.

4.2.3 Effect of cement content on the loading-rate dependent material stiffness of CPB under mode-II loading

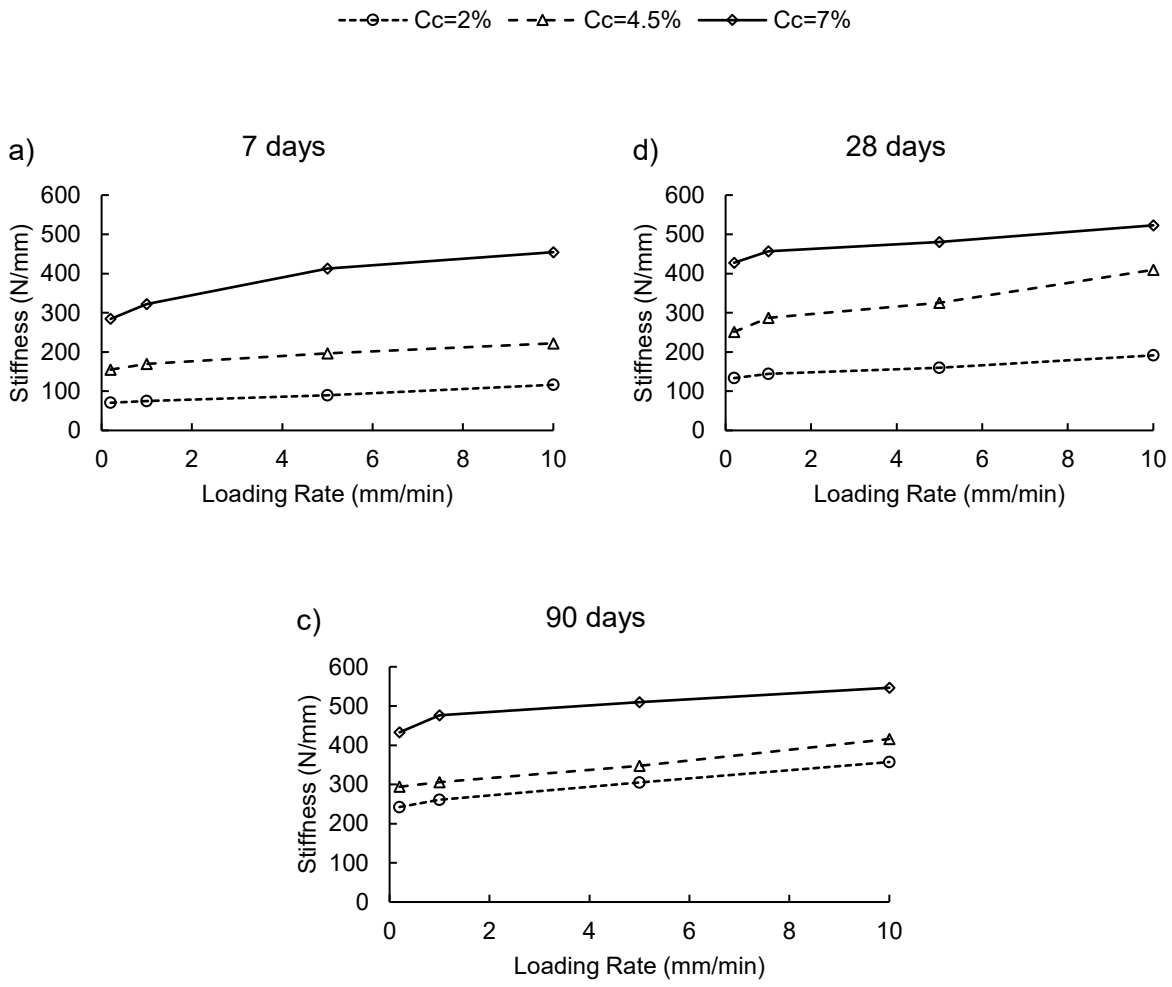

Figure 4.16. Effect of cement content on the loading rate-dependent mode-II material stiffness of CPB.

The influence of loading rate on the mode-II material stiffness of CPB due to change in cement content is depicted in Figure 4.16. Under mode-II loading circumstances, the stiffness of CPB is influenced by the loading rate and curing duration irrespective of cement content. Overall, the

material stiffness of CPB rises with increasing loading rates and curing time. For the A1-0 (2 wt.%) and B1-0 (4.5 wt.%) Cc samples, stiffness increases linearly with increasing loading rate at 7 days. However, at the same curing period, the C1-0 (7 wt.%) Cc sample shows a considerable improvement in material stiffness. There is a significant improvement in stiffness with increasing loading rate and cement content in the 28-day and 90-day samples. Notably, the stiffness of the sample C1-0 after 28 and 90 days of curing is comparable, indicating that the hydration process is completed.

4.2.4 Effect of sulphate concentration content on the loading-rate dependent material stiffness of CPB under mode-II loading

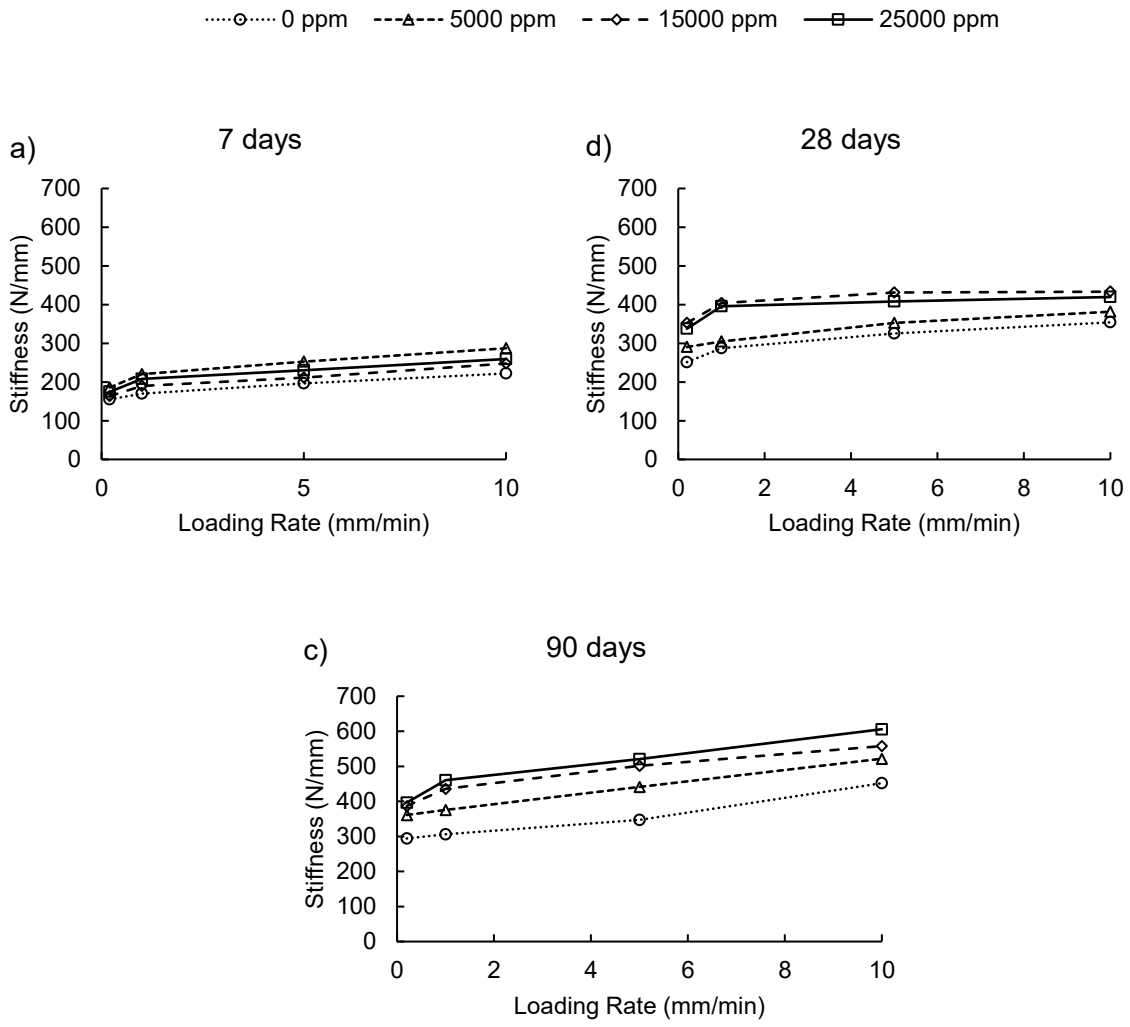

Figure 4.17. Effect of sulphate concentration on the loading rate-dependent mode-II material stiffness of CPB.

Figure 4.17 illustrates the significant impact of sulphate concentration on material stiffness in CPB. At early age (7 days) the higher sulphate concentration (Sc) in CPB have detrimental effect on gaining the material stiffness. The sample with lower Sc D1-0 (5000 ppm) have higher stiffness followed by F1-0 (25000 ppm) and E1-0 (15000 ppm) sample for all the loading rates. The formation of the hydration product is contained by the presence of more Sc on the sample there by reducing the early strength development of CPB. However, with increased sulphate concentration, stiffness keeps getting better after 28 days. The sample E1-0 becomes stiffer than the sample F1-0 followed by D1-0. Eventually at 90 days the higher Sc concentration sample become more stiffer than the corresponding lower Sc samples, it is to be noted that for all the curing period the sample with B1-0 (0 ppm) is less stiff than the sulphate concentrated sample. The hardened bulk matrix predominates the development of material stiffness on CPB. Higher sulphate concentrations cause the pore structure in the bulk matrix to develop further, resulting in a denser matrix. This streamlined microstructure aids in improving the macroscopic stiffness of the material. This change is brought about by the sulphate anion-induced hydration process, which promotes ettringite growth and reduces cementitious composites' moisture content. A stronger interparticle contact and overall improvement in material stiffness follow from the strengthening of interparticle friction resistance. This microstructural development with respect to curing time can be observed through the SEM images as shown in Figure 4.5. As the pore space gradually fills with hydration products over time by CSH and ettringite (AFt), cementation and densification processes produce a more refined bulk matrix.

4.2.5 Effect of cement content on the loading-rate dependent material stiffness of CPB under mode-III loading

Figure 4.18 illustrates the impact of mode III loading rate on the material stiffness of CPB. Notably, CPB exhibits a linear relationship between load and displacement in the pre-peak region, regardless of the age of the specimen, highlighting the validity of linear elastic fracture mechanics for CPB materials. Increasing the loading rate intensifies the linear pre-peak branch and enhances the material stiffness. This elevated stiffness enables CPB to provide more effective support to restrict stope convergence in field loading conditions. The mode III stiffness of CPB demonstrates significant improvement with higher cement content and longer curing time. This improvement can be attributed to factors such as cohesion, frictional resistance, and the mobilization of

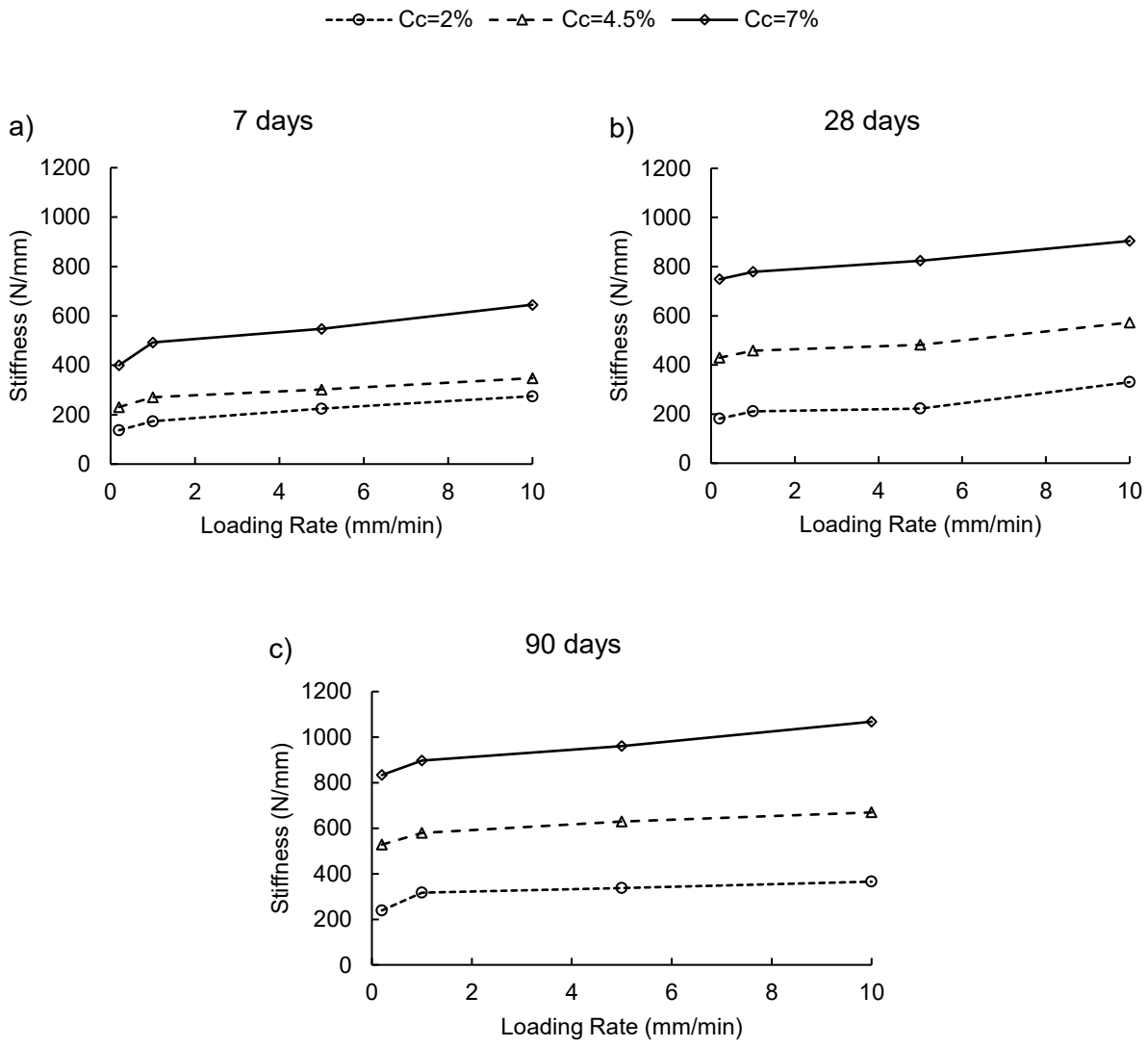

Figure 4.18. Effect of cement content on the loading rate-dependent mode-III material stiffness of CPB.

interparticle friction along the shear crack surface (Fang & Cui, 2022). The interface friction between tailings particles also contributes to a higher mode III stiffness. It is important to note that CPB exhibits enhanced resistance to crack propagation at higher loading rates, regardless of curing time and cement content. This is due to the inertia effect, which increases the cohesive strength between tailings particles and reduces the available time for crack propagation (Zhang et al., 2009). However, the kinetics of hydration are influenced by the diffusion velocity of pore water between the outer surface of hydration products and the internally anhydrous cement grains. Additionally, as the cement content (Cc) increases, there is a higher production of hydration products, leading to reduced moisture dispersion and a slower cement hydration rate at advanced ages. Furthermore,

the rate of stiffness increase diminishes with curing time due to the sudden release of strain energy associated with the peak load. The area beneath the load-displacement curves represents the accumulated strain energy within the CPB system (Fang & Cui, 2023).

4.2.6 Effect of sulphate concentration content on the loading-rate dependent material stiffness of CPB under mode-III loading

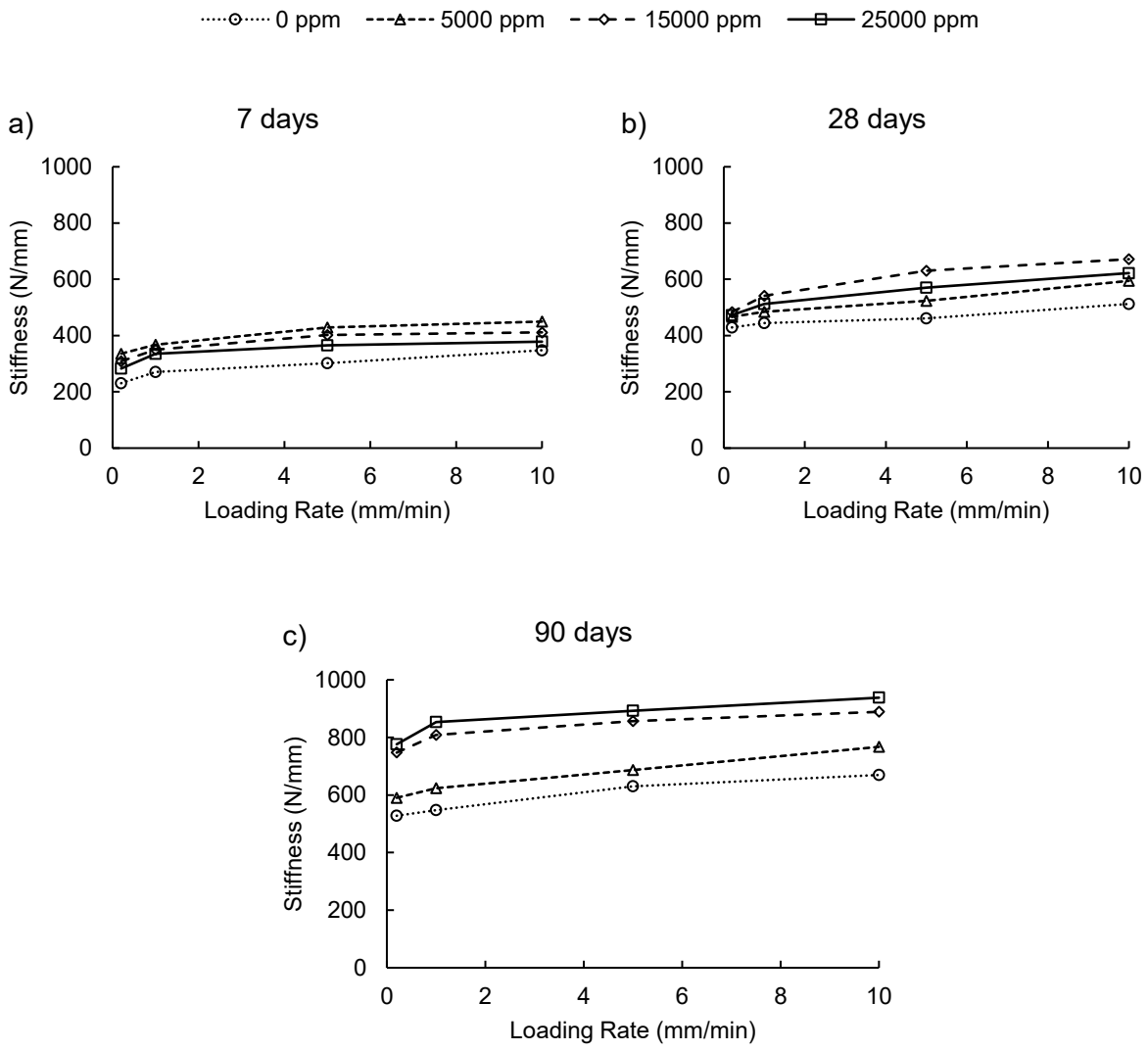

Figure 4.19. Effect of sulphate concentration on the loading rate-dependent mode-III material stiffness of CPB.

Figure 4.19 shows how a rise in sulphate concentration results in continual improvements in material stiffness after 7 days. The stiffness measurements are derived from the pre-peak branches of load displacement curves, where the hardened bulk matrix plays a significant role. The

microstructure of the bulk matrix is crucial in influencing material stiffness. As more hydration products, such as CSH and AFt (ettringite), precipitate into the pore space during curing, the bulk matrix gradually refines as shown in Figure 4.5. As the bulk matrix matures, the continuous cementation and densification process gets more prominent, resulting in a stiffer and stronger bulk matrix. Additionally, increasing the sulphate concentration improves the pore structure inside the bulk matrix. This finer microstructure aids in the formation of a denser bulk matrix, increasing material stiffness on a macroscopic scale. The presence of a sulphate-rich solution in pore promotes the early formation of ettringite, resulting in the consumption of a large amount of capillary water. As a result, CPB with a higher sulphate concentration has a lower moisture content which increases the particles friction there by increasing the material stiffness in advance ages. This pattern is especially visible in the analysis of CPB samples with high sulphate concentration at advanced ages. The rapid hydration of expansive phases in the early stages of CPB formation results in the consumption of surplus pore water. As a result, the fall in pore water content increases the material stiffness. In summary, mode III loading has a significant influence on the material stiffness of CPB, and factors such as loading rate cement content, curing time, and interparticle friction contribute to the observed stiffness variations.

4.3 Loading rate-dependent fracture toughness of CPB

4.3.1 Effect of cement content on the loading-rate dependent fracture toughness of CPB under mode-I loading

From Figure 4.20, the mode-I fracture toughness (K_{IC}) is sensitive to the change in loading rate irrespective of cement content and curing time. Cement hydration is associated with improving fracture toughness (Cui & Fall, 2018). Hydration products facilitate the formation of the cohesive matrix, leading to increased bonding strength and self-densification within the CPB matrix due to the increment in chemical shrinkage associated with dry density (Libos & Cui, 2020). For example, let's use the sample group with the labels A1-0, B1-0, and C1-0 with varied Cc, as shown in Figure 4.20. The K_{IC} value for sample A1-0 measures 5.30, 6.65, 8.22 and 9.52 kPa·m$^{1/2}$ at 7 days that rises by 114%, 110%, 121%, and 116% with a loading rate of 0.2, 1, 5, 10 mm/min respectively at 90 days. Similarly, for sample group B1-0, the 7-day K_{IC} value 12.80, 13.56, 14.08, and 15.78 kPa·m$^{1/2}$, which exceeds by 51%, 75% and 125% and 119%, respectively, with an increase in

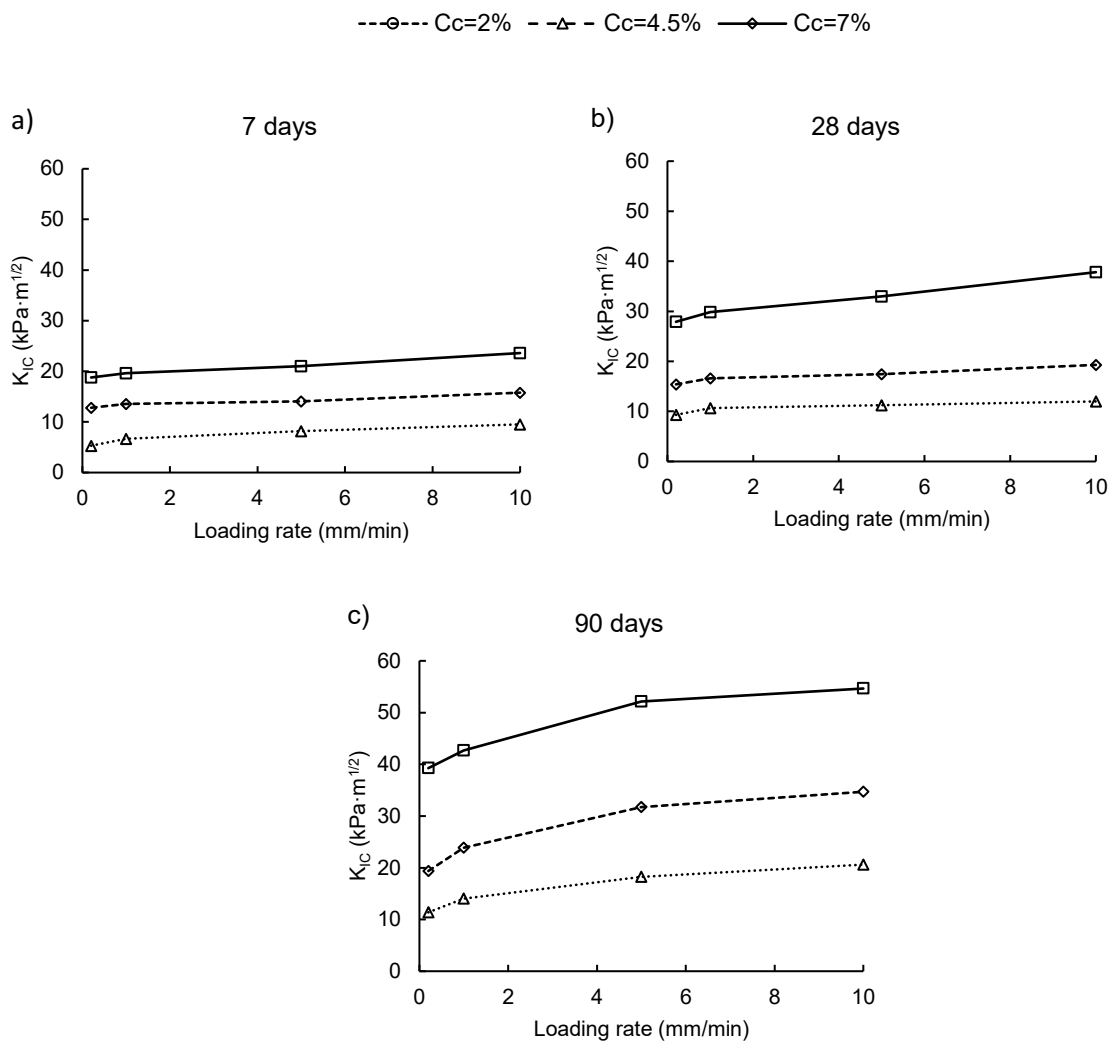

Figure 4.20. Effect of loading rate on development of mode-I fracture toughness at (a) 7 days, (b) 28 days, and (c) 90 days.

loading rate for 90 days. Additionally, sample C1-0 K_{IC} value at 7 days is 8.78, 19.61, 21 and 23.61 kPa·m$^{1/2}$ at a loading rate of 0.2,1, 5 and 10 mm/min, respectively. This result exceeds the toughness values of 39.26, 42.65, 52.16 and 54.65 kPa·m$^{1/2}$ by 347%, 117%, 147%, and 131%, respectively, under an increase in loading rate. Thus, results show no proportional link between the rise in fracture properties and the loading rate. This implies that the fracture characteristics may not grow linearly with increasing loading rate but may exhibit a variable rate of improvement. The fracture toughness enhancement is mainly due to self-desiccation and increased hydration production with the curing period.

Moreover, the EC results show a decreasing value which reflects the completion of the hydration process due to the nonlinear development of fracture toughness in advanced ages of CPB with the increase in cement content. This attribute can be explained by the formation of excessive hydration product with increase in cement content at early age as shown in SEM image (Figure 4.2), which surrounds the anhydrous cement particles by limiting the moisture diffusion to complete the hydration process. The evolution of EC in CPB provides additional evidence for the decline of cement hydration as shown in Figure 4.21. Cement hydration kinetics can be assessed using EC, which defines ion mobility. In the very early curing phases, the measured EC of CPB with a 7 wt.% Cc rises quickly. The EC, however, displays a declining trend after attaining a peak value, indicating a nonlinear slowdown of the cement hydration process. It confirms no correlation between the loading rate and increased fracture characteristics. Indicating that the relationship between fracture properties, such as fracture toughness, and loading rates are not always linear. Instead, the improvement in fracture properties may change for various loading rates. The rate sensitivity for advanced-age CPB at a lower loading rate is less due to a reduced VWC (Mindess et al., 2003).

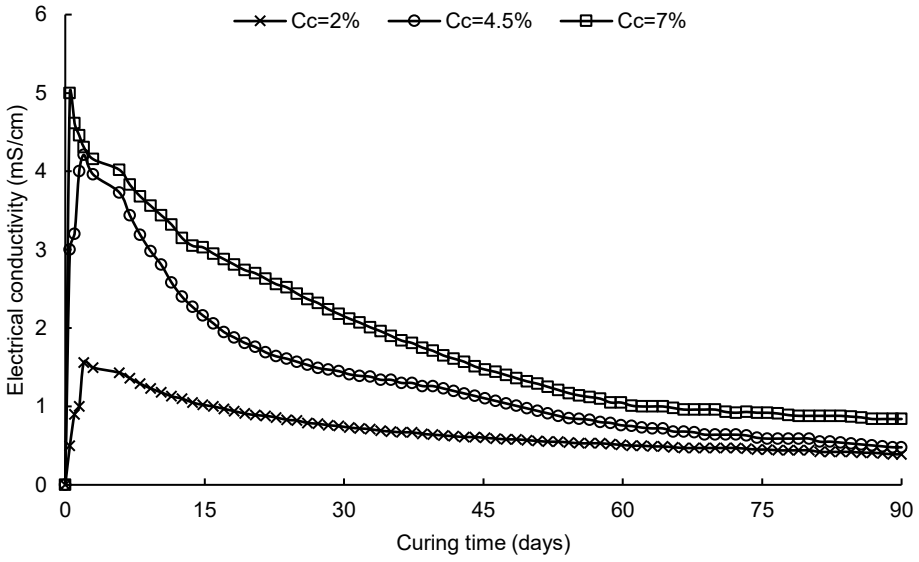

Figure 4.21. Effect of cement content on development of electrical conductivity (EC) of CPB.

As shown in Figure 4.22, the VWC with advanced curing time decreases with the increase in Cc in CPB. The abrupt increase of VWC in early-age CPB is observed in the monitoring process. The massive increment is due to the gap between the sensor and the associated chemical shrinkage

after contact with the CPB paste. The initial presence of a w/c ratio of 0.36 fills the gap within the CPB matrix to raise the water level. But with the start of cement hydration, water is used and gradually reduces the VWC on the CPB (Jiang et al., 2017). Following Figure 4.22, more capillary water was ingested during the cement hydration process in CPB when a more significant cement percentage was applied. A greater degree of unsaturation is generated in CPB due to increased matric suction and higher cement content. The CPB's mode-I fracture toughness (K_{IC}) showed an upward trend with increasing cement content under unsaturated conditions. This indicates that the CPB's unsaturated K_{IC} grew along with the cement concentration.

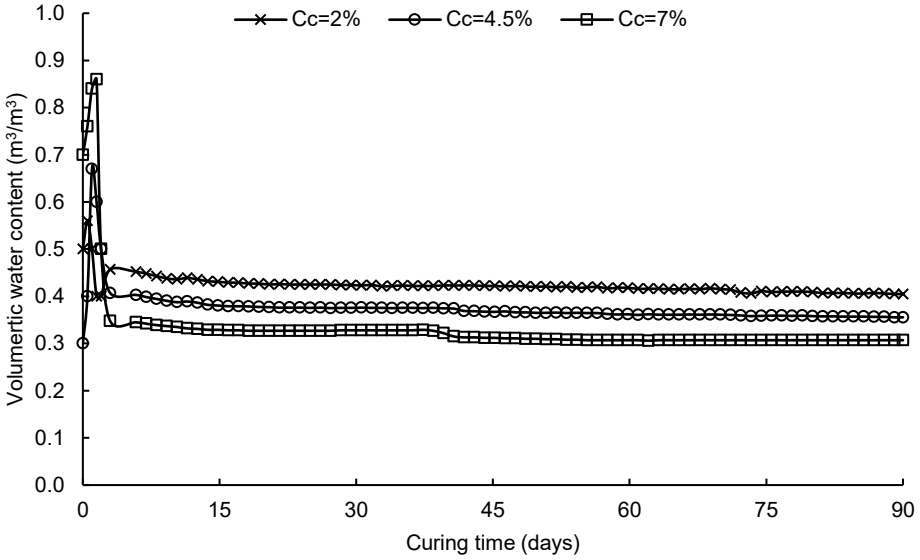

Figure 4.22. Effect of cement content on evolution of VWC with curing time.

Thus, the saturation state of the CPB is thought to be the cause of the varying rate of improvement in fracture characteristics with increasing loading rate. The particles and matrix interfacial debonding happened more easily at slow loading rates. This implies that well-bonded particles would dissociate from the matrix towards the fracture tip, lowering the material's resistance to fracture (Jacob et al., 2005). The debonding phenomena reduced the material's capacity for shear deformation and brought about early failure. This can be observed with the change in VWC, as shown in Figure 4.22. When the water content in CPB is reduced, interparticle friction within the material rises and thus increases the resistance to crack propagation with the increase in Cc and loading rate. We can observe the increase in VWC with an increase in Cc at a shorter period and gradually decreasing along the curing time, indicating the completion of the hydration process. In

addition to interfacial debonding, impact loading effects were also significant. Compared to the specimen's stiffness, the contact stiffness between the loading surface and the specimen interface is slightly higher (Koh et al., 1993).

4.3.2 Effect of sulphate concentration content on the loading-rate dependent fracture toughness of CPB under mode-I loading

The inhibitory effect of sulphate ions on cement hydration, which reduces water access to cement compounds, is the cause of the reduced fracture toughness with increasing sulphate concentration at an early age (Yilmaz & Fall, 2017). From Figure 4.23, CPB with a 5000 ppm sulphate concentration shows higher fracture toughness at 7 days, followed by 15000 ppm and 25000 ppm. The slight increment is due to the formation of gypsum at an early age, reducing porosity. The retardation effect on cement hydration predominates at high sulphate concentrations (15000 ppm and 25000 ppm), which lowers fracture toughness at an early age. However, for advanced curing times exceeding seven days, the pore structure by cement hydration products increases fracture toughness. To further explain the sulphate-induced retardation by analyzing EC value at different sulphate concentrations. EC values have grown, supporting the sulphate-induced delay in cement hydration. We can see the delay in achieving the peak value for 25000 ppm and 15000 ppm. The retardation effect due to the increased concentration of sulphate ion at the early age of CPB causes the time extension to reach the EC peak value. The sulphate ion inhibition effect prevents the typical course of hydration reactions and slows the formation of hydration products (Li & Fall, 2018; Tzouvalas et al., 2004). Figure 4.24 shows how the starting sulphate concentrations (0, 5000, 15000 and 25,000 ppm) affect the EC over time for CPB samples. The peak of electrical conductivity is delayed as the initial sulphate concentration rises, following a trend that shows a delay in binder hydration. In just 5 hours after mixing, the CPB sample without any sulphate (0 ppm) obtains a peak EC value of 9.9 mS/cm. Similarly, Sc of 5000 ppm needs about a day to attain the peak value of 8.8mS/cm, and the sample with Sc of 15,000 ppm would require 2.5 days to attain a peak value of 10.37 mS/cm and 5.5 days for 25,000 ppm to achieve the peak value of 11.58 mS/cm. The noticeable reduction in electrical conductivity over time is the initial rapid dissolution of sulphate ions and reactive alumina, and ettringite production, which begins to slow down after achieving the peak value. This drop aligns with the cited references, which state that C_3A inhibits the fast reaction between cement and water (Li & Fall, 2018; Pokharel & Fall, 2013; Tzouvalas

et al., 2004). A reduction in hydration products, specifically calcium silicate hydrate (C-S-H) and calcium hydroxide (CH), associated with higher Sc (15,000 and 25,000 ppm) (Li & Fall, 2018).

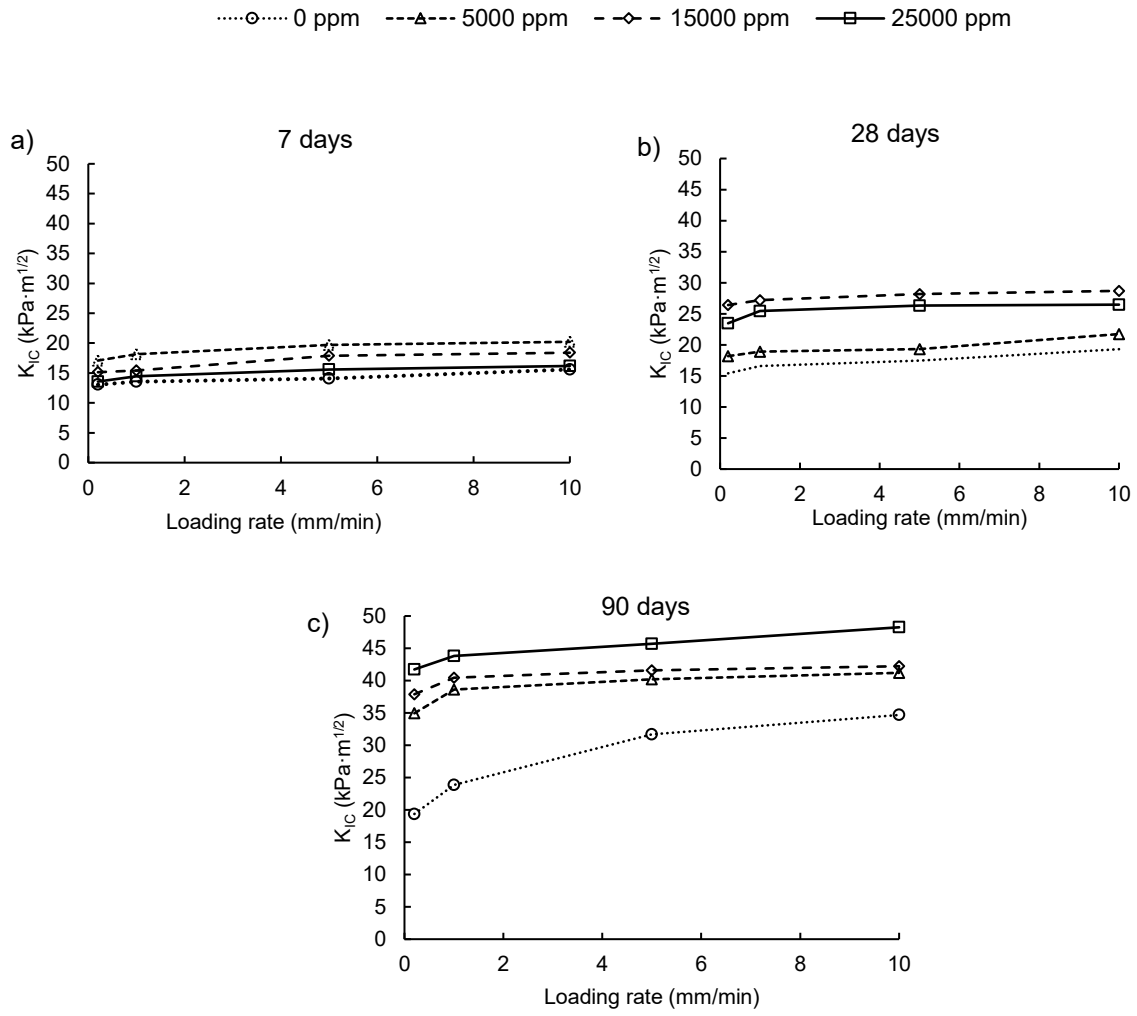

Figure 4.23. Effect of loading rate on the development of fracture toughness under mode-I loading condition.

The C-S-H and CH peak intensities are relatively more significant in the sulphate-free CPB than in the samples with sulphate concentrations of 15,000 ppm and 25,000 ppm. This implies that less C-S-H and CH are produced in the sulphate-containing samples, negatively affecting CPB's strength development (Li & Fall, 2018). Likewise, CPB resists the propagation of cracks by improving interparticle friction through the reduction of water content as shown in Figure 4.25. This effect is amplified by concurrently increasing loading rate and coefficient of curvature . Early rise in initial volumetric water content (VWC) associated with increases in Cc at early age. VWC steadily drops as the curing process progresses, indicating full hydration.

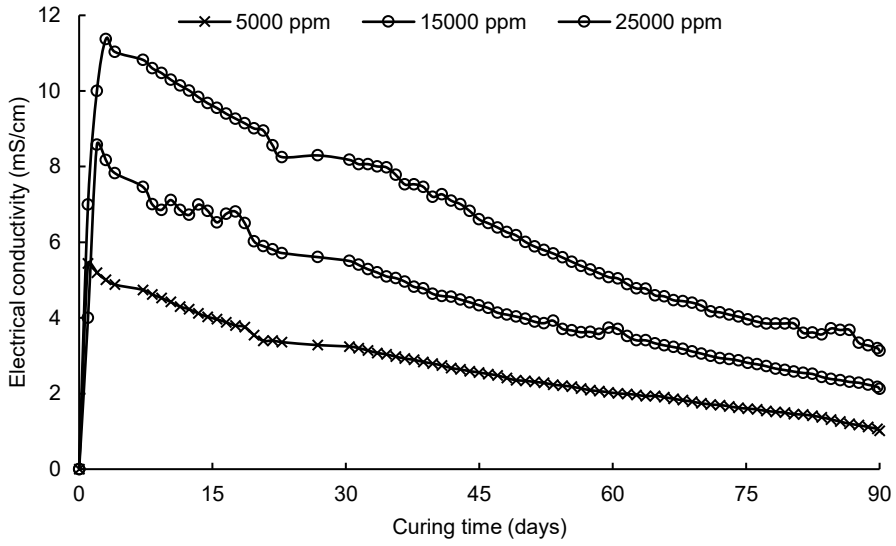

Figure 4.24. Effect of sulphate concentration on development of electrical conductivity (EC) of CPB.

In addition to interfacial debonding, impact loading has a major effect on the material's reaction due to somewhat increased contact stiffness at the loading interface (Koh et al., 1993). Raise in VWC and Sc show that interparticle friction increases with decreasing water content. Increased contact stiffness and impact loading improve the material's resistance to outside pressures.

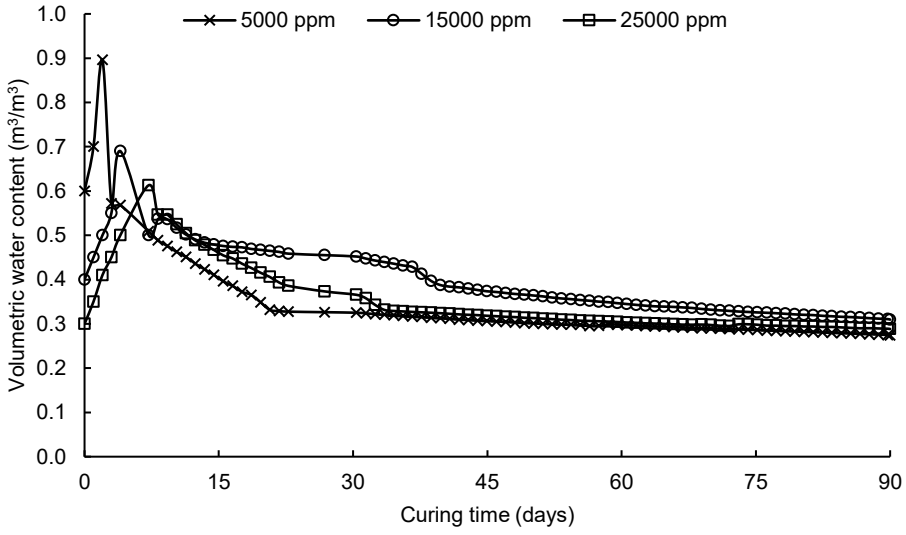

Figure 4.25. Effect of sulphate concentration on evolution of VWC in CPB.

4.3.3 Effect of cement content on the loading-rate dependent fracture toughness of CPB under mode-II loading

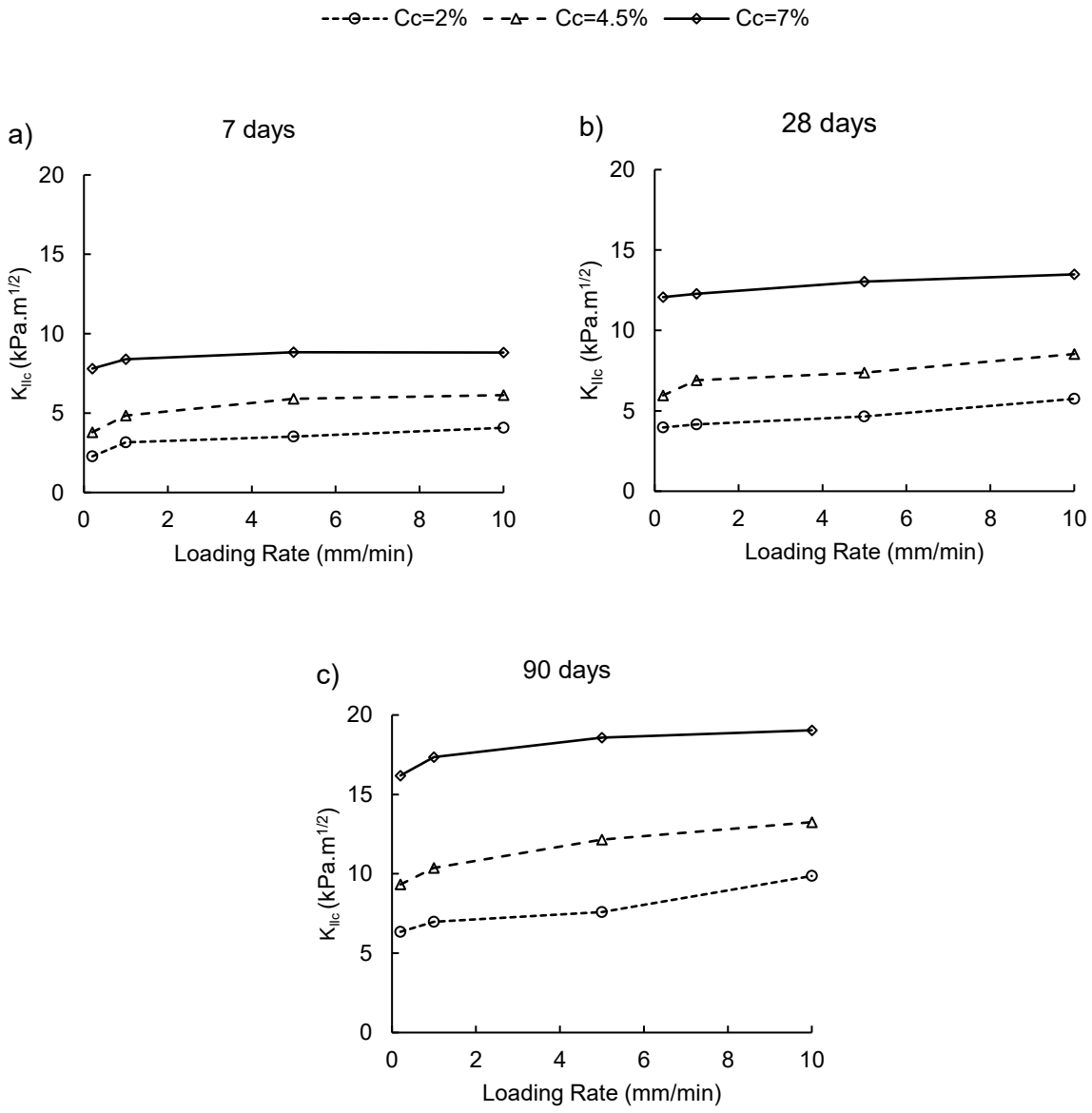

Figure 4.26. Effect of cement content on the loading rate-dependent mode-II facture toughness of CPB.

Figure 4.26 illustrates the outcomes of evaluating mode-II loading under different loading rates (0.2, 1, 5, and 10 mm/min) and curing times (7, 28, and 90 days). The fracture toughness (K_{IIc}) of the 7-day samples noticeably increases with higher loading rates and cement content (Cc). Moreover, for all loading rates, the mode II loading on group C1-0 (7 wt.% Cc) yields a K_{IIc} three times greater than that of the A1-0 (2 wt.% Cc) sample, as curing time increases. However, the

A1-0 sample, which has the lowest Cc, demonstrates the least variation concerning changes in loading rate and curing time. The increase in the fracture toughness parameter is determined by cohesion, matric suction, and the frictional resistance between tailings particles. This variance in fracture toughness is related to increased cement hydration products such as C-S-H, gypsum, and ettringite. These products influence particle bonding forces and can refine or coarsen the microstructure of the CPB (Pokharel & Fall, 2013). The rise in K_{IIc} is mostly due to increased cohesiveness, matric suction and frictional resistance. As soon as the matric suction reaches the air entry value, air begins to infiltrate the porous material, causing the transition from full saturation to partial saturation. An increase in matric suction causes the tailings particles to consolidate and move closer together in the unsaturated state. In the beginning, it encourages an increase in the contact area between particles, strengthening the resistance to interparticle friction. Second, as the particles are pulled closely together, it helps to create a matrix that is denser (Fang & Cui, 2023). This transition is accompanied by variations in fracture surface roughness, with intergranular fractures having rougher surfaces than transgranular fractures. The results show that intergranular fractures dominate at low loading rates, and transgranular fractures dominate at higher loading rates (Fang & Cui, 2023; Zhang & Zhao, 2013).

The variance in fracture behaviour is due to stress redistribution around the crack tip during loading. These stress fields have enough time to redistribute at low loading rates, resulting in increased damage along the weak regions near the crack tip, particularly the grain boundaries, and encouraging intergranular fracture. On the other hand, high loading rates limit plastic strain development due to insufficient time, resulting in stiffer behaviour and a greater proclivity for transgranular fractures (Liang et al., 2015; Wasantha et al., 2015). According to the study's findings, mode II fracture has the most applied energy independent of loading rate because it generates a better fracture surface area (Mahanta et al. 2017). As a result, mode II fractures require additional energy to fail. The higher energy absorption is aided by the bigger surface area generated as a result of the shear opening. The cracks propagate along the fracture plane, resulting in the development of many smaller fracture surfaces and the fracture became sudden and brittle with the higher loading rate (Dai et al., 2013; Liang et al., 2015).

4.3.4 Effect of sulphate concentration content on the loading-rate dependent fracture toughness of CPB under mode-II loading

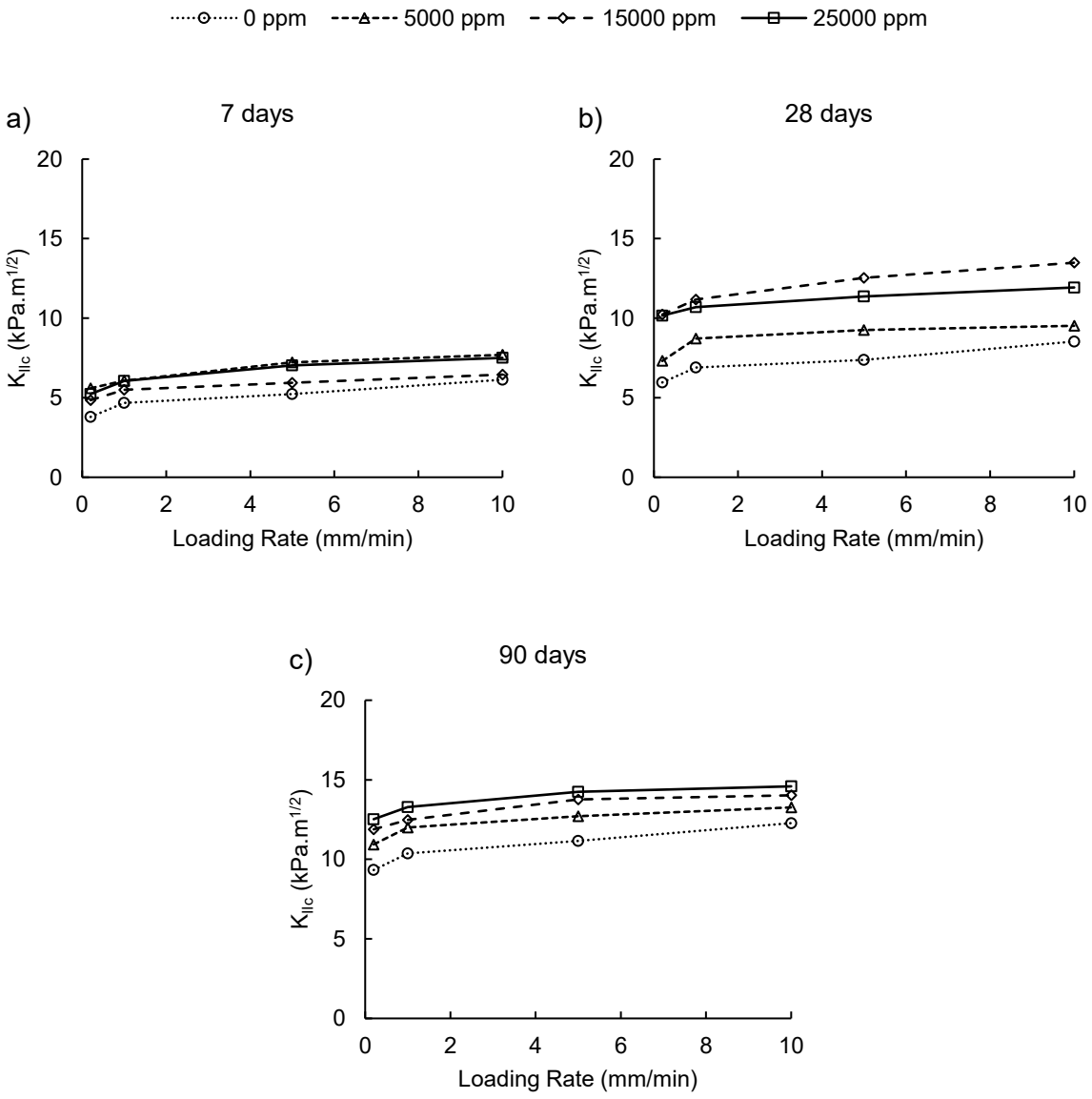

Figure 4.27. Effect of sulphate concentration on the loading rate-dependent mode-II facture toughness of CPB.

The experimental results shown in Figures 4.27 provide important insights into the fracture behaviour of specimens under various loading rates, sulphate concentration and curing time. It can be observed that sulphate ions influence the fracture toughness of the CPB varies over time. The consequences differ based on the sulphate concentration. After 7 days of curing, the sample D1-0 5000 ppm sulphate concentration has the highest fracture toughness. However, after 28 days of

curing, the samples with sulphate concentrations of E1-0 15000 ppm and F1-0 25000 ppm show progressively increase in fracture toughness. The addition of sulphate solution gradually reduces the interparticle bond strength, which affects the pre-peak behaviour of cementitious materials. Flatter pre-peak branches and a lower peak force in CPB serve as indicators of this weakening behaviour in mode II loading condition. Additionally, calcium hydroxide (CH) crystals inside the CPB matrix become fewer when sulphate concentrations rise as a result of the interaction between sulphate anions and CH (Fang & Fall, 2019). The constant depletion of CH caused by the development of ettringite worsens the early weakening of the cementation process since it is a vital byproduct of cement hydration that is responsible for particle binding strength (Yilmaz & Fall, 2017). The inhibitory effect of sulphate ions on binder hydration can be linked to the decrease in modes II fracture toughness at the early age of cement hydration. Sulphate ions impede the hydration process by producing a layer of ettringite on the un-hydrated cement particles, which acts as a barrier and inhibits water from reaching and hydrating the key binder components, such as C_3S and C_2S. With increasing sulphate ion concentrations, this inhibitory action becomes more prominent. As a result, macroscale softening behaviour is more pronounced in sulphate-rich CPB samples, and it gets stronger as sulphate concentration increases at early age CPB (Li & Fall, 2016).

The CPB matrix's microstructural alterations can be observed using scanning electron microscopy (SEM) as shown in Figure 4.5. Ettringite crystals, which have an acicular structure, are formed more frequently as sulphate concentration rises. These needle-like ettringite crystals slowly develop into longer rod-like crystals within the CPB matrix at the seven-day stage. It is crucial to remember that the strength of particle connections is unaffected by the ettringite's precipitation. However, due to the considerable amount of expansive ettringite crystals present in early aged cementation process in CPB matrix is significantly impacted. Expanding ettringite raises the resistance to particle friction by lowering the moisture content of the matrix, which also reduces the lubricating effect of pore water between particles. Furthermore, expansive ettringite induces a state of passive confinement within the toughened CPB matrix, strengthening the contact between the CPB matrix.

Additionally, the presence of sulphate ions in CPB has a retarding effect on binder hydration, which can be seen by evaluating EC values at various sulphate concentrations. Figure 4.28 depicts

how increasing sulphate concentrations (0, 5000, 15000, and 25000 ppm) alter the EC in CPB samples over time. As the initial sulphate concentration increases, the peak of electrical conductivity lags, indicating a delay in binder hydration. For example, after only 24 hours of mixing, the CPB sample without sulphate (0 ppm) has a peak EC value of 4.2 mS/cm. In comparison, the sample with 5000 ppm sulphate concentration takes around 36 hrs to reach a peak value of 5.4 mS/cm, while the sample with 15000 ppm and 25000 ppm sulphate concentrations take 48 hrs and 72 hrs, respectively, to reach their peak values (8.6 mS/cm and 11.4 mS/cm). The gradual decrease in EC can be due to the quick initial dissolution of sulphate ions and reactive alumina, followed by the formation of ettringite, which slows down after reaching its maximal value. This decrease is consistent with prior research highlighting C_3A inhibitory effect on the fast interaction between cement and water.

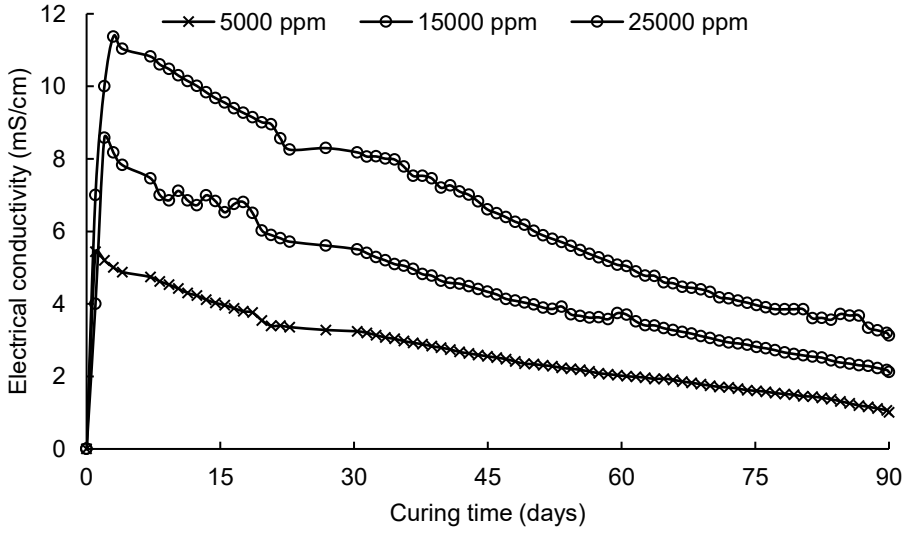

Figure 4.28. Effect of sulphate concentration on the evolution of electrical conductivity.

4.3.5 Effect of cement content on the loading-rate dependent fracture toughness of CPB under mode-III loading

In Figure 4.29, the relationship between loading rate and mode-III fractures toughness of CPB is presented. The figure demonstrates that an increase in loading rate leads to an improvement in mode-III fracture toughness. Notably, the influence of loading rate on fracture toughness appears to be more significant compared to the Cc and curing time, especially in the advanced age samples. The 7-day samples exhibit a linear trend, indicating that as loading rate increases, there is a

proportional increase in mode-III fracture toughness. From Figure 18 it is observed that the increase

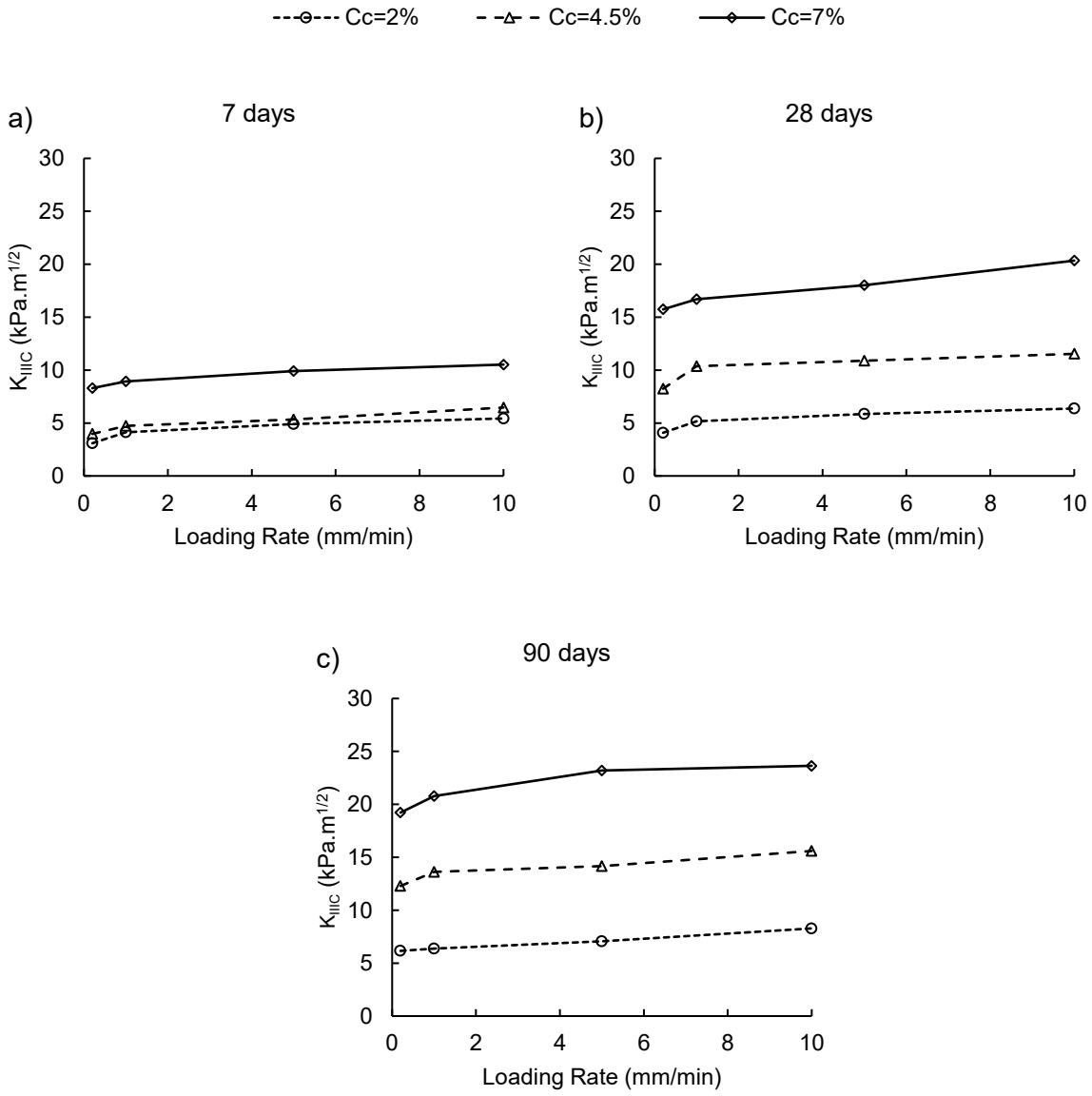

Figure 4.29. Effect of cement content on the loading rate-dependent mode-III fracture toughness of CPB.

in loading rate has a direct effect on its resistance to mode-III fracture toughness. The fracture toughness (K_{IIIC}) of the C1-0 (7 wt.% Cc) samples is much higher than that of the A1-0 (2 wt.% Cc) samples. This means that, regardless of Cc raise in loading rate promotes improved resistance to mode-III fracture. This is mostly due to creating a wide surface area following specimen failure. When a material fractures in mode III loading, a shear opening occurs along the fracture plane, significantly separating the two fracture surfaces. The applied energy creates new fracture surfaces

during mode III fracture. The cracks propagate along the fracture plane, resulting in the development of many smaller surfaces. Compared to other fracture types, this material fragmentation into smaller fragments necessitates a higher energy input. As a result, throughout the failure process, mode III fracture consumes more energy. The enhanced energy absorption is due to the wider surface area generated due to the shear opening results in increase fracture toughness (Mahanta et al., 2017).

However, the fracture toughness of the 28-day 7 wt.% Cc sample, on the other hand, is comparable to that of the 90-day 7 wt.% Cc sample as shown in Figure 4.29 (b &c). This implies that a longer curing time does not always result in a significant increase in mode-III fracture toughness above a specific cement content threshold and loading rate. This phenomenon can be linked to the completion of hydration process as because of the use of pore water by cement. Likewise, self-desiccation and the suction mechanism, in which water is drawn out of water-filled voids due to hydration processes, are thought to be responsible for creating capillary pore spaces in CPB materials. In the early phases of curing, linked capillary holes emerge because the rate of water loss through voids is higher than the rate at which hydration products precipitate. Hydration products like C-S-H and CH eventually fill these capillary holes as the hydration process advances. Additionally, the physical characteristics of the components affect the CPB transition from a paste phase to a solid phase as cement and water undergo chemical reactions at various speeds and during various curing stages. So that four phases of cement hydration products such as unreacted cement, surface products (including linked pores), pore products (without connected pores), and capillary pore space helps to determine the strength of CPB at different curing time.

4.3.6 Effect of sulphate concentration content on the loading-rate dependent fracture toughness of CPB under mode-III loading

The primary influence of the chemical reaction on the mechanical process is the bonding force between the CPB interface, which is a result of the increased degree of cement hydration. The presence of sulphate ions in CPB is typically having detrimental impacts, such as impeding cement hydration and affecting the microstructure of the interface through the development of ettringite (Cui & Fall, 2018). These ions can considerably affect the shear behaviour and characteristics of the CPB interface at early ages in the mode III loading condition. In addition to inhibiting cement hydration, the presence of sulphate ions can cause the formation of ettringite, which can either

refine or coarsen the microstructure of the interface, affecting its shear strength (Aldhafeeri & Fall, 2016; Cui & Fall, 2018; Fang & Fall, 2019). In Figure 4.30 the detrimental effect of higher conc-

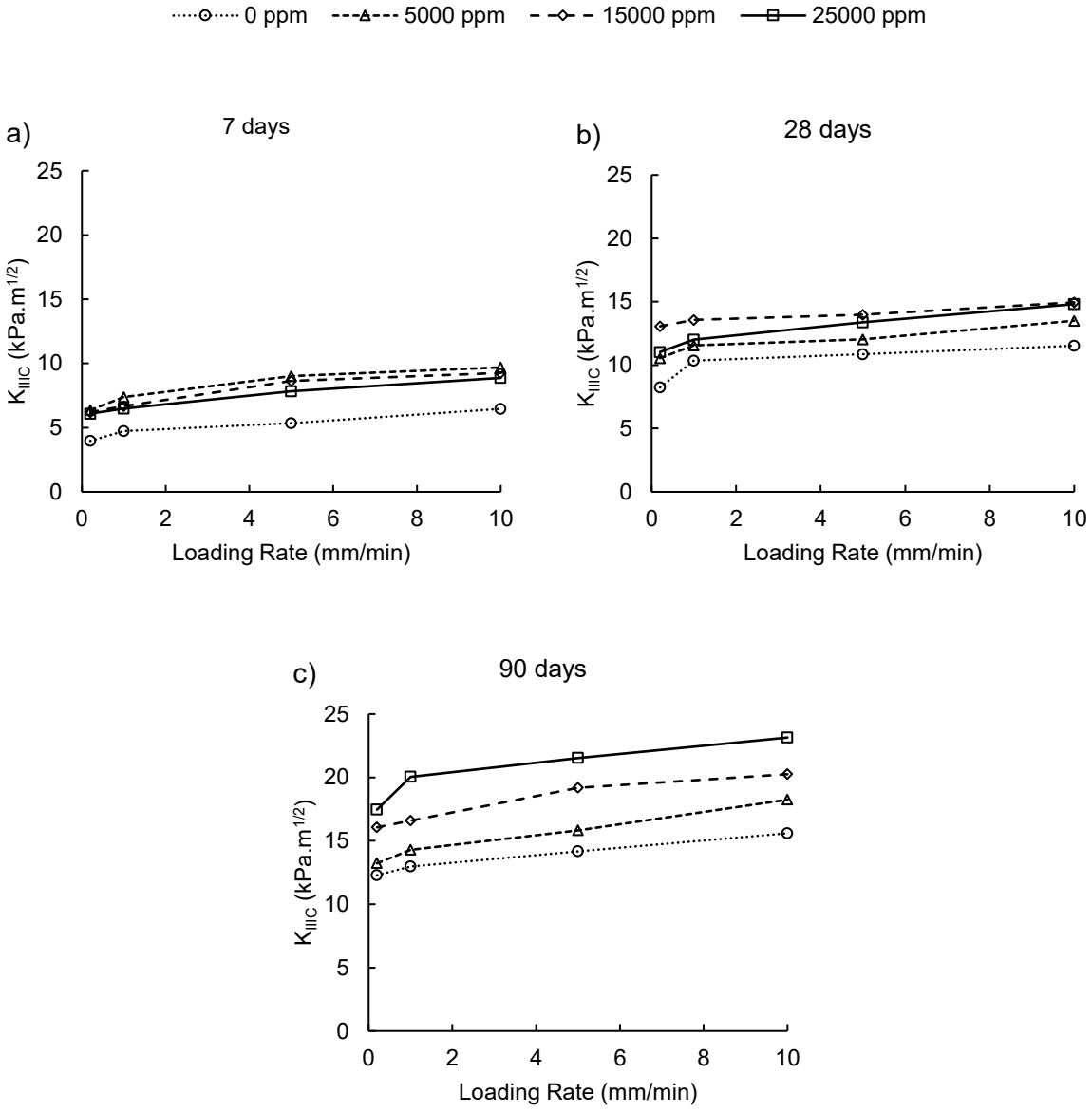

Figure 4.30. Effect of sulphate concentration on the loading rate-dependent mode-III fracture toughness of CPB.

centration of sulphate can be seen with lower concentration D1-0, E1-0 and F1-0 respectively having higher fracture toughness. This is consistent with study findings by Li & Fall (2018) which shows the negative effect of sulphate concentration on early day for strength development. However, the higher sulphate concentrated sample possess improved K_{IIIC} than the one without sulphate concentration B1-0 which is due to the formation of binding product in the presence of

sulphate and development of particles friction. The sample higher Sc sample E1-0, F1-0 and D1-0 start gaining its strength with the span of 28 days and at the end of 90 days the sample with higher Sc F1-0 possess higher fracture toughness followed by lower concentration E1-0 and D1-0 respectively. The interaction between sulphate concentration, adhesion, and the time-dependent evolution of shear strength sheds light on the complex nature of the behaviour at the interface (Fang et al., 2020).

The time-dependent evolution of the shear strength of interface samples with different sulphate concentrations demonstrates that adhesion and friction contribute to the formation of interface shear strength. Hence, it is reasonable to assume that the shear strength of pure mode III loading focuses solely on shear loading conditions is equivalent to the adhesion of the interface. The shear strength of the interface with varied degrees of sulphate concentration shows that the adhesion and friction between the materials contribute to the overall strength development on CPB (Fang et al., 2020; Fang & Fall, 2019). The loss in early-age strength is the coarsening of the pore structure of CPB matrix induced by the excessive production of expansive minerals such as ettringite (Ghirian & Fall, 2015). Likewise, the substantial inhibition of binder hydration in specimens with high sulphate concentrations (15,000 and 25,000 ppm) results in a reduction in the strength due to self-desiccation in CPB samples, developing the low matric suction. In Figure 4.11 we can observed that the sample with 5000 ppm Sc took 2 days to achieve matric suction of 12.7 kPa. Likewise, the sample with 15000 and 2500 ppm took 5 days and 8 days respectively to develop the matrix suction of 13.6 and 14.3 kPa respectively. The early age slowdown of matric suction is due to the inhibition effect of sulphate concentration in CPB which limits self-desiccation and restrain the matric suction development. Similarly, a decrease in the consumption of pore water as a result of higher sulphate concentrations in CPB lowers capillary pressure and hinders the processes that lead to self-desiccation (Bentz, 2008). The significant inhibition of binder hydration results in lower matric suction is often associated with reduced strength in unsaturated porous media. Similarly, from Figure 11, following 28 days curing period, the matric suction in CPB steadily rises with advancing age, reaching values of 11.1, 12.7, and 14.1 kPa at 90 days respectively for 5000, 15,000, and 25,000 ppm Sc sample. The improvement of matric suction in CPB at an advanced age is essential for encouraging self-desiccation and improving fracture toughness. The presence of sulphate ion on CPB goes through the different mechanism including C-S-H absorption, the production of ettringite, and reactions with CH that result in the production of gypsum (Li & Fall,

2018). The production of low-quality C-S-H due to absorption results in formation of inferior quality C-S-H gel thereby reduces the strength at early age. Furthermore, in a study by Pokharel & Fall (2011) illustrate that the reduced production of C-S-H and CH as an effect of sulphate concentration at early 7 and 28 days. The intensity of C-S-H and CH is found to be higher in the sulphate-free cemented paste than in the samples with a sulphate concentration of 25,000 ppm, demonstrating that sulphate inhibits the formation of C-S-H and CH. Additionally, high intensity of ettringite formation with the increase sulphate concentration creates expansive pressure due to ettringite crystallization, and these pressures have the potential to adversely reducing strength at the early age CPB (Pokharel & Fall, 2011). Along with from the early phases of the chemical reaction forming ettringite are seen in SEM image (Figure 4.5) as rod-like crystals with a significant filling of capillary holes. Ettringite is the predominant cement hydration product at young ages (7 days), with low formation of CH, according to analysis of SEM images from samples with various curing periods. The production of C-S-H, which is essential for connecting tailings particles and filling capillary spaces, is relatively less significant in the initial stages but increment is significant as the cement hydration progresses. SEM photos of the samples at 28 and 90 days show substantial C-S-H production and negligible ettringite which reflect the advance age bonding strength due to cement hydration.

4.4 Loading rate-dependent fracture work of CPB

4.4.1 Effect of cement content on the loading-rate dependent fracture work of CPB under mode-I loading

When crack propagation is investigated, the 7-day and 28-day samples require less energy to initiate the crack propagation as the loading rates increase from 0.2, 1, 5, and 10 mm/min. The 90-day sample, however, reveals an increase in work of crack initiation with respect to an increase in loading rate, curing duration, and cement content. These findings are consistent with the resultant effect of fracture toughness and material stiffness. The failure process in the materials is characterized by the simultaneous spread of many microcracks under high loading rates. High loading rates prevent microcracks from having enough time to determine routes with the least energy or resistance, unlike quasi-static loading, where a single macro-crack is initiated and propagates relatively sluggishly. As we can see from Figure 4.31, fracture energy required to

initiate the crack for 7-day group A1-0, B1-0 and C1-0 samples showed a significant increment with the increase in loading rate. For instance, fracture energy required for the 7-day B1-0 sample is 4.34, 5.39, 5.90 and 6.60 mJ at 0.2,1,5, and 10 mm/min loading rates, respectively. The increment for the same test group B1-0 at 90 days is 7.64, 9.78, 11.73 and 13.84 mJ which is 176%, 181%, 198% and 234% higher than the 7-day sample. The consumption of free water in advanced ages CPB reduces VWC, which decreases the rate sensitivity for dry CPB material at a lower loading rate, but its rate effect is significantly increased at a higher loading rate. This explanation supports the higher fracture energy required to initiate the crack for a higher loading rate (Mindess et al., 2003). The inertia effect in the specimen substantially contributes to the strength growth when exposed to higher loading rates. Fracture propagation becomes difficult due to the inertia of the entire material and the micro-inertia surrounding the crack tip. The increased inertia slows the progression of cracks and requires more energy to cause fractures.

Furthermore, the development of numerous microcracks amplified as the loading rate rose. Thus, more significant crack initiation and propagation density result from increased microcracks inside the material as the loading rate increases. This accelerated crack growth contributes to the overall loading rate influence on the CPB's mechanical response (Vegt, 2007). Rapid loading forces these micro-cracks to spread along the shortest pathways, frequently with higher resistances. The microcracks spread throughout the material, resulting in smaller-scale deterioration and disintegration. The critical deformation and energy needed for fracture under high loading rate increase significantly when many microcracks are dispersed throughout the material. The particular fracture energy needed to initiate new fracture surfaces per unit area is anticipated to rise as loading rates increase (Brara & Klepaczko, 2007; Bischoff & Perry, 1991). This is because compared to the propagation of a single macro-crack, the simultaneous propagation of many micro-cracks requires more energy. The limited time available for micro-cracks to identify optimum propagation channels at high loading rates promotes their caused propagation down suboptimal paths. As a result, the material sustains more damage and fragmentation, needing more energy to sustain a fracture. Therefore, the specific fracture energy tends to rise as a function of the loading rate. However, rate sensitivity for that to quasi-static loading rate (0.2 mm/min), the effect is slight, ascribed to the viscous effect caused due to the presence of free water in pores of CPB matrix (Zhang et al., 2009)

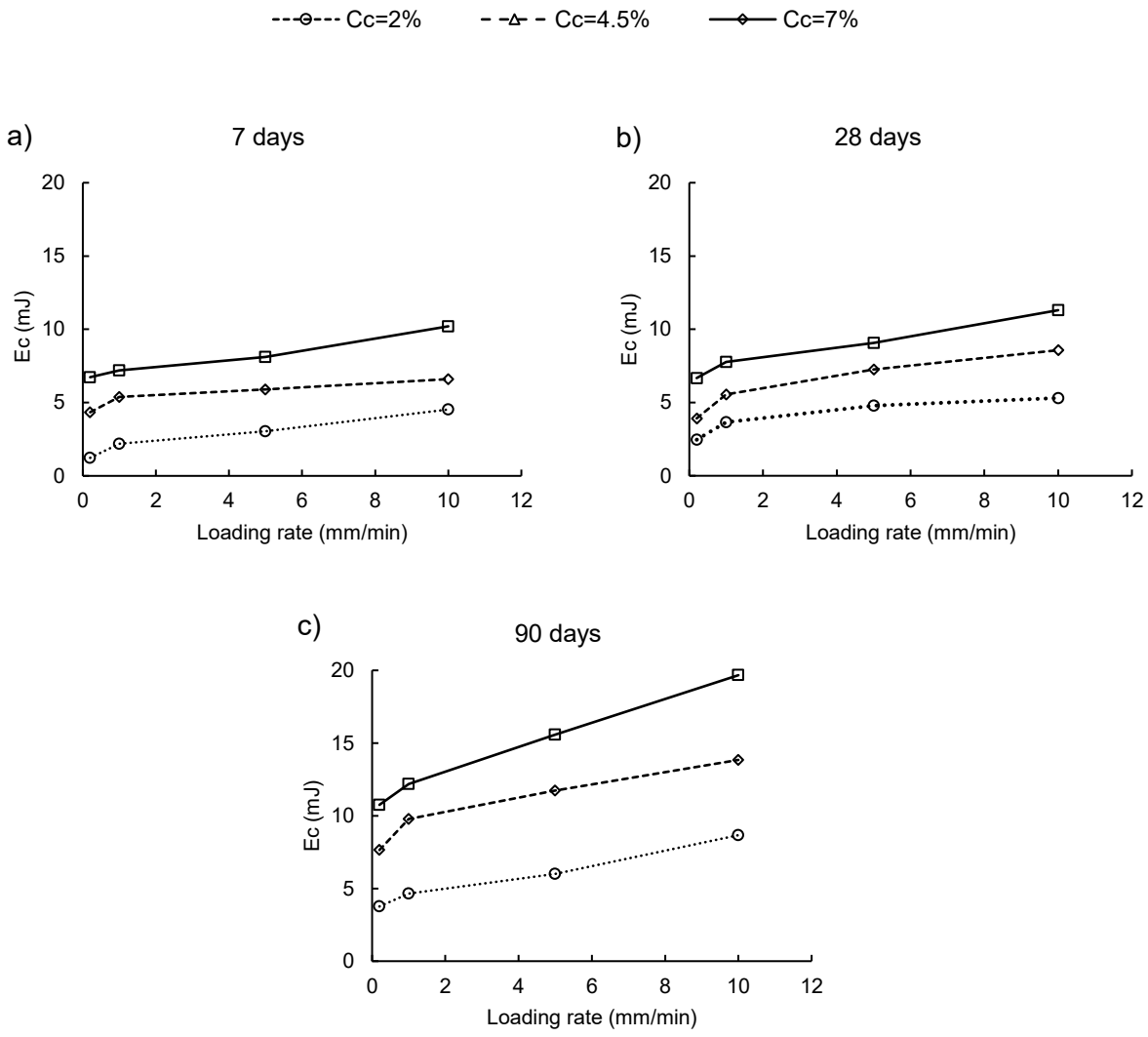

Figure 4.31. Effect of loading rate on evolution of work of crack initiation at (a) 7 days, (b) 28 days, and (c) 90 days.

4.4.2 Effect of sulphate concentration content on the loading-rate dependent fracture work of CPB under mode-I loading

To further support the fracture toughness behaviour with the increase in Sc concentration, we can observe a similar graph pattern for the fracture energy requirement to initiate the crack growth. For early 7-day sample the 5000 ppm Sc sample required 5.69, 6.14, 6.81 and 7.60 mJ to initiate the crack in 0.2, 1, 5 and 10 mm/min loading rate. This is 8% (5.22), 4% (5.88), 6% (6.04) mJ and 11% (6.90) higher than 1500 ppm Sc and 113% (5), 1% (5.66), 4% (5.91) and 11% (6.73) mJ higher than 2500 ppm Sc for the same curing period. However, the change in chemical reaction between the sulphate ion with cement changes the pore structure with respect to curing time. The higher sulphate-concentrated sample gradually starts to gain more bonding strength. The

intermediate curing time of 28 days explains the gradual rise of fracture energy as CPB starts to begin cement hydration that is caused due to the retardation effect for the higher concentration of sulphate. As we can see in Figure 4.32 the 90-day sample with higher Sc of 25000 ppm has higher fracture energy of 14.67, 15.61, 18.08 and 19.91 mJ which is 48%, 42%, 48% and 49%higher than the 15000 ppm sample and 65%, 63%, 67% and 66% higher than 5000 ppm sample. The strength development w.r.t change in matric suction, VWC, and EC result discussed above to comply with the fracture energy requirement for initiating the crack on the CPB sample.

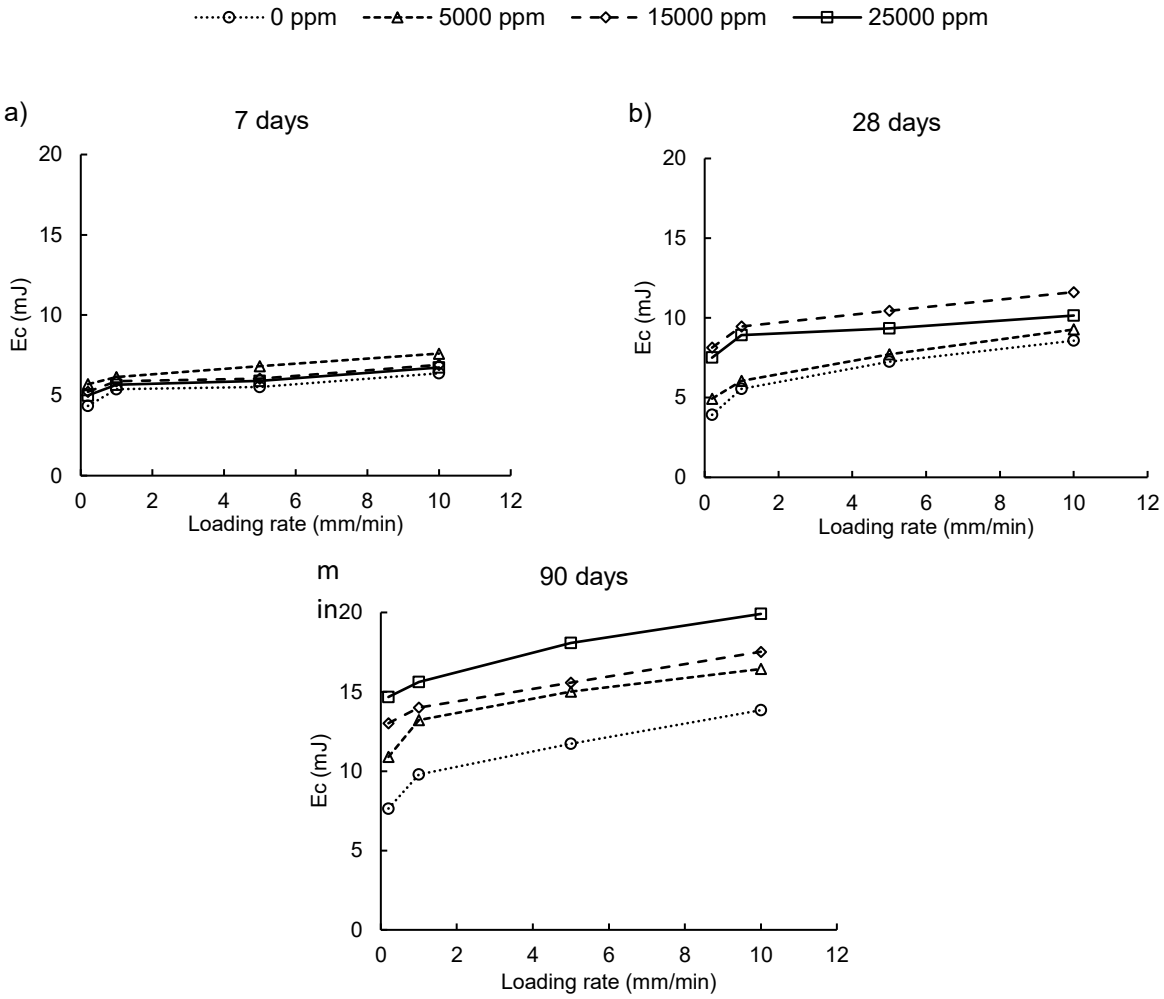

Figure 4.32. Effect of loading rate effect on evolution of work of crack initiation at (a) 7 days, (b) 28 days, and (c) 90 days.

4.4.3 Effect of cement content on the loading-rate dependent fracture work of CPB under mode-II loading

Significant variations in the energy required to initiate cracks (fracture energy) were observed in Figure 4.33 for samples belonging to groups A1-0, B1-0, and C1-0 at 7 days, depending on the loading rate. Notably, as the loading rate increased, the fracture energy also showed a substantial increase. For example, the B1-0 sample at 7 days exhibited fracture energies of 16.96, 18.02, 20.77, and 21.36 mJ for loading rates of 0.2, 1, 5, and 10 mm/min, respectively. This indicates a clear upward trend in fracture energy with higher loading rates. Comparing the 7-day sample to the same B1-0 test group after 90 days, even more significant increments in fracture energy were observed. The fracture energies at 90 days were recorded as 31.54, 44.11, 52.49, and 63.72 mJ for loading rates of 0.2, 1, 5, and 10 mm/min, respectively. These values represent substantial increases of 85%, 144%, 152%, and 198%, respectively, compared to the fracture energies of the 7-day sample. The growth of multiple microcracks becomes increasingly obvious as the loading rate rises. As a result, the material experiences a higher density of crack initiation and spread. According to (Vegt, 2007), the overall effect of loading rate on the mechanical response of CPB is influenced by the faster crack propagation under a higher loading rate. Under increased loading, microcracks frequently find stronger resistances as they spread over shorter routes. As a result, the material begins to degrade and break on a smaller scale and develops microcracks all around. Numerous microcracks scattered throughout the material considerably raise the critical deformation and energy needed for fracture under accelerated loading. Accordingly, as observed by (Bischoff & Perry, 1991; Brara & Klepaczko, 2007), the specific fracture energy required to begin new fracture surfaces per unit area is projected to increase with rising loading rates. This is due to the fact that numerous microcracks propagating simultaneously use more energy than a single macrocrack does. When loading rates are high, microcracks have little time to discover the best channels for their propagation, which encourages them to go through less-than-ideal routes. Because of the increased damage and fragmentation, the material requires more energy to fracture. So, as the loading rate increases, the specific fracture energy tends to do so as well. According to (Zhang et al., 2009), the rate sensitivity effect is modest under lower loading rates (e.g., 0.2 mm/min), mostly because of the viscous effect brought on by the presence of free water in the CPB matrix's pores. A decrease in rate sensitivity for CPB material at lower loading rates is brought about by the

consumption of free water in advanced aged CPB, which lowers the VWC as shown in Figure 4.22. However, when loading rates are higher, the inertia effect is noticeably more pronounced. These phenomena can be explained by the fact that, when exposed to increasing rates of loading, both the material's inertia and the micro-inertia surrounding the crack tip significantly contribute to the rise of strength. As a result of the increased inertia, it takes more energy to create fractures and slows down crack development.

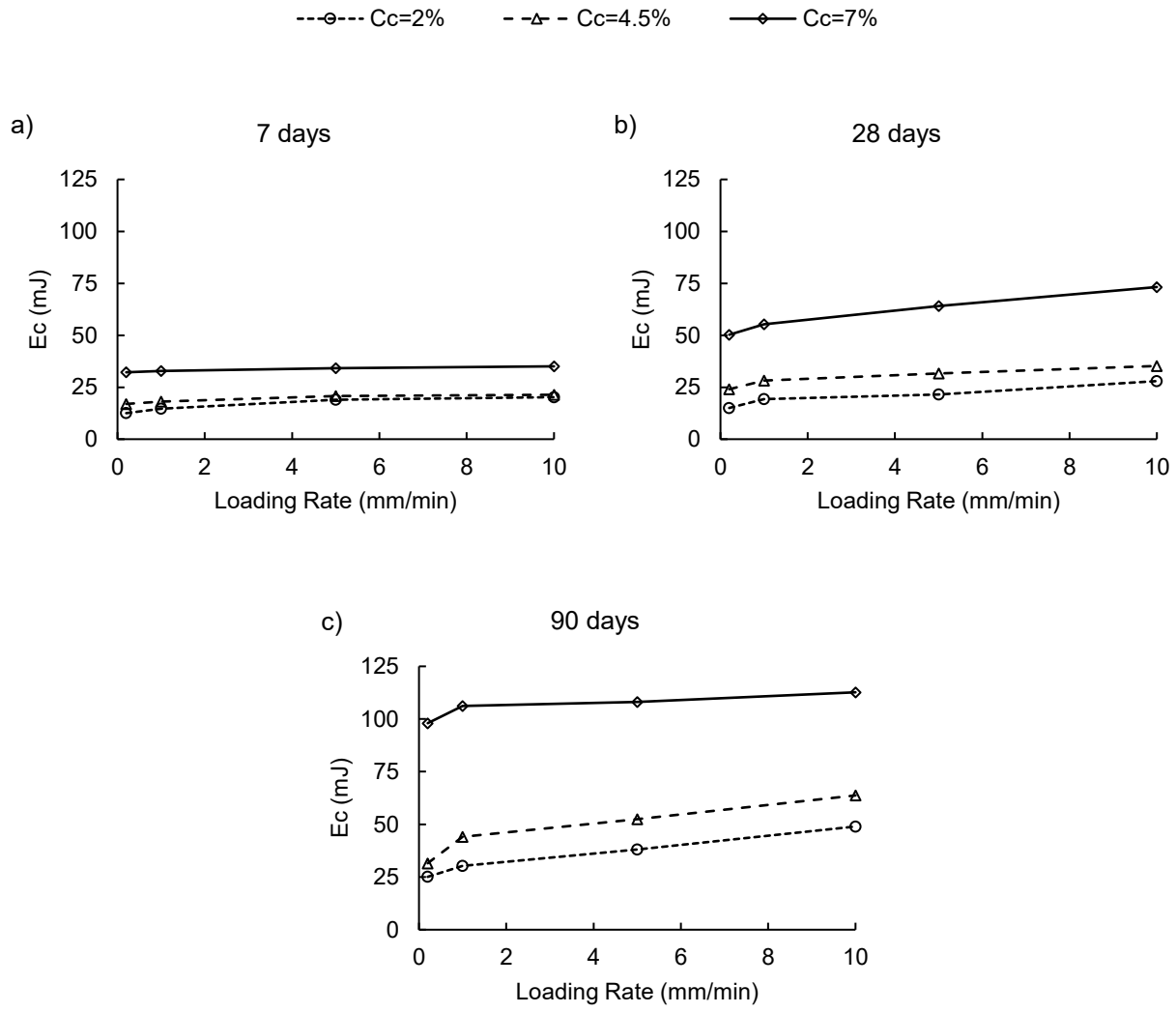

Figure 4.33. Effect of cement content on the loading rate-dependent mode-II fracture work of CPB.

Furthermore, the presence of angular aggregates with sharp edges in tailings, which are made up of the byproducts of crushed and milled materials following the ore refining process, helps to improve both strength and stability (Ismailov et al., 2020). This is because the tailings particles can interlock more effectively by hydration product. The denser matrix that is created as a result

of the higher cement content is a major contributor to this improvement. By increasing internal friction and adhesiveness of the material, this interlocking effect increases resistance to movement and displacement when the material is loaded (Qi & Fourie, 2019). The material's resistance to fracture initiation and propagation is aided by the denser matrix created by the increased cement concentration and made possible by the interlocking of tailings particles. As a result, with the increase in loading rate more energy is needed to start cracks in the CPB material. The CPB matrix's increased cohesiveness and internal friction cause a stronger resistance to fracture formation, requiring more energy to initiate cracks.

4.4.4 Effect of sulphate concentration content on the loading-rate dependent fracture work of CPB under mode-II loading

Figure 4.34 shows how the loading rate affects the mode II work of crack initiation in CPB due to the concentration of sulphate. The findings demonstrate that the retardation effect seen in the early day samples is influenced by the sulphate concentration. In particular, the sample with 5000 ppm requires more energy to initiate a crack at 7 days than the samples with 15000 ppm and 25000 ppm. The higher concentrated samples, however, gradually become stronger and require more energy to start cracking as the curing period progresses. The sample with the highest energy needs for crack initiation at 28 days is the one with 15000 ppm, followed by samples with 25000 ppm and 5000 ppm, respectively. After 90 days, the samples with 15000 ppm and 5000 ppm require the least amount of energy for crack initiation, whereas the CPB sample with 25000 ppm requires the most energy. This shows that as the curing period increases, the higher cement concentration results in increased strength and makes it harder to start cracks. Furthermore, the samples show that higher loading rates significantly increase the amount of energy required. This further emphasizes the connection between the loading rate and the fracture energy needed for crack initiation in CPB by implying that a higher loading rate necessitates more effort to achieve crack initiation. Likewise Figure 4.35 demonstrates the behaviour of the crack and its path of propagation under mode II loading, specifically the wing fracture originating from the crack tip. The initiation position of the wing crack gradually shifts toward the crack tip. This shift indicates that the wing crack tends to originate closer to the tip of the pre-existing crack.

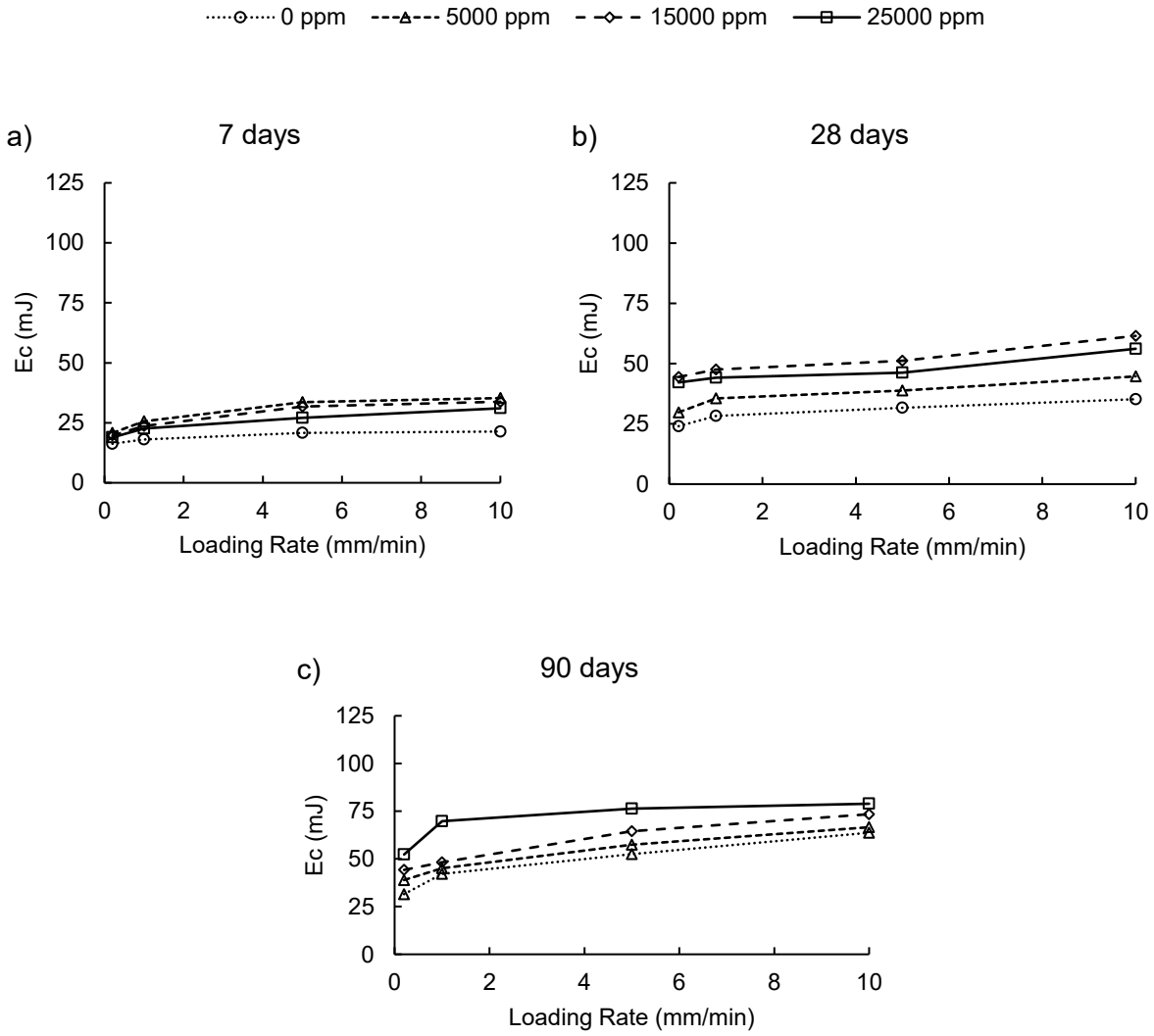

Figure 4.34. Effect of sulphate concentration on the loading rate-dependent mode-II fracture work of CPB.

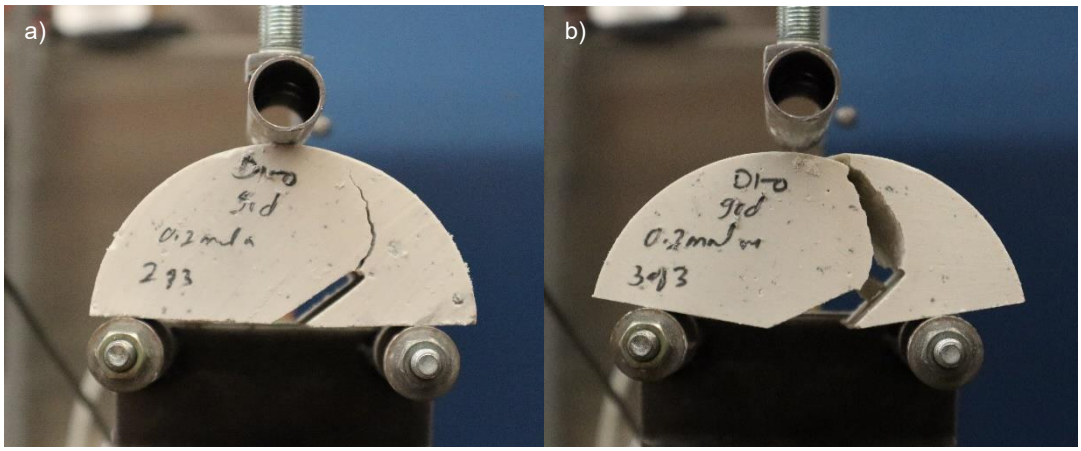

Figure 4.35. Mode II failure pattern.

4.4.5 Effect of cement content on the loading-rate dependent fracture work of CPB under mode-III loading

Depending on the loading rate, Figure 4.36 showed noticeable changes in the fracture energy needed to start cracks in samples containing 2 wt.% Cc, 4.5 wt.% Cc, and 7 wt.% Cc at 7 days. With higher loading rates, it was seen that the fracture energy significantly increased. The 4.5% Cc sample, for instance, showed fracture energies of 24.09, 31.34, 46.99, and 64.23 mJ at 7 days for loading rates of 0.2, 1, 5, and 10 mm/min. Even more significant increases in fracture energy were seen when comparing the 90-day sample to the 7-day 4.5 wt.% Cc sample.

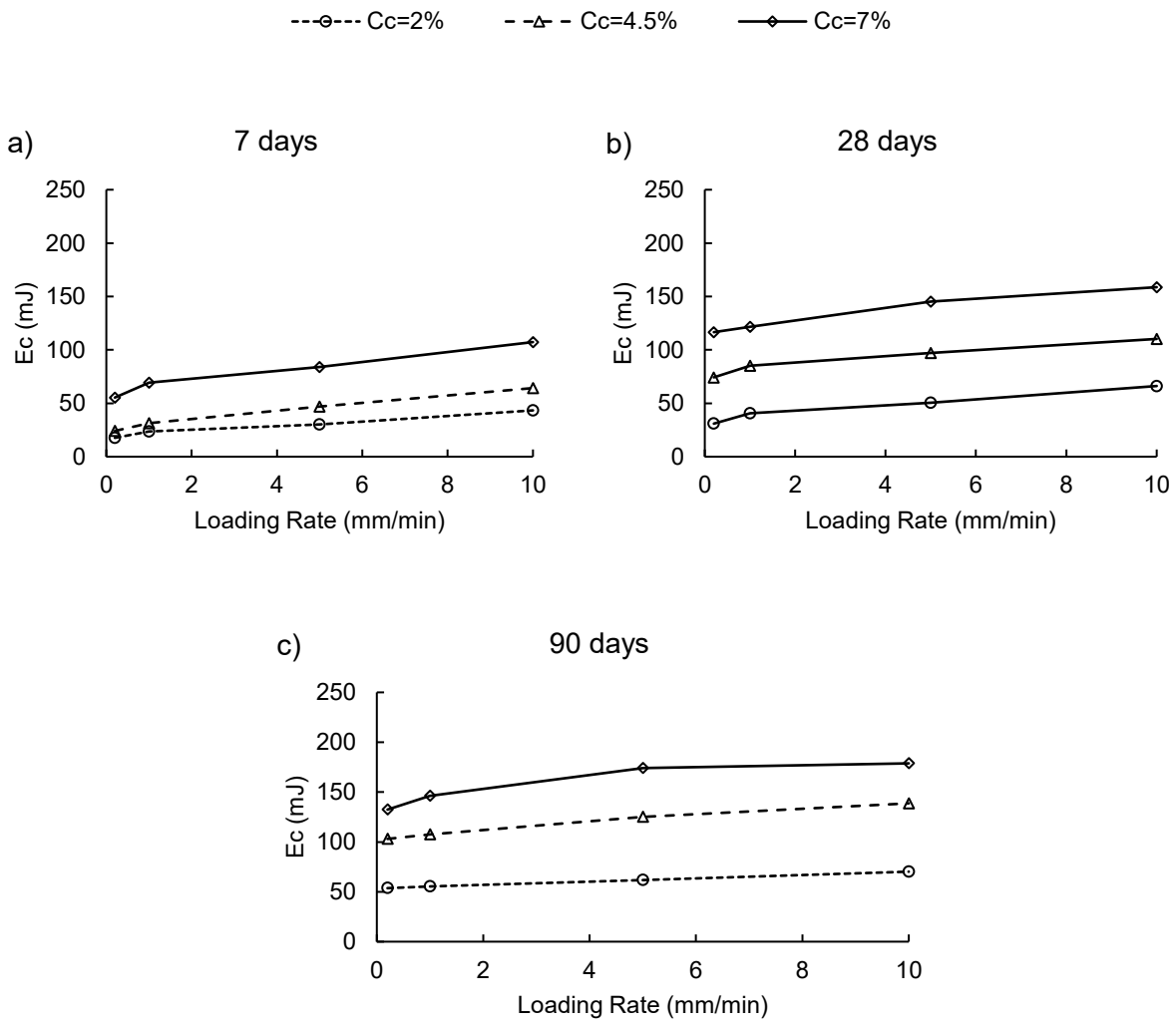

Figure 4.36. Effect of cement content on the loading rate-dependent mode-III fracture work of CPB.

For loading rates of 0.2, 1, 5, and 10 mm/min, the fracture energies at 90 days were calculated as 103.06, 107.59, 125.25, and 138.70 mJ, respectively. These numbers demonstrated significant increases over the fracture energies of the 7-day sample by amounts of 327%, 243%, 166%, and 115%, respectively. In mode III loading the region around the original crack, where microcracks develop, is referred to as the fracture process zone. These microcracks occur at an angle rather than parallel because they are inclined to the fracture plane. The complicated stress distribution experienced during shear loading results in inclined microcracks. In order to carry compression stresses, the intact material situated between two adjacent inclined fissures is quite important. These angled microcracks pass along some of the stress from the main crack as it develops to the intact CPB matrix that is situated between them. The initial crack cannot form and spread quickly because of the compression forces exerted on this material. The inclined microcracks contribute to preventing early failure by transferring stress. They enable the material to absorb additional energy before total fracture takes place. This means that it increases the CPB material's overall energy requirement to initiate the fracture by allowing it to endure greater loads and improving its capacity to resist crack development (Firoozi et al., 2018). With rising loading rates, the fracture energy clearly trended upward. The results clearly indicated a strong correlation between loading rate and fracture energy. As the loading rate increased, the energy required to initiate cracks in the samples with 4.5 wt.% Cc at both 7, 28 and 90 days exhibited significant rises. This observation underscores the influence of loading rate on the fracture behaviour of the CPB samples.

4.4.6 Effect of sulphate concentration content on the loading-rate dependent fracture work of CPB under mode-III loading

The relationship between fracture energy and sulphate concentration, as well as curing time, is visually represented in Figure 4.37. Notably, fluctuations in sulphate concentration have a significant influence on fracture energy, particularly at advanced ages. However early age samples with higher sulphate concentration have detrimental effect for achieving the higher fracture energy. This consistent pattern is found for CPB across mode II and mode III loading circumstances. CPB specimens with higher sulphate concentrations have a greater ability to absorb strain energy as they mature, thus limiting the onset and advancement of cracks within the matrix. Fracture surface formation requires the conversion of strain energy for energy dissipation. The addition of sulphate anions increases fracture energy, indicating an improvement in the crack surface energy of CPB.

This improvement can be due to the confinement given by expanding hydration products, which strengthens the material's resistance to crack propagation. As a result, CPB specimens with higher sulphate concentrations require more strain energy to promote crack formation. Additionally, Figure 4.38 illustrates the pure mode III fracture patterns frequently seen for the tested materials. From the image, it can be seen that the pure mode III fracture path has a twisted configuration about the middle section. The fracture path's trajectory follows an anti-symmetric curved surface about the initial crack plane.

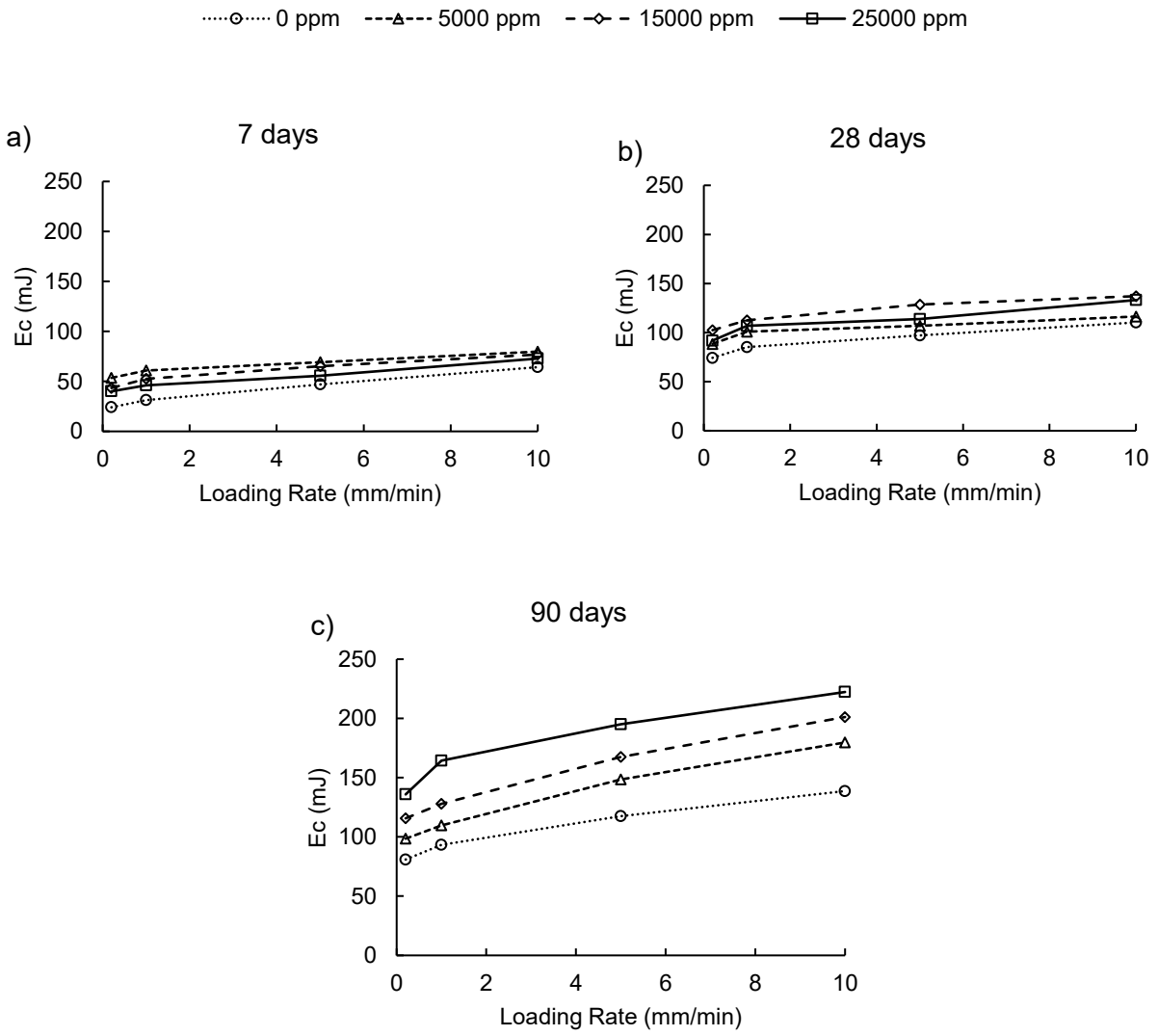

Figure 4.37. Effect of sulphate concentration on the loading rate-dependent mode-III fracture work of CPB.

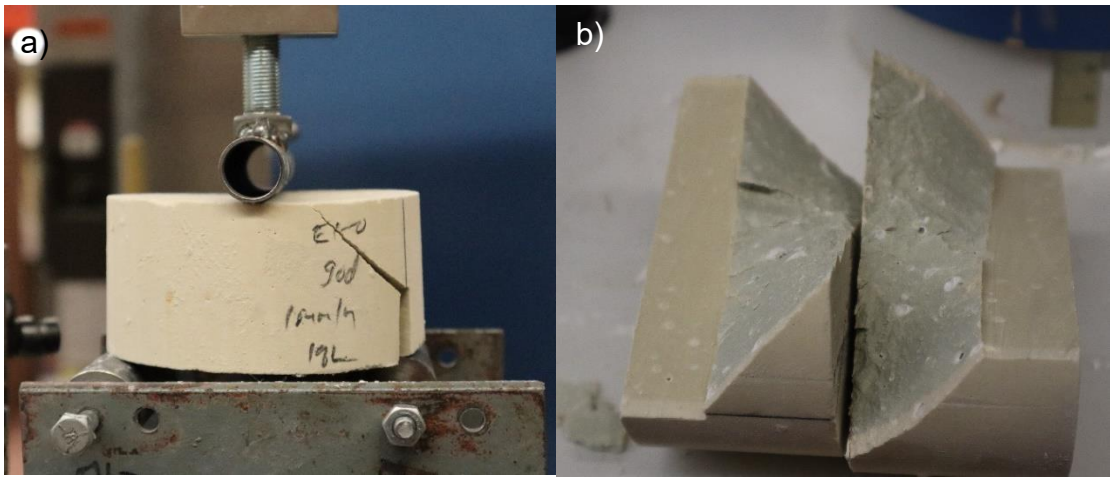

Figure 4.38. Mode III failure pattern.

Chapter 5 Conclusions and recommendations

5.1 Conclusions

This comprehensive experimental testing program has been successfully conducted to investigate the complex effects of cement content (2 wt.%, 4.5 wt.%, and 7 wt.%) and sulfate concentration (5000 ppm, 15000 ppm, and 25000 ppm) on the loading-rate dependent (0.2 mm/min, 1 mm/min, 5 mm/min, and 10 mm/min) fracture behaviour and properties of CPB at three different curing times (7, 28, and 90 days). To consider different loading conditions, a series of SCB tests and ENDB tests were employed to explore the mode-I (tensile stress), mode-II (in-plane shear stress), and mode-III (out-of-plane shear stress) fracture behaviour and properties under different loading rates, respectively. Moreover, auxiliary analysis, including SEM observation and a mould-based monitoring program (i.e., measurement of matric suction, volumetric water content, and electrical conductivity), were also performed to reveal the mechanisms responsible for the evolution of loading-rate dependent fracture behaviour and properties. Based on the obtained results, the key findings of this study can be summarised as follows:

(1) The load-displacement curves under mode-I, mode-II, and mode-III loading conditions demonstrate a noticeable sensitivity to variations in loading rates. As the loading rate increases, CPB shows a steeper pre-peak portion of the load-displacement curves and an increased peak load. However, CPB constantly exhibits unnoticeable post-peak resistance irrespective of changes in loading rates.

(2) As the cement content increases, the sensitivity of load-displacement curves to the loading rate becomes more evident. Nonetheless, changes in cement content cannot improve CPB's post-peak response.

(3) Increasing sulphate concentration results in the changes in dependence of load-displacement curves on the loading rate. The results show that the load-displacement curves become more sensitive to the loading rate as the sulphate concentration increases. Similarly, no changes in post-peak resistance were measured when the sulphate concentration changed.

(4) Material stiffness consistently increases with the loading rates, especially when a higher cement content is adopted. The stiffer CPB materials can potentially promote the immediate support of the backfill structure to the surrounding rock.

(5) The loading-rate dependent material stiffness can be further improved by increasing sulphate concentration (up to 15000ppm) from early to advanced ages. When sulphate concentration reaches 25000ppm, the continuous improvement in stiffness was only measured at 90 days, and a degradation in stiffness was detected at 7 and 28 days.

(6) The fracture toughness (K_{IC}, K_{IIC}, and K_{IIIC}) of CPB are highly sensitive to the loading rates, especially at a cement content of 7 wt.%. However, the rate of changes in fracture toughness decreases as the loading rate increases.

(7) The effects of sulphate concentration on the loading-rate dependent fracture toughness are similar to those observed from material stiffness; namely, increasing sulphate concentration up to 15000 ppm can steadily promote fracture toughness, while the addition of 25000ppm sulphate solution negatively affects 7-day and 28-day fracture toughness. The similarity between fracture toughness and stiffness indicates these two fracture toughness are strength-related properties.

(8) Compared with stiffness and fracture toughness, fracture work shows weaker sensitivity to the loading rates, especially under mode-I loading conditions. As the cement content increases, fracture work of CPB shows an improvement in the dependence on the loading rates, especially at advanced ages.

(9) The influence of sulphate concentration on the fracture work is relatively limited, especially at early ages. Therefore, CPB shows a similar change in fracture work as the sulphate concentration increases. This is because the resultant expansive phase, such as AFt, can reduce the deformation tolerance of CPB and weaken its energy dissipation capacity.

(10) The SEM observations confirm that a higher cement content results in more C-S-H precipitated in the CPB matrix and thus promotes the bond strength between tailing particles. Consequently, a stiffer and more rigid CPB can be obtained as curing time increases. However, CPB with a higher cement content also leads to weakened ductility and reduces the deformation tolerance of CPB, especially at a higher loading rate.

(11) A considerable amount of expansive ettringite was observed from CPB, especially at a higher sulphate concentration. The generated expansive ettringite adversely affects the integrity of the CPB matrix at early ages. However, the resultant crystallisation pressure can facilitate a passive confining pressure in the CPB matrix, thus promoting advanced-age stiffness, fracture toughness, and fracture work.

(12) As cement content and sulphate concentration increased, a mould-based monitoring program recorded a higher matric suction associated with a lower water content. The higher matric suction can pull the tailing particles to a greater extent and thus improve the material resistance to stress, which can contribute to the improvement of loading-rate dependent stiffness, fracture toughness, and fracture work.

(13) The measurement of EC confirms that the changes in cement content and sulphate concentration can influence the evolution of electrical conductivity and the progression of hydration in the CPB matrix. Consequently, the chemical factors, including cement content and sulphate concentration, must be fully considered for the reliable and accurate assessment of fracture behaviour and properties of CPB under different loading rates.

This thesis research work reveals the effect of cement content and sulphate concentration on the evaluative fracture behaviour and properties of CPB under various loading rates, and the obtained findings have the potential to promote the safe and optimal design of CPB materials in underground mining operation.

5.2 Recommendations for future work

As the mine backfill technology progresses, it becomes clear that there are still unexplored pathways and obstacles in comprehending the complex interplay of factors impacting its behaviour and performance. The preceding study shed insight into the sulphate induced effect on fracture behaviour on CPB, providing exciting findings, but it also underlines the need for additional research to improve our understanding of this crucial backfill technique. In this context, the following recommendations serve as a road map for future research endeavors aimed at filling gaps in present knowledge and propelling CPB understanding to new heights.

1. Development of Mathematical Modeling

Create thorough mathematical models that account for the amount of cement, the ratio of water to cement, the concentration of sulphate, and the duration of curing time. By digging further into the complex interrelationships between these variables, this modeling technique can offer a more comprehensive comprehension of CPB behaviour. Utilize experimental data to validate the models.

2. Validation under Dynamic Loading Circumstances

To simulate and study CPB behaviour under intricate loading conditions, use dependable mathematical models. This stage is crucial for bridging the knowledge gap between controlled laboratory settings and real-world mining operations, where loading circumstances are frequently complex and difficult to mimic.

3. Investigating Excessive Sulphate Concentrations

Examine sulphate concentrations higher than 25000 ppm to determine the point at which material performance starts to deteriorate. Understanding the top bounds of sulphate inclusion in CPB-type materials and how it affects long-term behaviour is essential.

4. Combining Data from Models and Experiments

Make a strong link between the predictions of mathematical modeling and the outcomes of experiments. With this integration, forecasts will be more reliable and the CPB response under

different conditions will be more accurately represented. This is particularly important to guarantee that the results can be applied to real-world mining situations.

5. Comprehensive Analysis of Fracture Behaviour

Examine the mode-I, mode-II, and mode-III fracture behaviour in CPB at various curing durations and sulphate concentrations. Use other mechanical observation methods to obtain a more thorough understanding of the material qualities, such as XRD analysis. This method will help characterize CPB's reaction to sulphate inclusion in a comprehensive way.

6. Interdisciplinarity Cooperation:

To improve the study, promote cooperation with professionals in relevant disciplines including materials science, chemistry, and geology. Multidisciplinary perspectives can offer a more comprehensive understanding of CPB behaviour and inspire creative problem-solving and research methodologies.

7. Long term Durability Studies

Expand the research to incorporate durability studies that evaluate the long-term performance of CPB. This will give important information for long-lasting and sustainable backfill solutions in mining applications by illuminating the material's durability and behaviour over time. Researchers may further our understanding of CPB behaviour and ensure the development of more robust and efficient backfill systems in mining operations by focusing on these areas of future research.

References

Akcil, A. (2003). Destruction of cyanide in gold mill effluents: Biological versus chemical treatments. *Biotechnology Advances*, *21*(6), 501–511. https://doi.org/10.1016/S0734-9750(03)00099-5

Alainachi, I., & Fall, M. (2021). Chemically induced changes in the geotechnical response of cementing paste backfill in shaking table test. *Journal of Rock Mechanics and Geotechnical Engineering*, *13*(3), 513–528. https://doi.org/10.1016/j.jrmge.2020.11.002

Al-Amoudi, O. S. B. (1998). Sulfate attack and reinforcement corrosion in plain and blended cements exposed to sulfate environments. *Building and Environment*, *33*(1), 53–61. https://doi.org/10.1016/S0360-1323(97)00022-X

Aldhafeeri, Z., & Fall, M. (2016). Time and damage induced changes in the chemical reactivity of cemented paste backfill. *Journal of Environmental Chemical Engineering*, *4*(4, Part A), 4038–4049. https://doi.org/10.1016/j.jece.2016.09.006

Aliha, M. R. M., Bahmani, A., & Akhondi, Sh. (2015). Determination of mode III fracture toughness for different materials using a new designed test configuration. *Materials & Design*, *86*, 863–871. https://doi.org/10.1016/j.matdes.2015.08.033

Araújo, E. E. B. de, Simon, D., França, F. A. N. de, Neto, O. de F., & Jr, O. F. dos S. (2017). Shear Strength of a Cemented Paste Backfill Submitted to High Confining Pressure. *Applied Mechanics and Materials*, *858*, 219–224. https://doi.org/10.4028/www.scientific.net/AMM.858.219

Aubertin, M., Li, L., Arnoldi, S., Belem, T., Bussière, B., Benzaazoua, M., & Simon, R. (2003). *Interaction between backfill and rock mass in narrow stopes*.

Ayatollahi, M. R., & Aliha, M. R. M. (2006). On determination of mode II fracture toughness using semi-circular bend specimen. *International Journal of Solids and Structures*, *43*(17), 5217–5227. https://doi.org/10.1016/j.ijsolstr.2005.07.049

Ayatollahi, M. R., & Saboori, B. (2015). A new fixture for fracture tests under mixed mode I/III loading. *European Journal of Mechanics - A/Solids*, *51*, 67–76. https://doi.org/10.1016/j.euromechsol.2014.09.012

Bentz, D. P. (2008). A review of early-age properties of cement-based materials. *Cement and Concrete Research*, *38*(2), 196–204. https://doi.org/10.1016/j.cemconres.2007.09.005

Bentz, D. P., Ehlen, M. A., Ferraris, C. F., Winpigler, J. A., & United States. Federal Highway Administration. Office of Infrastructure Research and Development. (2002). *Service Life Prediction Based on Sorptivity for Highway Concrete Exposed to Sulfate Attack and Freeze-Thaw Conditions.* (FHWA-RD-01-162). https://rosap.ntl.bts.gov/view/dot/54487

Benzaazoua, M., Fall, M., & Belem, T. (2004). A contribution to understanding the hardening process of cemented pastefill. *Minerals Engineering*, *17*(2), 141–152. https://doi.org/10.1016/j.mineng.2003.10.022

Bischoff, P. H., & Perry, S. H. (1991). Compressive behaviour of concrete at high strain rates. *Materials and Structures*, *24*(6), 425–450. https://doi.org/10.1007/BF02472016

Bonen, D., & Cohen, M. D. (1992). Magnesium sulfate attack on portland cement paste-I. Microstructural analysis. *Cement and Concrete Research*, *22*(1), 169–180. https://doi.org/10.1016/0008-8846(92)90147-N

Brara, A., & Klepaczko, J. R. (2007). Fracture energy of concrete at high loading rates in tension. *International Journal of Impact Engineering*, *34*(3), 424–435. https://doi.org/10.1016/j.ijimpeng.2005.10.004

Carvalho, S. Z., Vernilli, F., Almeida, B., Oliveira, M. D., & Silva, S. N. (2018). Reducing environmental impacts: The use of basic oxygen furnace slag in portland cement. *Journal of Cleaner Production*, *172*, 385–390. https://doi.org/10.1016/j.jclepro.2017.10.130

Chen, S., Yilmaz, E., Wang, W., & Wang, Y. (2022). Curing stress effect on stability, microstructure, matric suction and electrical conductivity of cementitious tailings backfills. *Construction and Building Materials*, *360*, 129601. https://doi.org/10.1016/j.conbuildmat.2022.129601

Chen, X., Shi, X., Zhou, J., Chen, Q., Li, E., & Du, X. (2018). Compressive behavior and microstructural properties of tailings polypropylene fibre-reinforced cemented paste backfill. *Construction and Building Materials*, *190*, 211–221. https://doi.org/10.1016/j.conbuildmat.2018.09.092

Chhorn, C., Hong, S. J., & Lee, S. W. (2018). Relationship between compressive and tensile strengths of roller-compacted concrete. *Journal of Traffic and Transportation Engineering (English Edition)*, *5*(3), 215–223. https://doi.org/10.1016/j.jtte.2017.09.002

Cohen, M. D., & Bentur, A. (1988). Durability of Portland Cement-Silica Fume Pastes in Magnesium and Sodium Sulfate Solutions. *Materials Journal*, *85*(3), 148–157. https://doi.org/10.14359/1809

Courard, L., Michel, F., Perkowicz, S., & Garbacz, A. (2014). Effects of limestone fillers on surface free energy and electrical conductivity of the interstitial solution of cement mixes. *Cement and Concrete Composites*, *45*, 111–116. https://doi.org/10.1016/j.cemconcomp.2013.09.014

Cui, L. (2023). Experimental investigation of evolutive mode-I and mode-II fracture behavior of fiber-reinforced cemented paste backfill: Effect of curing temperature and curing time. *Frontiers of Structural and Civil Engineering*. https://doi.org/10.1007/s11709-022-0924-z

Cui, L., & Fall, M. (2015). A coupled thermo–hydro-mechanical–chemical model for underground cemented tailings backfill. *Tunnelling and Underground Space Technology*, *50*, 396–414. https://doi.org/10.1016/j.tust.2015.08.014

Cui, L., & Fall, M. (2016a). An evolutive elasto-plastic model for cemented paste backfill. *Computers and Geotechnics*, *71*, 19–29. https://doi.org/10.1016/j.compgeo.2015.08.013

Cui, L., & Fall, M. (2016b). Mechanical and thermal properties of cemented tailings materials at early ages: Influence of initial temperature, curing stress and drainage conditions. *Construction and Building Materials*, *125*, 553–563. https://doi.org/10.1016/j.conbuildmat.2016.08.080

Cui, L., & Fall, M. (2018). Modeling of self-desiccation in a cemented backfill structure. *International Journal for Numerical and Analytical Methods in Geomechanics*, *42*(3), 558–583. https://doi.org/10.1002/nag.2756

Cui, L., & Fall, M. (2019). Mathematical modelling of cemented tailings backfill: A review. *International Journal of Mining, Reclamation and Environment*, *33*(6), 389–408. https://doi.org/10.1080/17480930.2018.1453320

Cui, L., & Fall, M. (2020). Numerical Simulation of Consolidation Behavior of Large Hydrating Fill Mass. *International Journal of Concrete Structures and Materials*, *14*(1), 23. https://doi.org/10.1186/s40069-020-0398-0

Dai, F., Xia, K., & Nasseri, M. H. B. (2013). Micromechanical model for the rate dependence of the fracture toughness anisotropy of Barre granite. *International Journal of Rock*

Mechanics and Mining Sciences, *63*, 113–121. https://doi.org/10.1016/j.ijrmms.2013.08.011

Dehwah, H. A. F. (2007). Effect of sulfate concentration and associated cation type on concrete deterioration and morphological changes in cement hydrates. *Construction and Building Materials*, *21*(1), 29–39. https://doi.org/10.1016/j.conbuildmat.2005.07.010

Ercikdi, B., Baki, H., & İzki, M. (2013). Effect of desliming of sulphide-rich mill tailings on the long-term strength of cemented paste backfill. *Journal of Environmental Management*, *115*, 5–13. https://doi.org/10.1016/j.jenvman.2012.11.014

Ercikdi, B., Kesimal, A., Cihangir, F., Deveci, H., & Alp, İ. (2009). Cemented paste backfill of sulphide-rich tailings: Importance of binder type and dosage. *Cement and Concrete Composites*, *31*(4), 268–274. https://doi.org/10.1016/j.cemconcomp.2009.01.008

Fall, M., Belem, T., Samb, S., & Benzaazoua, M. (2007). Experimental characterization of the stress–strain behaviour of cemented paste backfill in compression. *Journal of Materials Science*, *42*(11), 3914–3922. https://doi.org/10.1007/s10853-006-0403-2

Fall, M., & Benzaazoua, M. (2005). Modeling the effect of sulphate on strength development of paste backfill and binder mixture optimization. *Cement and Concrete Research*, *35*(2), 301–314. https://doi.org/10.1016/j.cemconres.2004.05.020

Fall, M., Célestin, J. C., Pokharel, M., & Touré, M. (2010). A contribution to understanding the effects of curing temperature on the mechanical properties of mine cemented tailings backfill. *Engineering Geology*, *114*(3–4), 397–413. https://doi.org/10.1016/j.enggeo.2010.05.016

Fall, M., & Pokharel, M. (2010). Coupled effects of sulphate and temperature on the strength development of cemented tailings backfills: Portland cement-paste backfill. *Cement and Concrete Composites*, *32*(10), 819–828. https://doi.org/10.1016/j.cemconcomp.2010.08.002

Fang, K., & Cui, L. (2022). Experimental investigation of fiber content and length on curing time-dependent mode-I fracture behavior and properties of cemented paste backfill and implication to engineering design. *Fatigue & Fracture of Engineering Materials & Structures*, *45*(11), 3302–3318. https://doi.org/10.1111/ffe.13819

Fang, K., & Cui, L. (2023). Experimental investigation of evolutive mode-I and mode-II fracture behavior of fiber-reinforced cemented paste backfill: Effect of curing temperature and

curing time. *Frontiers of Structural and Civil Engineering*, *17*(2), 256–270. https://doi.org/10.1007/s11709-022-0924-z

Fang, K., Cui, L., & Fall, M. (2020). A coupled chemo-elastic cohesive zone model for backfill-rock interface. *Computers and Geotechnics*, *125*, 103666. https://doi.org/10.1016/j.compgeo.2020.103666

Fang, K., & Fall, M. (2018). Effects of curing temperature on shear behaviour of cemented paste backfill-rock interface. *International Journal of Rock Mechanics and Mining Sciences*, *112*, 184–192. https://doi.org/10.1016/j.ijrmms.2018.10.024

Fang, K., & Fall, M. (2019). Chemically Induced Changes in the Shear Behaviour of Interface Between Rock and Tailings Backfill Undergoing Cementation. *Rock Mechanics and Rock Engineering*, *52*(9), 3047–3062. https://doi.org/10.1007/s00603-019-01757-0

Fang, K., & Fall, M. (2020a). Insight into the mode I and mode II fracture toughness of the cemented backfill-rock interface: Effect of time, temperature and sulphate. *Construction and Building Materials*, *262*, 120860. https://doi.org/10.1016/j.conbuildmat.2020.120860

Fang, K., & Fall, M. (2020b). Shear Behavior of the Interface Between Rock and Cemented Backfill: Effect of Curing Stress, Drainage Condition and Backfilling Rate. *Rock Mechanics and Rock Engineering*, *53*(1), 325–336. https://doi.org/10.1007/s00603-019-01909-2

Fang, K., & Fall, M. (2021). Shear Behaviour of Rock–Tailings Backfill Interface: Effect of Cementation, Rock Type, and Rock Surface Roughness. *Geotechnical and Geological Engineering*, *39*(3), 1753–1770. https://doi.org/10.1007/s10706-020-01586-x

Fang, K., & Fall, M. (2022). Shear characteristics of the rock/cemented tailings interface exposed to sulfate attack. *Geotechnical Research*, *9*(4), 186–195. https://doi.org/10.1680/jgere.22.00017

Fang, K., Ren, L., & Jiang, H. (2021). Development of Mode I and Mode II fracture toughness of cemented paste backfill: Experimental results of the effect of mix proportion, temperature and chemistry of the pore water. *Engineering Fracture Mechanics*, *258*, 108096. https://doi.org/10.1016/j.engfracmech.2021.108096

Firoozi, S., Dehestani, M., & Navayi Neya, B. (2018). Effect of water to cement ratio on the mode III fracture energy of self-compacting concrete. *Materials and Structures*, *51*(4), 80. https://doi.org/10.1617/s11527-018-1208-x

Fu, J. X., Song, W. D., & Tan, Y. Y. (2016). Study on Microstructural Evolution and Strength Growth and Fracture Mechanism of Cemented Paste Backfill. *Advances in Materials Science and Engineering*, *2016*. https://doi.org/10.1155/2016/8792817

Ghirian, A., & Fall, M. (2014). Coupled thermo-hydro-mechanical–chemical behaviour of cemented paste backfill in column experiments: Part II: Mechanical, chemical and microstructural processes and characteristics. *Engineering Geology*, *170*, 11–23. https://doi.org/10.1016/j.enggeo.2013.12.004

Ghirian, A., & Fall, M. (2015). Coupled Behavior of Cemented Paste Backfill at Early Ages. *Geotechnical and Geological Engineering*, *33*(5), 1141–1166. https://doi.org/10.1007/s10706-015-9892-6

Guo, L., Peng, X., Zhao, Y., Liu, G., Tang, G., & Pan, A. (2022). Experimental Study on Direct Tensile Properties of Cemented Paste Backfill. *Frontiers in Materials*, *9*, 864264. https://doi.org/10.3389/fmats.2022.864264

Haufe, J., & Vollpracht, A. (2019). Tensile strength of concrete exposed to sulfate attack. *Cement and Concrete Research*, *116*, 81–88. https://doi.org/10.1016/j.cemconres.2018.11.005

Helinski, M., Fourie, A., Fahey, M., & Ismail, M. (2007). Assessment of the self-desiccation process in cemented mine backfills. *Canadian Geotechnical Journal*, *44*(10), 1148–1156. https://doi.org/10.1139/T07-051

Hua, W., Li, J., Gan, Z., Huang, J., & Dong, S. (2022). Degradation response of mode I and mode III fracture resistance of sandstone under wetting–drying cycles with an acidic solution. *Theoretical and Applied Fracture Mechanics*, *122*, 103661. https://doi.org/10.1016/j.tafmec.2022.103661

Huang, S., Xia, K., & Qiao, L. (2011). Dynamic tests of cemented paste backfill: Effects of strain rate, curing time, and cement content on compressive strength. *Journal of Materials Science*, *46*(15), 5165–5170. https://doi.org/10.1007/s10853-011-5449-0

Hustrulid, W. A., Hustrulid, W. A., & Bullock, R. L. (2001). *Underground Mining Methods: Engineering Fundamentals and International Case Studies*. SME.

Ismailov, A., Merilaita, N., Solismaa, S., Karhu, M., & Levänen, E. (2020). Utilizing mixed-mineralogy ferroan magnesite tailings as the source of magnesium oxide in magnesium potassium phosphate cement. *Construction and Building Materials*, *231*, 117098. https://doi.org/10.1016/j.conbuildmat.2019.117098

Jaber, A., Gorgis, I., & Hassan, M. (2018). Relationship between splitting tensile and compressive strengths for self-compacting concrete containing nano- and micro silica. *MATEC Web of Conferences*, *162*, 02013. https://doi.org/10.1051/matecconf/201816202013

Jacob, G. C., Starbuck, J. M., Fellers, J. F., Simunovic, S., & Boeman, R. G. (2005). The effect of loading rate on the fracture toughness of fiber reinforced polymer composites. *Journal of Applied Polymer Science*, *96*(3), 899–904. https://doi.org/10.1002/app.21535

Jafari, M. (2020). *Experimental Study of Physical and Mechanical Properties of a Cemented Mine Tailings—ProQuest* [University of Toronto]. https://www.proquest.com/openview/606b1c2ee0743b19e5297d6ce82e7e5c/1?pq-origsite=gscholar&cbl=51922&diss=y

Jafari, M., & Grabinsky, M. (2021). Effect of hydration on failure surface evolution of low sulfide content cemented paste backfill. *International Journal of Rock Mechanics and Mining Sciences*, *144*, 104749. https://doi.org/10.1016/j.ijrmms.2021.104749

Jiang, H., Fall, M., & Cui, L. (2017). Freezing behaviour of cemented paste backfill material in column experiments. *Construction and Building Materials*, *147*, 837–846. https://doi.org/10.1016/j.conbuildmat.2017.05.002

Jiang, H., Fall, M., Li, Y., & Han, J. (2019). An experimental study on compressive behaviour of cemented rockfill. *Construction and Building Materials*, *213*, 10–19. https://doi.org/10.1016/j.conbuildmat.2019.04.061

Jiang, H., Han, J., Ren, L., Guo, Z., & Yilmaz, E. (2023). Study of early-age performance of cementitious backfills with alkali activated slag under internal sulfate attack. *Construction and Building Materials*, *371*, 130786. https://doi.org/10.1016/j.conbuildmat.2023.130786

Ke, Y., Shen, Y., Qing, C., Hu, K., Wang, S., Chen, Q., & Guan, H. (2022). Mechanical Properties and Microstructure Evolution of Cemented Tailings Backfill Under Seepage Pressure. *Frontiers in Materials*, *8*, 818698. https://doi.org/10.3389/fmats.2021.818698

Kesimal, A., Ercikdi, B., & Yilmaz, E. (2003). The effect of desliming by sedimentation on paste backfill performance. *Minerals Engineering*, *16*(10), 1009–1011. https://doi.org/10.1016/S0892-6875(03)00267-X

Kesimal, A., Yilmaz, E., & Ercikdi, B. (2004). Evaluation of paste backfill mixtures consisting of sulphide-rich mill tailings and varying cement contents. *Cement and Concrete Research*, *34*(10), 1817–1822. https://doi.org/10.1016/j.cemconres.2004.01.018

Kinnunen, P. (2018). Sulphate removal from mine water with chemical, biological and membrane technologies. *Water Science and Technology*, *2017*(1), 194–205. https://doi.org/10.2166/wst.2018.102

Klepaczko, J. R., & Brara, A. (2001). An experimental method for dynamic tensile testing of concrete by spalling. *International Journal of Impact Engineering*, *25*(4), 387–409. https://doi.org/10.1016/S0734-743X(00)00050-6

Koh, S.-W., Kim, J.-K., & Mai, Y.-W. (1993). Fracture toughness and failure mechanisms in silica-filled epoxy resin composites: Effects of temperature and loading rate. *Polymer*, *34*(16), 3446–3455. https://doi.org/10.1016/0032-3861(93)90474-O

Komurlu, E., Kesimal, A., & Demir, S. (2016a). Experimental and numerical analyses on determination of indirect (splitting) tensile strength of cemented paste backfill materials under different loading apparatus. *Geomechanics and Engineering*, *10*(6), 775–791. https://doi.org/10.12989/gae.2016.10.6.775

Koupouli, N. J. F., Belem, T., Rivard, P., & Effenguet, H. (2016). Direct shear tests on cemented paste backfill–rock wall and cemented paste backfill–backfill interfaces. *Journal of Rock Mechanics and Geotechnical Engineering*, *8*(4), 472–479. https://doi.org/10.1016/j.jrmge.2016.02.001

Kuruppu, M. D., & Chong, K. P. (2012). Fracture toughness testing of brittle materials using semi-circular bend (SCB) specimen. *Engineering Fracture Mechanics*, *91*, 133–150. https://doi.org/10.1016/j.engfracmech.2012.01.013

Kuruppu, M. D., Obara, Y., Ayatollahi, M. R., Chong, K. P., & Funatsu, T. (2014). ISRM-Suggested Method for Determining the Mode I Static Fracture Toughness Using Semi-Circular Bend Specimen. *Rock Mechanics and Rock Engineering*, *47*(1), 267–274. https://doi.org/10.1007/s00603-013-0422-7

Landes, J. D. (1996). *Fracture Toughness Testing*. https://doi.org/10.31399/asm.hb.v19.a0002380

Li, L. (2014). Analytical solution for determining the required strength of a side-exposed mine backfill containing a plug. *Canadian Geotechnical Journal*, *51*(5), 508–519. https://doi.org/10.1139/cgj-2013-0227

Li, W., & Fall, M. (2016). Sulphate effect on the early age strength and self-desiccation of cemented paste backfill. *Construction and Building Materials*, *106*, 296–304. https://doi.org/10.1016/j.conbuildmat.2015.12.124

Li, W., & Fall, M. (2018). Strength and self-desiccation of slag-cemented paste backfill at early ages: Link to initial sulphate concentration. *Cement and Concrete Composites*, *89*, 160–168. https://doi.org/10.1016/j.cemconcomp.2017.09.019

Li, Y., Jin, L., & Zhang, L. (2016). *Mechanical Parameters of Cemented Paste Backfilling and Its Failure Modes Under Different Loading Rates*. *21*, 10.

Liang, C., Wu, S., Li, X., & Xin, P. (2015). Effects of strain rate on fracture characteristics and mesoscopic failure mechanisms of granite. *International Journal of Rock Mechanics and Mining Sciences*, *76*, 146–154. https://doi.org/10.1016/j.ijrmms.2015.03.010

Libos, I. L. S. (2020). *Experimental Testing of Geomechanical Behavior of Fiber- Reinforced Cemented Paste Backfill (FR-CPB) under Warmer Curing Temperature*. Lakehead University.

Libos, I. L. S., & Cui, L. (2020). Effects of curing time, cement content, and saturation state on mode-I fracture toughness of cemented paste backfill. *Engineering Fracture Mechanics*, *235*, 107174. https://doi.org/10.1016/j.engfracmech.2020.107174

Liu, G., Li, L., Yang, X., & Guo, L. (2016). A numerical analysis of the stress distribution in backfilled stopes considering nonplanar interfaces between the backfill and rock walls. *International Journal of Geotechnical Engineering*, *10*(3), 271–282. https://doi.org/10.1080/19386362.2015.1132123

Liu, G., Li, L., Yang, X., & Guo, L. (2017). Numerical Analysis of Stress Distribution in Backfilled Stopes Considering Interfaces between the Backfill and Rock Walls. *International Journal of Geomechanics*, *17*(2), 06016014. https://doi.org/10.1061/(ASCE)GM.1943-5622.0000702

Liu, L., Song, M., Peng, Y., & Li, J. (2019). A novel fusion framework of infrared and visible images based on RLNSST and guided filter. *Infrared Physics & Technology*, *100*, 99–108. https://doi.org/10.1016/j.infrared.2019.05.019

Liu, L., Xin, J., Huan, C., Qi, C., Zhou, W., & Song, K.-I. (2020). Pore and strength characteristics of cemented paste backfill using sulphide tailings: Effect of sulphur content. *Construction and Building Materials*, *237*, 117452. https://doi.org/10.1016/j.conbuildmat.2019.117452

Liu, L., Zhu, C., Qi, C., Zhang, B., & Song, K.-I. (2019). A microstructural hydration model for cemented paste backfill considering internal sulfate attacks. *Construction and Building Materials*, *211*, 99–108. https://doi.org/10.1016/j.conbuildmat.2019.03.222

Liu, X., Liu, K., Zhao, K., & Hu, J. (2013). *Strain Rate Effects and Acoustic Emission Characteristics of Tailing Cement Backfill Under Uniaxial Compression*. *18*.

Lu, D. X., Bui, H. H., & Saleh, M. (2021). Effects of specimen size and loading conditions on the fracture behaviour of asphalt concretes in the SCB test. *Engineering Fracture Mechanics*, *242*, 107452. https://doi.org/10.1016/j.engfracmech.2020.107452

Lura, P., Jensen, O. M., & Weiss, J. (2009). Cracking in cement paste induced by autogenous shrinkage. *Materials and Structures*, *42*(8), 1089–1099. https://doi.org/10.1617/s11527-008-9445-z

Mahanta, B., Tripathy, A., Vishal, V., Singh, T. N., & Ranjith, P. G. (2017). Effects of strain rate on fracture toughness and energy release rate of gas shales. *Engineering Geology*, *218*, 39–49. https://doi.org/10.1016/j.enggeo.2016.12.008

McLean, J., & Cui, L. (2021). Multiscale Geomechanical Behavior of Fiber-Reinforced Cementitious Composites Under Cyclic Loading Conditions—A Review. *Frontiers in Materials*, *8*, 759126. https://doi.org/10.3389/fmats.2021.759126

Mehta, P. K. (1983). Mechanism of sulfate attack on portland cement concrete—Another look. *Cement and Concrete Research*, *13*(3), 401–406. https://doi.org/10.1016/0008-8846(83)90040-6

Mindess, S., Young, J. F., & Darwin, D. (2003). *Concrete* (2nd ed). Prentice Hall.

Nasir, O., & Fall, M. (2008). Shear behaviour of cemented pastefill-rock interfaces. *Engineering Geology*, *101*(3), 146–153. https://doi.org/10.1016/j.enggeo.2008.04.010

Obara, Y., Yoshinaga, T., & Hirata, A. (2009, October 29). *Fracture Toughness in Mode I and II of Rock Under Water Vapor Pressure*. ISRM Regional Symposium - EUROCK 2009. https://dx.doi.org/

Ouattara, D., Yahia, A., Mbonimpa, M., & Belem, T. (2017). Effects of superplasticizer on rheological properties of cemented paste backfills. *International Journal of Mineral Processing*, *161*, 28–40. https://doi.org/10.1016/j.minpro.2017.02.003

Pan, A., & Grabinsky, M. (2023). Mechanical Characterization of Cemented Paste Backfill. *Eng*, *4*, 738–747. https://doi.org/10.3390/eng4010044

Pan, A. N., & Grabinsky, M. W. F. (2021). Tensile Strength of Cemented Paste Backfill. *Geotechnical Testing Journal*, *44*(6), 1886–1897. https://doi.org/10.1520/GTJ20200206

Pokharel, M., & Fall, M. (2011). Coupled Thermochemical Effects on the Strength Development of Slag-Paste Backfill Materials. *Journal of Materials in Civil Engineering*, *23*(5), 511–525. https://doi.org/10.1061/(ASCE)MT.1943-5533.0000192

Pokharel, M., & Fall, M. (2013). Combined influence of sulphate and temperature on the saturated hydraulic conductivity of hardened cemented paste backfill. *Cement and Concrete Composites*, *38*, 21–28. https://doi.org/10.1016/j.cemconcomp.2013.03.015

Qi, C., & Fourie, A. (2019). Cemented paste backfill for mineral tailings management: Review and future perspectives. *Minerals Engineering*, *144*, 106025. https://doi.org/10.1016/j.mineng.2019.106025

Richard, H. A., Schramm, B., & Schirmeisen, N.-H. (2014). Cracks on Mixed Mode loading – Theories, experiments, simulations. *International Journal of Fatigue*, *62*, 93–103. https://doi.org/10.1016/j.ijfatigue.2013.06.019

Rosa, A. L., Yu, R. C., Ruiz, G., Saucedo, L., & Sousa, J. L. A. O. (2012). A loading rate dependent cohesive model for concrete fracture. *Engineering Fracture Mechanics*, *82*, 195–208. https://doi.org/10.1016/j.engfracmech.2011.12.013

Schuler, H., Mayrhofer, C., & Thoma, K. (2006). Spall experiments for the measurement of the tensile strength and fracture energy of concrete at high strain rates. *International Journal of Impact Engineering*, *32*(10), 1635–1650. https://doi.org/10.1016/j.ijimpeng.2005.01.010

Shahsavari, M., & Grabinsky, M. (2016). *Pore Water Pressure Variations in Cemented Paste Backfilled Stopes*. 331–342. https://doi.org/10.1061/9780784480137.033

Sheshpari, M. (2015a). *A Review of Underground Mine Backfilling Methods with Emphasis On Cemented Paste Backfill*. *20*.

Stoddart, E. P., Byfield, M. P., Davison, J. B., & Tyas, A. (2013). Strain rate dependent component based connection modelling for use in non-linear dynamic progressive collapse analysis. *Engineering Structures*, *55*, 35–43. https://doi.org/10.1016/j.engstruct.2012.05.042

Tariq, A., & Yanful, E. K. (2013). A review of binders used in cemented paste tailings for underground and surface disposal practices. *Journal of Environmental Management*, *131*, 138–149. https://doi.org/10.1016/j.jenvman.2013.09.039

Thomson, D. M., Cui, H., Erice, B., Hoffmann, J., Wiegand, J., & Petrinic, N. (2017). Experimental and numerical study of strain-rate effects on the IFF fracture angle using a

new efficient implementation of Puck's criterion. *Composite Structures*, *181*, 325–335. https://doi.org/10.1016/j.compstruct.2017.08.084

Tian, B., & Cohen, M. D. (2000). Does gypsum formation during sulfate attack on concrete lead to expansion? *Cement and Concrete Research*, *30*(1), 117–123. https://doi.org/10.1016/S0008-8846(99)00211-2

Tian, X., & Fall, M. (2021). Non-isothermal evolution of mechanical properties, pore structure and self-desiccation of cemented paste backfill. *Construction and Building Materials*, *297*, 123657. https://doi.org/10.1016/j.conbuildmat.2021.123657

Tzouvalas, G., Dermatas, N., & Tsimas, S. (2004). Alternative calcium sulfate-bearing materials as cement retarders: Part I. Anhydrite. *Cement and Concrete Research*, *34*(11), 2113–2118. https://doi.org/10.1016/j.cemconres.2004.03.020

Vegt, I. (2007). *Failure mechanisms of concrete under impact loading*.

Wagner, A. C., de Sousa Silva, J. P., de Azambuja Carvalho, J. V., Cezar Rissoli, A. L., Cacciari, P. P., Chaves, H. M., Scheuermann Filho, H. C., & Consoli, N. C. (2022). Mechanical behavior of iron ore tailings under standard compression and extension triaxial stress paths. *Journal of Rock Mechanics and Geotechnical Engineering*. https://doi.org/10.1016/j.jrmge.2022.11.013

Walker, W. J., Montoy, J., & Chatriand, T. (2015). Sulfate removal from coal mine water in western Pennsylvania: Regulatory requirements, design, and performance. *Journal American Society of Mining and Reclamation*, *4*(1), 73–93. https://doi.org/10.21000/jasmr15010073

Wang, C., Harbottle, D., Liu, Q., & Xu, Z. (2014). Current state of fine mineral tailings treatment: A critical review on theory and practice. *Minerals Engineering*, *58*, 113–131. https://doi.org/10.1016/j.mineng.2014.01.018

Wang, C., Ren, Z., Huo, Z., Zheng, Y., Tian, X., Zhang, K., & Zhao, G. (2021). Properties and hydration characteristics of mine cemented paste backfill material containing secondary smelting water-granulated nickel slag. *Alexandria Engineering Journal*, *60*(6), 4961–4971. https://doi.org/10.1016/j.aej.2020.12.058

Wang, Y., Cao, Y., Cui, L., Si, Z., & Wang, H. (2020). Effect of external sulfate attack on the mechanical behavior of cemented paste backfill. *Construction and Building Materials*, *263*, 120968. https://doi.org/10.1016/j.conbuildmat.2020.120968

Wang, Y., Yu, Z., Cui, L., & Wang, Y. (2020). Effect of Moisture Content on the Ductility of Cemented Paste Backfill. *IOP Conference Series: Earth and Environmental Science*, *514*, 022019. https://doi.org/10.1088/1755-1315/514/2/022019

Wasantha, P. L. P., Ranjith, P. G., Zhao, J., Shao, S. S., & Permata, G. (2015). Strain Rate Effect on the Mechanical Behaviour of Sandstones with Different Grain Sizes. *Rock Mechanics and Rock Engineering*, *48*(5), 1883–1895. https://doi.org/10.1007/s00603-014-0688-4

Weilv, W., Xu, W., & Jianpin, Z. (2021). Effect of inclined interface angle on shear strength and deformation response of cemented paste backfill-rock under triaxial compression. *Construction and Building Materials*, *279*, 122478. https://doi.org/10.1016/j.conbuildmat.2021.122478

Wenbin, X., Tian, X., & Wan, C. (2018). Prediction of Mechanical Performance of Cemented Paste Backfill by the Electrical Resistivity Measurement. *Journal of Testing and Evaluation*, *46*, 20160183. https://doi.org/10.1520/JTE20160183

Wisetsaen, S., Walsri, C., & Fuenkajorn, K. (2015). Effects of loading rate and temperature on tensile strength and deformation of rock salt. *International Journal of Rock Mechanics and Mining Sciences*, *73*, 10–14. https://doi.org/10.1016/j.ijrmms.2014.10.005

Wu, D., Liu, Y., Zheng, Z., & Wang, S. (2016). Impact Energy Absorption Behavior of Cemented Coal Gangue-Fly Ash Backfill. *Geotechnical and Geological Engineering*, *34*(2), 471–480. https://doi.org/10.1007/s10706-015-9958-5

Wu, J., Feng, M., Chen, Z., Mao, X., Han, G., & Wang, Y. (2018). Particle Size Distribution Effects on the Strength Characteristic of Cemented Paste Backfill. *Minerals*, *8*(8), Article 8. https://doi.org/10.3390/min8080322

Xiapeng, P., Fall, M., & Haruna, S. (2019). Sulphate induced changes of rheological properties of cemented paste backfill. *Minerals Engineering*, *141*, 105849. https://doi.org/10.1016/j.mineng.2019.105849

Xiu, Z., Wang, S., Ji, Y., Wang, F., Ren, F., & Nguyen, V.-T. (2021a). Loading rate effect on the uniaxial compressive strength (UCS) behavior of cemented paste backfill (CPB). *Construction and Building Materials*, *271*, 121526. https://doi.org/10.1016/j.conbuildmat.2020.121526

Xiu, Z., Wang, S., Ji, Y., Wang, F., Ren, F., & Nguyen, V.-T. (2021b). The effects of dry and wet rock surfaces on shear behavior of the interface between rock and cemented paste backfill. *Powder Technology*, *381*, 324–337. https://doi.org/10.1016/j.powtec.2020.11.053

Xu, W., & Cao, P. (2018a). Fracture behaviour of cemented tailing backfill with pre-existing crack and thermal treatment under three-point bending loading: Experimental studies and particle flow code simulation. *Engineering Fracture Mechanics*, *195*, 129–141. https://doi.org/10.1016/j.engfracmech.2018.04.008

Xu, W., Cao, P., & Tian, M. (2018). Strength Development and Microstructure Evolution of Cemented Tailings Backfill Containing Different Binder Types and Contents. *Minerals*, *8*(4), Article 4. https://doi.org/10.3390/min8040167

Xu, W., Li, Q., & Liu, B. (2020). Coupled effect of curing temperature and age on compressive behavior, microstructure and ultrasonic properties of cemented tailings backfill. *Construction and Building Materials*, *237*, 117738. https://doi.org/10.1016/j.conbuildmat.2019.117738

Xu, X., Wu, W., & Xu, W. (2020). Sulfate-Dependent Shear Behavior of Cementing Fiber-Reinforced Tailings and Rock. *Minerals*, *10*(11), Article 11. https://doi.org/10.3390/min10111032

Yang, L., Hou, C., Zhu, W., Liu, X., Yan, B., & Li, L. (2022). Monitoring the failure process of cemented paste backfill at different curing times by using a digital image correlation technique. *Construction and Building Materials*, *346*, 128487. https://doi.org/10.1016/j.conbuildmat.2022.128487

Yilmaz, E. (2018). Stope depth effect on field behaviour and performance of cemented paste backfills. *International Journal of Mining, Reclamation and Environment*, *32*(4), 273–296. https://doi.org/10.1080/17480930.2017.1285858

Yilmaz, E., Benzaazoua, M., Belem, T., & Bussière, B. (2009). Effect of curing under pressure on compressive strength development of cemented paste backfill. *Minerals Engineering*, *22*(9), 772–785. https://doi.org/10.1016/j.mineng.2009.02.002

Yilmaz, E., & Fall, M. (2017). Introduction to Paste Tailings Management. In E. Yilmaz & M. Fall (Eds.), *Paste Tailings Management* (pp. 1–5). Springer International Publishing. https://doi.org/10.1007/978-3-319-39682-8_1

Yilmaz, E., Kesimal, A., Deveci, H., & Ercikdi, B. (2003). The factors affecting the performance of paste backfill: Physical, chemical and mineralogical characterization. *First Engineering Sciences Congress for Young Researcher (MBGAK'03), Istanbul*.

Yin, S., Yan, Z., Chen, X., Yan, R., Chen, D., Chen, J., & Li, G. (2023). Active roof-contact: The future development of cemented paste backfill. *Construction and Building Materials*, *370*, 130657. https://doi.org/10.1016/j.conbuildmat.2023.130657

Zhang, Q. B., & Zhao, J. (2013). Effect of loading rate on fracture toughness and failure micromechanisms in marble. *Engineering Fracture Mechanics*, *102*, 288–309. https://doi.org/10.1016/j.engfracmech.2013.02.009

Zhang, X. X., Ruiz, G., Yu, R. C., & Tarifa, M. (2009). Fracture behaviour of high-strength concrete at a wide range of loading rates. *International Journal of Impact Engineering*, *36*(10), 1204–1209. https://doi.org/10.1016/j.ijimpeng.2009.04.007

Zhao, G., Li, J., Shi, M., Fan, H., Cui, J., & Xie, F. (2020). Degradation mechanisms of cast-in-situ concrete subjected to internal-external combined sulfate attack. *Construction and Building Materials*, *248*, 118683. https://doi.org/10.1016/j.conbuildmat.2020.118683

Zhou, J., Pan, J., & Leung, C. K. Y. (2015). Mechanical Behavior of Fiber-Reinforced Engineered Cementitious Composites in Uniaxial Compression. *Journal of Materials in Civil Engineering*, *27*(1), 04014111. https://doi.org/10.1061/(ASCE)MT.1943-5533.0001034

Zhou, X., Hu, S., Zhang, G., Li, J., Xuan, D., & Gao, W. (2019). Experimental investigation and mathematical strength model study on the mechanical properties of cemented paste backfill. *Construction and Building Materials*, *226*, 524–533. https://doi.org/10.1016/j.conbuildmat.2019.07.148

Zhou, Y., Yu, X., Guo, Z., Yan, Y., Zhao, K., Wang, J., & Zhu, S. (2021). On acoustic emission characteristics, initiation crack intensity, and damage evolution of cement-paste backfill under uniaxial compression. *Construction and Building Materials*, *269*, 121261. https://doi.org/10.1016/j.conbuildmat.2020.121261

Zhu, W. C., Niu, L. L., Li, S. H., & Xu, Z. H. (2015). Dynamic Brazilian Test of Rock Under Intermediate Strain Rate: Pendulum Hammer-Driven SHPB Test and Numerical Simulation. *Rock Mechanics and Rock Engineering*, *48*(5), 1867–1881. https://doi.org/10.1007/s00603-014-0677-7